



1 **Anthropogenic CO₂, air-sea CO₂ fluxes and acidification in the Southern**
2 **Ocean: results from a time-series analysis at station OISO-KERFIX (51°S-**
3 **68°E).**

4
5 Nicolas Metzl¹, Claire Lo Monaco¹, Coraline Leseurre^{1,2}, Céline Ridame¹, Gilles Reverdin¹,
6 Thi Tuyet Trang Chau³, Frédéric Chevallier³, Marion Gehlen³

7
8 ¹ Laboratoire LOCEAN/IPSL, Sorbonne Université-CNRS-IRD-MNHN, Paris, 75005, France

9 ² Flanders Marine Institute (VLIZ), 8400 Ostend, Belgium

10 ³ Laboratoire LSCE/IPSL, CEA-CNRS-UVSQ, Université Paris-Saclay Gif-sur-Yvette, 91191, France

11
12 *Correspondence to:* Nicolas Metzl (nicolas.metzl@locean.ipsl.fr)

13
14 **Abstract:** The temporal variation of the carbonate system, air-sea CO₂ fluxes and pH is analyzed in the Southern
15 Indian Ocean, south of the Polar Front, based on in-situ data obtained from 1985 to 2021 at a fixed station
16 (50°40'S-68°25'E) and results from a neural network model that reconstructs the fugacity of CO₂ (fCO₂) and
17 fluxes at monthly scale. Anthropogenic CO₂ (C_{ant}) was estimated in the water column and detected down to the
18 bottom (1600m) in 1985 resulting in an aragonite saturation horizon at 600m that migrated up to 400m in 2021
19 due to the accumulation of C_{ant}. In subsurface, the trend of C_{ant} is estimated at +0.53 (±0.01) μmol.kg⁻¹.yr⁻¹ with a
20 detectable increase in recent years. At the surface during austral winter the oceanic fCO₂ increased at a rate close
21 or slightly lower than in the atmosphere. To the contrary, in summer, we observed contrasting fCO₂ and
22 dissolved inorganic carbon (C_T) trends depending on the decade and emphasizing the role of biological drivers
23 on air-sea CO₂ fluxes and pH inter-annual variability. The region moved from an annual source of 0.8 molC.m⁻²
24 .yr⁻¹ in 1985 to a sink of -0.5 molC.m⁻².yr⁻¹ in 2020. In 1985-2020, the annual pH trend in surface of -0.0165 (±
25 0.0040).decade⁻¹ was mainly controlled by anthropogenic CO₂ but the trend was modulated by natural processes.
26 Using historical data from November 1962 we estimated the long-term trend for fCO₂, C_T and pH confirming
27 that the progressive acidification was driven by atmospheric CO₂ increase. In 59 years this leads to a diminution
28 of 11% for both aragonite and calcite saturation state. As atmospheric CO₂ will desperately continue rising in the
29 future, the pH and carbonate saturation state will decrease at a faster rate than observed in recent years. A
30 projection of future C_T concentrations for a high emission scenario (SSP5-8.5) indicates that the surface pH in
31 2100 would decrease to 7.32 in winter. This is up to -0.86 lower than pre-industrial pH and -0.71 lower than pH
32 observed in 2020. The aragonite under-saturation in surface waters would be reached as soon as 2050 (scenario
33 SSP5-8.5) and 20 years later for a stabilization scenario (SSP2-4.5) with potential impacts on phytoplankton
34 species and higher trophic levels in the rich ecosystems of the Kerguelen Island area.

35
36 **Keywords:** Ocean Carbonate System, Ocean acidification, anthropogenic CO₂, air-sea CO₂ fluxes, Southern
37 Ocean, Time-series station

38



39

40 1 Introduction

41 The ocean plays an important role in mitigating climate change by taking up since decades a large part
42 of the excess of heat (Cheng et al., 2020; Fox-Kemper et al., 2021) and of CO₂ released by human activities
43 (Sabine et al., 2004; Gruber et al., 2019a; Canadell et al., 2021). Since 1750, the global ocean has captured 185
44 (± 35) PgC (Petagram of Carbon) from a total of 700 (± 75) PgC of anthropogenic carbon emissions from
45 fossils fuels and land-used changes (Friedlingstein et al., 2022). From year to year, the ocean anthropogenic CO₂
46 sink increased progressively from 1.1 (± 0.4) PgC.yr⁻¹ in the 1960s to 2.3 (± 0.4) PgC.yr⁻¹ in the 2000s. Over the
47 decade 2012-2021, the partitioning of the anthropogenic CO₂ sinks was roughly equal between the ocean (2.9 \pm
48 0.4 PgC.yr⁻¹) and the land (3.1 \pm 0.6 PgC.yr⁻¹) (Friedlingstein et al., 2022).

49 Ocean observations indicate that since the 1990s the Southern Ocean (SO) south of 45°S has been
50 accumulating each year about 0.5 PgC.yr⁻¹ (e.g. Takahashi et al., 2009; Lenton et al., 2013; Rödenbeck et al.,
51 2013; Long et al., 2021; Fay et al., 2023; Gray, 2024). Results based on BGC-Argo floats (Southern Ocean
52 Carbon and Climate Observations and Modeling project, SOCCOM) suggest that the CO₂ sink in the SO might
53 be much lower (0.16 PgC.yr⁻¹ south of 44°S for the period 2015-2017, Gray et al. 2018; Bushinsky et al., 2019)
54 but there is an ongoing debate (Long et al., 2021; Sutton et al., 2021; Gray, 2024). It is also well established that
55 the CO₂ sink in the SO undergoes substantial decadal variability first documented for the 1990s (Le Quéré et al.,
56 2007; Metzl, 2009; Lenton et al., 2013) and subsequently identified for the period 1982-2018 (Landschützer et
57 al., 2015; Keppler and Landschützer, 2019; Mackay et al., 2022; Hauck et al., 2023). A recent extension of the
58 period to 1957-2020 suggests that the inter-annual to decadal variability of the SO CO₂ sink was most
59 pronounced after the 1980s (Rödenbeck et al., 2022; Bennington et al., 2022). Whatever the variability of the SO
60 CO₂ sink since the 1960s, the ocean continuously absorbs atmospheric CO₂ and the distribution of anthropogenic
61 CO₂ (C_{ant}) in the SO is now relatively well documented (e.g. Pardo et al., 2014; Gruber et al., 2019a) thanks to
62 the GLODAP data synthesis effort for the global ocean (Global Ocean Data Analysis Project, Olsen et al., 2016,
63 2019, 2020). The SO takes up about 40% of the total anthropogenic carbon that enters the ocean (Khatiwala et
64 al., 2013; Gruber et al., 2019a).

65 The anthropogenic CO₂ uptake in the ocean results in lowering carbonate ion concentrations and pH, a
66 chemical process termed “ocean acidification” (OA) (Caldeira and Wickett 2003; Doney et al., 2009). This
67 decreases the saturation state with respect to carbonate minerals (aragonite, Ω_{ar} and calcite, Ω_{ca}), a process most
68 pronounced in the cold and naturally at a low saturation state waters in high latitudes (Orr et al., 2005; Takahashi
69 et al., 2014; Jiang et al., 2015). The first estimate of C_{ant} distribution in the global ocean (for a nominal year
70 1994, Sabine et al., 2004) shows that C_{ant} uptake led to an upward migration of the Ω_{ar} and Ω_{ca} saturation
71 horizon in all ocean basins (Feely et al., 2004). This change is particularly pronounced south of the Polar Front
72 (PF) in the SO linked to both C_{ant} uptake and the upwelling of dissolved inorganic carbon (C_T) C_T-rich deep
73 waters (e.g. Hauck et al., 2010; Pardo et al., 2017). It has been suggested, through numerical studies, that
74 depending on future CO₂ emission levels, surface waters could reach under-saturation state for aragonite by
75 2030-2050 in the SO (Orr et al., 2005; Gangstø et al., 2008; McNeil and Matear, 2008; Negrete-Garcia et al.,
76 2019). Such a change would have multiple and detrimental impacts on marine ecosystems (Fabry et al., 2008;
77 Doney et al., 2012; Bopp et al., 2013), in particular calcifying marine organisms especially aragonite producers
78 such as pteropods (Hunt et al., 2008; Gardner et al., 2023), but also calcite producing planktonic foraminifera
79 (Moy et al., 2009), coccolithophorids (Beaufort et al., 2011), and non-calcifying species such as the abundant SO



80 diatoms (e.g. Benoiston et al., 2017; Petrou et al., 2019; Weir et al., 2020; Duncan et al., 2022) and krill
81 (Kawaguchi et al., 2013).

82 Hindcast simulations with Global Ocean Biogeochemical Models (GOBM), as well as projections with
83 Earth System Models (ESM) have been used to evaluate the ocean carbon cycle over the past decades and future
84 changes in C_{am} storage, ocean acidification or impacts of global change on marine ecosystems. However, current
85 model-based estimates of the contemporary SO CO_2 sink are subject to relatively large uncertainties (e.g. Long
86 et al., 2013; Hauck et al., 2020; Gooya et al., 2023; Hauck et al., 2023; Mayot et al., 2023; DeVries et al., 2023).
87 Difference between GOBM models can reach 0.7 PgC.yr^{-1} in the SO (Hauck et al., 2020), which is roughly
88 equivalent to the mean climatological flux of 0.5 PgC.yr^{-1} (McNeil et al., 2007; Takahashi et al., 2009; Lenton et
89 al., 2013). In the high latitudes of the SO ($> 50^\circ\text{S}$) for the 2010s, ESM from the Coupled Model Intercomparison
90 Project Phase 6 (CMIP6) simulated either a large sink or a modest source of CO_2 (McKinley et al., 2023). This is
91 mainly due to incorrect or missing physical and/or biological processes in the models (e.g. Pilcher et al., 2015;
92 Kessler and Tjiputra, 2016; Mongwe et al., 2018; Lerner et al., 2021) leading to biases in the seasonality of
93 temperature, C_T , partial pressure of CO_2 ($p\text{CO}_2$), air-sea CO_2 fluxes, pH or Ω (e.g. McNeil and Sasse 2016;
94 Rodgers et al., 2023; Rustogi et al., 2023; Joos et al., 2023). Such model imperfections should be resolved to
95 have future projections of CO_2 uptake, OA, productivity and the responses of the marine ecosystems, gain in
96 reliability (Frölicher et al., 2015; Hauck et al., 2015; Sasse et al., 2015; Kessler and Tjiputra, 2016; McNeil and
97 Sasse 2016; Kwiatkowski and Orr, 2018; Negrete-Garcia et al., 2019; Burger et al., 2020; Terharr et al., 2021;
98 Krumhardt et al., 2022; Jiang et al., 2023; Mongwe et al., 2023). In this context, as often concluded in modeling
99 studies (e.g. Kessler and Tjiputra, 2016; Gooya et al., 2023; Wright et al., 2023; Hauck et al., 2023; Mayot et al.,
100 2023; Rodgers et al., 2023), long-term biogeochemical observations are particularly valuable to quantify and
101 understand recent past and current changes, and ultimately evaluate model simulations.

102 Although the SO south of the Polar Front remains much less observed than other oceanic regions,
103 several observations based studies have allowed to estimate the decrease in pH in the surface waters in response
104 to the increase in oceanic CO_2 fugacity, $f\text{CO}_2$ (Mirodikwa et al., 2012; Takahashi et al., 2014; Lauvset et al.,
105 2015; Munro et al., 2015; Xue et al., 2018; Iida et al., 2021; Leseurre et al., 2022; Brandon et al., 2022). Results
106 showed a large range of the pH trends from $-0.008.\text{decade}^{-1}$ to $-0.035.\text{decade}^{-1}$ depending on the period and
107 regions of interest. Most of these analyses were based on summer observations (Table 1) and some studies
108 highlighted contrasting pH trends on a 5-10 year time probably linked to large scale climate variability such as
109 the Southern Annular Mode (SAM) (e.g. Xue et al., 2018). Given such variability, it is important to continue
110 monitoring $f\text{CO}_2$ and pH trend and, if possible, at different seasons as future change in CO_2 uptake and potential
111 tipping points of that carbonate saturation state also depends on seasonality (Sasse et al., 2015). The above
112 observational studies were dedicated to pH changes in surface waters. In contrast to Northern high latitudes (e.g.
113 Olafsson et al., 2009, 2010; Franco et al., 2021; Skjelvan et al., 2022) few studies in the SO attempted to
114 evaluate decadal changes of carbonate system properties and acidification in the water column based on time-
115 series stations. These changes in the SO water column were investigated from data collected during cruises
116 generally 3 to 15 years apart (Hauck et al., 2010; Van Heuven et al., 2011; Pardo et al., 2017; Tanhua et al.,
117 2017; Carter et al., 2019).

118



119

120 Table 1: Trends of oceanic $f\text{CO}_2$ ($\mu\text{atm.yr}^{-1}$) and pH (decade^{-1}) in the Southern Ocean south of the Polar Front
 121 based on observations and from this study. IO: Indian Ocean sector. PO: Pacific Ocean sector. AO: Atlantic
 122 Ocean sector. SO SPSS: Southern Ocean SubPolar Seasonally Stratified biome (around 50-60°S). PZ: Polar
 123 Zone. NR: Not Reported. Standard-deviations when available are in bracket.
 124

125	126	127	128	129	130	131	132	133	134	135	136	137	138	139	140	141	142	143	144	145	146	147	148	149	150	151	152	153	154	155
Period	Season	Zone	Trend $f\text{CO}_2$ $\mu\text{atm.yr}^{-1}$	Trend pH decade^{-1}	Reference																									
1991-2000	Summer	IO PZ 55-60°S	2.93	-0.035	Xue et al (2018)																									
2001-2011	Summer	IO PZ 55-60°S	1.41	-0.016	Xue et al (2018)																									
2005-2019	Summer	IO PZ 54-64°S	NR	-0.026(0.003)	Brandon et al (2022)																									
1998-2019	Summer	IO 50°S-68°E	1.9 (0.3)	-0.019 (0.004)	Leseurre et al (2022)																									
1998-2019	Summer	IO 55°S-63°E	2.1 (0.3)	-0.022 (0.003)	Leseurre et al (2022)																									
1998-2007	Summer	IO 55°S-63°E	5.3 (0.4)	-0.050 (0.016)	Leseurre et al (2022)																									
2006-2019	Summer	IO 55°S-63°E	0.3 (0.2)	no trend	Leseurre et al (2022)																									
1969-2003	Summer	PO 55-62°S	1.7 (0.2)	-0.020 (0.003)	Midorikawa (2012)																									
2002-2012	Annual	Drake North	2.21 (0.55)	-0.023 (0.007)	Takahashi (2014)																									
2002-2012	Annual	Drake South	1.50 (0.65)	-0.015 (0.008)	Takahashi (2014)																									
2002-2015	Summer	Drake North	1.95 (0.55)	-0.021 (0.006)	Munro et al (2015)																									
2002-2015	Winter	Drake North	1.92 (0.24)	-0.018 (0.003)	Munro et al (2015)																									
2002-2015	Summer	Drake South	1.30 (0.85)	-0.017 (0.010)	Munro et al (2015)																									
2002-2015	Winter	Drake South	0.67 (0.39)	-0.008 (0.004)	Munro et al (2015)																									
2002-2015	Annual	Drake North	1.74 (0.15)	-0.019 (0.002)	Munro et al (2015)																									
2002-2015	Annual	Drake South	1.16 (0.27)	-0.015 (0.003)	Munro et al (2015)																									
1981-2011	Annual	SO SPSS	1.44 (0.10)	-0.020 (0.002)	Lauvset et al (2015)																									
1991-2011	Annual	SO SPSS	1.46 (0.11)	-0.021 (0.002)	Lauvset et al (2015)																									
1993-2018	Annual	SO 44-75°S	NR	-0.0165 (0.0001)	Iida et al (2021)																									
1962-2016	November	IO 50°S-68°E	1.31 (0.20)	-0.014 (0.002)	This study, Obs.																									
1991-2021	Summer	IO 50°S-68°E	2.10 (0.22)	-0.022 (0.002)	This study, Obs.																									
1991-2001	Summer	IO 50°S-68°E	0.76 (0.90)	-0.009 (0.010)	This study, Obs.																									
2001-2010	Summer	IO 50°S-68°E	3.23 (1.07)	-0.035 (0.011)	This study, Obs.																									
2010-2020	Summer	IO 50°S-68°E	0.84 (0.77)	-0.008 (0.008)	This study, Obs.																									
1985-2020	Summer	IO 50°S-68°E	1.71 (0.08)	-0.018 (0.001)	This study, FFNN																									
1991-2020	Summer	IO 50°S-68°E	1.85 (0.11)	-0.020 (0.001)	This study, FFNN																									
1991-2001	Summer	IO 50°S-68°E	1.18 (0.26)	-0.013 (0.004)	This study, FFNN																									
2001-2010	Summer	IO 50°S-68°E	2.87 (0.25)	-0.030 (0.003)	This study, FFNN																									
2010-2020	Summer	IO 50°S-68°E	0.98 (0.40)	-0.010 (0.004)	This study, FFNN																									
1991-2001	Winter	IO 50°S-68°E	0.98 (0.09)	-0.010 (0.001)	This study, FFNN																									
2001-2010	Winter	IO 50°S-68°E	1.99 (0.10)	-0.021 (0.001)	This study, FFNN																									
2010-2020	Winter	IO 50°S-68°E	2.21 (0.17)	-0.022 (0.002)	This study, FFNN																									
1985-2020	Annual	IO 50°S-68°E	1.57 (0.03)	-0.0165(0.0004)	This study, FFNN																									

172

173

174

175

176

177

178

179

180

181

182

183

184

185

186

The present study complements in time, seasons, and in the water column, the surface $f\text{CO}_2$ and pH trends investigated by Leseurre et al., (2022) in different regions of the Southern Indian Ocean for the period 1998-2019 during austral summer. South of the PF around 50°S, Leseurre et al. (2022) showed that in summer the surface $f\text{CO}_2$ increase and pH decrease over 20 years were mainly driven by the increase in anthropogenic CO_2 sequestration about $+0.6 (\pm 0.2) \mu\text{mol.kg}^{-1}.\text{yr}^{-1}$ and by a small warming of $+0.03 (\pm 0.02) ^\circ\text{C.yr}^{-1}$. In addition Leseurre et al. (2022) showed that in the recent decade, 2007-2019, the $f\text{CO}_2$ trend was low $+0.3 (\pm 0.2) \mu\text{atm yr}^{-1}$ compared to $+5.3 (\pm 0.4) \mu\text{atm yr}^{-1}$ in 1998-2007, highlighting the sensitivity of the $f\text{CO}_2$ and pH trends to the



181 selected time period (especially during summer). In particular, they observed relatively stable pH values over
182 2010-2019 (i.e. no decrease in pH) with no clear explanation on the origin of the slow-down of the $f\text{CO}_2$ and pH
183 trends in surface waters south of the PF in recent years. To complement the analysis by Leseurre et al. (2022)
184 based on summer observations in 1998-2019 this study focusses on one location regularly visited south of the
185 Polar Front (around 50°S - 68°E south-west of Kerguelen Island, Figure 1). The analysis period is extended back
186 to 1985 and forward to 2021 to investigate the recent status of $f\text{CO}_2$ and pH. We also evaluate the trends for
187 different seasons using sparse spring/winter data. The combination of in situ observations and monthly estimates
188 from a neural network model over the period 1985-2020 (Chau et al., 2022) enables to assess potential changes
189 in seasonality of the surface ocean carbonates system (including $f\text{CO}_2$, C_T , pH, Ω) as suggested in recent decades
190 or in future scenarios (Gallego et al., 2018; Landschützer et al., 2018; Kwiatkowski and Orr, 2018; Kwiatkowski
191 et al., 2020; Lerner et al., 2021; Fassbender et al., 2022; Yun et al., 2022; Rodgers et al., 2023; Joos et al., 2023).
192 The variability in surface waters will be related to changes in C_{ant} concentrations observed in the water column
193 and will be complemented by an analysis of OA at depth between 1985 and 2021. Finally we will explore the
194 long-term variability of $f\text{CO}_2$ and pH since 1960s and potential future changes of the carbonate system at this
195 time series site.

196

197 **2 Data selection, methods and quality control**

198

199 **2.1 Study area and data selection**

200

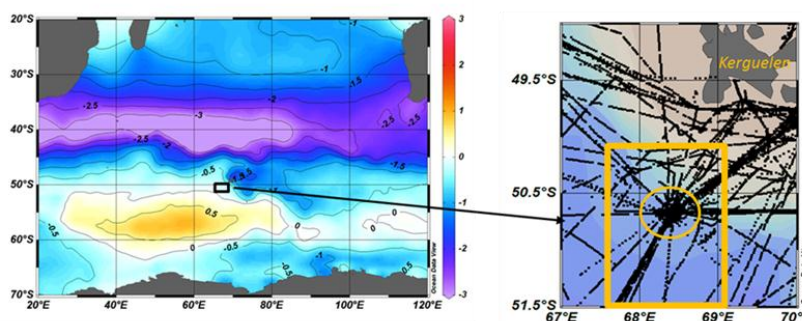
201 This study focused on a High Nutrients Low Chlorophyll area (HNLC, Minas and Minas, 1992) of the
202 Indian sector of the Southern ocean (SO) in the Permanent Open Ocean Zone (POOZ) south of the Polar Front
203 (PF) and south-west of Kerguelen Islands (around 50°S - 68°E , Figure 1). The Kerguelen Plateau is an extended
204 topographic feature that controls part of the Antarctic Circumpolar Current (ACC), generates eddies (Daniault
205 and Ménard, 1985) and the northward deflection of the PF near the Island (Pauthenet et al., 2018). The Plateau is
206 also a region of relatively high Chl-a (Moore and Abbott, 2000; Mongin et al., 2008) and strong CO_2 uptake
207 during austral spring-summer that contrasts with the weaker sink over the POOZ/HNLC (Metzl et al., 2006;
208 Jouandet et al., 2008, 2011; Lo Monaco et al., 2014; Leseurre et al., 2022). The POOZ/HNLC region west
209 (upstream) of the Kerguelen Plateau is characterized by rather stable water mass properties (temperature,
210 salinity, oxygen or nutrients) over time and low eddy activity compared to the Plateau (Daniault and Ménard,
211 1985; Chapman et al., 2015; Dove et al., 2022). In this region, located in the deep Enderby Basin, the flow is not
212 constrained by topography and there is no local upwelling that would import C_T -rich water to surface layers as
213 observed on the eastern side of the Kerguelen Plateau (Brady et al., 2021).

214 The Indian austral sector is also recognized to host the strongest winds in the SO leading to year-round
215 high gas transfer coefficients (Wanninkhof and Trinanes 2017). As a result, and in contrast to the Atlantic sectors
216 of the SO, the Indian region south of 45°S was a periodic CO_2 source, especially in the 1960s to the 1980s
217 (Rödenbeck et al., 2022; Bennington et al., 2022; Prend et al., 2022; Gray, 2024). In the POOZ-HNLC region,
218 high winter wind speed (monthly average up to $16 \text{ m}\cdot\text{s}^{-1}$) and associated heat loss drive deep mixing. Deep
219 winter mixing entrains subsurface properties to the surface layer, increases C_T concentrations leading to
220 wintertime outgassing of CO_2 (Metzl et al., 2006). This combination of characteristics makes the region an ideal
221 test-bed for 1-D modeling studies investigating the temporal dynamics and drivers of biogeochemical processes



222 including nutrients, iron, phytoplankton and carbon (Pondaven et al., 1998, 2000; Louanchi et al., 1999, 2001;
223 Jabaud-Jan et al., 2004; Metzl et al., 2006; Mongin et al., 2006, 2007; Kane et al., 2011; Pasquer et al., 2015;
224 Demuynek et al., 2020).

225
226
227
228
229
230
231
232
233
234
235
236
237



238 Figure 1: Left: Annual air-sea CO₂ flux (molC.m⁻².yr⁻¹) in the South Indian Ocean for year 2020 from the FFNN model
239 (negative flux for ocean sink, positive flux for ocean source). The black box identified the location of the study south-west of
240 Kerguelen. Right: Track of cruises with underway fCO₂ data South-West of Kerguelen Island. The station at 50°40'S-
241 68°25'E occupied in 1985, 1992-1993 and 1998-2021 is indicated by a yellow circle. The yellow square is the region selected
242 to calculate the mean values from the underway surface observations and from the FFNN model. Figures produced with
243 ODV (Schlitzer, 2018).
244

245 Here we used surface and water-column observations around location 50°40'S-68°25'E (Figure 1, Table
246 S1), historically called KERFIX station (KERguelen FIXed station) sampled in 1990-1995 in the framework of
247 the WOCE/JGOFS programs (Jeandel et al., 1998). The station was first occupied in March 1985 during the
248 INDIGO-1 cruise (Indian Ocean Geochemistry, Poisson, 1985; Poisson et al., 1988) and since 1998 it is
249 regularly visited during the OISO cruises (Océan Indien Service d'Observations, Metzl and Lo Monaco, 1998,
250 <https://doi.org/10.18142/228>). The regular occupation from 1985 to 2021 makes it the longest time-series station
251 in the Southern Ocean POOZ/HNLC area allowing investigating the inter-annual to decadal trends of carbonate
252 properties in surface waters and across the water-column (0-1600m). Despite the occasional variability in surface
253 waters properties (e.g. lower surface Salinity in 2011-2013) we consider all observations selected for this study
254 both in surface waters and the water-column to be representative of the water masses in this POOZ/HNLC region
255 upstream of the Kerguelen Plateau.

256 Data for 1985-2011 were extracted from the GLODAP data-product, version V2.2021 (Lauvset et al.,
257 2021 a, b; Table S1a). Observations collected during OISO cruises in 2012-2021 (Lo Monaco, 2020; Lo Monaco
258 et al., 2021) will be included in GLODAP-V3. For the surface water properties, all available underway fCO₂ data
259 were selected (Figure 1). This includes one cruise in November 1962 (Keeling and Waterman, 1968) and 41
260 cruises in 1991-2021 (Table S1b). All surface temperature, salinity and fCO₂ data were extracted from the
261 SOCAT data-product version v2022 (Surface Ocean CO₂ Atlas, Bakker et al., 2016, 2022).
262



263

264 2.2 Methods

265

266 The methods for surface underway $f\text{CO}_2$ and biogeochemical properties (Oxygen, A_T - C_T , nutrients) in
267 the water-column for the INDIGO-1, KERFIX and OISO cruises were described in previous studies (e.g.
268 Poisson et al., 1993; Louanchi et al., 2001; Metzl et al., 2006; Metzl, 2009; Mahieu et al., 2020; Leseurre et al.,
269 2022). Here we briefly recall the methods for underway $f\text{CO}_2$ and water-column observations.

270

271 2.2.1 Surface $f\text{CO}_2$ data

272

273 For $f\text{CO}_2$ measurements in 1991-2021, sea-surface water was continuously equilibrated with a "thin
274 film" type equilibrator thermostated with surface seawater (Poisson et al., 1993). The $x\text{CO}_2$ in the dried gas was
275 measured with a non-dispersive infrared analyser (NDIR, Siemens Ultramat 5F or 6F). Standard gases for
276 calibration (around 270, 350 and 490 ppm) were measured every 6 hours. To correct $x\text{CO}_2$ dry measurements to
277 $f\text{CO}_2$ *in situ* data, we used polynomials from Weiss and Price (1980) for vapour pressure and from Copin-
278 Montégut (1988, 1989) for temperature. Note that when incorporated in the SOCAT data-base, the original $f\text{CO}_2$
279 data are recomputed (Pfeil et al., 2013) using temperature correction from Takahashi et al. (1993). Given the
280 small difference between equilibrium temperature and sea surface temperature ($+0.56 \pm 0.30$ °C on average for
281 the cruises in 1998-2021), the $f\text{CO}_2$ data from SOCAT used in this analysis (Bakker et al., 2022) are almost
282 identical (within 1 μatm) to the original $f\text{CO}_2$ values from our cruises ([www.ncei.noaa.gov/access/ocean-carbon-
283 data-system/oceans/VOS_Program/OISO.html](http://www.ncei.noaa.gov/access/ocean-carbon-data-system/oceans/VOS_Program/OISO.html)).

284

285 2.2.2 Water column data

286

287 In 1990-1995, water samples were collected during the KERFIX program on the ship *La Curieuse* at
288 standard depths using 8 L Niskin bottles mounted on a stainless steel cable and equipped with reversing SIS
289 pressure and temperature probes. Methods and accuracy for the geochemical measurements used in this analysis
290 (A_T , C_T , oxygen, nutrients) are detailed by Jeandel et al. (1998) and by Louanchi et al. (2001). From 1998
291 onwards, the station was occupied within the framework of the OISO long-term monitoring program onboard the
292 *R.V. Marion-Dufresne*. We used Conductivity-Temperature-Depth (CTD) sensors mounted on a 24 bottles
293 rosette equipped with 12 L Niskin bottles. Temperature and salinity measurements have an accuracy of 0.002 °C
294 and 0.005 respectively (Mahieu et al., 2020). Samples for A_T and C_T were filled in 500 mL glass bottles and
295 poisoned with 100 μL of saturated mercuric chloride solution to halt biological activity. Discrete C_T and A_T
296 samples were analyzed onboard by potentiometric titration derived from the method developed by Edmond
297 (1970) using a closed cell. Based on replicate samples from the surface or depth, the repeatability for A_T and C_T
298 varies from 1 to 3.5 $\mu\text{mol.kg}^{-1}$ depending on the cruise. The accuracy of ± 3 $\mu\text{mol.kg}^{-1}$ was ensured by daily
299 analyses of Certified Reference Materials (CRMs) provided by Andrew Dickson's laboratory (Scripps Institute
300 of Oceanography).

301 Dissolved oxygen (O_2) concentration was determined by a sensor fixed on the rosette and values were
302 adjusted based on discrete measurements (Winkler method, Carpenter, 1965) using a potentiometric titration
303 system. Accuracy for O_2 is ± 2 $\mu\text{mol.kg}^{-1}$ (Mahieu et al., 2020). Although long-term deoxygenation in the



304 Southern ocean has been suggested (Ito et al., 2017; Schmidtko et al., 2017; Oschlies et al., 2018), no significant
305 trend in O_2 was identified over 1985-2021 at this station around $50^\circ S$ in both surface or in subsurface waters
306 (e.g. in the layer of the temperature minimum representing winter water for C_{am} calculations as described later).
307 However, in the station data a small O_2 decrease was detected around 800m in the O_2 minimum layer over 36
308 years ($-0.22 \pm 0.07 \mu\text{mol.kg}^{-1}.\text{yr}^{-1}$). As this has no impact on the interpretation for pH and Ω trends for this
309 analysis, the observed change of O_2 at depth will be not discussed further. Here the O_2 data are mainly used for
310 the calculation of anthropogenic CO_2 concentrations and the observed O_2 change at depth is too small to have an
311 impact on temporal variations of C_{am} concentrations.

312 Nitrate (NO_3) and silicate (DSi) were analyzed on board or at LOCEAN/Paris by colorimetry following
313 the methods described by Tréguer and Le Corre (1975) for 1998-2008 or from Coverly et al. (2009) for 2009-
314 2021. The uncertainty of NO_3 and DSi measurements is $\pm 0.1 \mu\text{mol.kg}^{-1}$. Based on replicate measurements for
315 deep samples, we estimate an error of about 0.3 % for both nutrients. Phosphate (PO_4) samples were analyzed in
316 samples from a few cruises following the method of Murphy and Riley (1962) revised by Strickland and Parsons
317 (1972) with uncertainty of $\pm 0.02 \mu\text{mol.kg}^{-1}$. When nutrient data are not available for a cruise, we used
318 climatological values based on seasonal nutrients cycles inferred from data from 1990 to 2021. This has a very
319 small impact on the carbonate system calculations and the trend analysis as we did not detect any significant
320 trends in nutrients in surface or at depth since 1985 (not shown) as opposed to what has been observed at higher
321 latitude of the SO (Iida et al., 2013; Hoppema et al., 2015). However, we will see that the inter-annual variability
322 of nutrients (especially DSi in the HNLC region) might inform on potential changes in biological processes.

323 For Chlorophyll-a (Chl-a), samples were taken in the top layers (0-150m). One to two liters of seawater
324 were filtered onto $0.7 \mu\text{m}$ glass microfiber filters (GF/F, Whatman) and filters were stored at $-80^\circ C$ onboard.
325 Back at the LOCEAN/Paris laboratory, samples were extracted in 90% acetone (Strickland and Parsons, 1972)
326 and fluorescence of Chl-a was measured on a Turner Type 450 fluorometer in 1998-2007 and since 2009 at 670
327 nm on a Hitachi F-4500 spectrofluorometer (Neveux and Lantoine, 1993).

328

329 **2.2.3 Data quality-control and data consistency**

330

331 When exploring the trends of ocean properties based on different cruises more than 35 years apart, it is
332 important to first verify the consistency of the data and if there is any bias or drift. The INDIGO data from 1985
333 (i.e. prior to CRM available for A_T and C_T) were first controlled prior to their incorporation into the original
334 GLODAP product (Sabine et al., 1999; Key et al., 2004) and corrections for A_T and C_T were revisited within the
335 framework of the CARINA project (CARbon IN the Atlantic, Lo Monaco et al., 2010). A secondary quality
336 control was performed on the data from the OISO cruises collected between 1998 and 2011 within the CARINA
337 and GLODAP-v2 initiatives (Lo Monaco et al., 2010; Olsen et al., 2016). Significant off-sets were identified for
338 A_T - C_T in samples from the KERFIX cruises (1990-1993) compared to INDIGO and OISO data and it was
339 proposed to correct the original values by $-35 \mu\text{mol.kg}^{-1}$ for C_T and $-49 \mu\text{mol.kg}^{-1}$ for A_T (Metzl et al., 2006).
340 These corrections were applied in GLODAP version v2.2019 (Olsen et al., 2019) and resulted in coherent A_T and
341 C_T concentrations for KERFIX in the deep layers compared to other cruises (Supp Mat., Table S2, Figure S1).
342 The same data quality control protocol as for GLODAP-v2 was applied to data from OISO cruises for the years
343 2012-2021 (Mahieu et al., 2020). Given the accuracy of the data no systematic bias (excepted in 2014) was
344 found for the properties measured in 2012-2021. The time-series of A_T and C_T at depth below 1450 m for all



345 cruises in 1985-2021 show some variability but no trend over 36 years as expected in the bottom waters in this
346 region (Supp. Mat, Figure S1). However, we identified a small bias for C_T in 2014 (cruise OISO-23) where C_T
347 concentrations in the deep water appeared slightly lower (2228-2234 $\mu\text{mol.kg}^{-1}$ in 2014 compared to the mean
348 value of $2240.7 (\pm 3.7) \mu\text{mol.kg}^{-1}$, Table S2, Figure S1). When compared to $f\text{CO}_2$ in surface waters, we also
349 suspect the C_T data in the mixed-layer in 2014 to be too low by about 10 $\mu\text{mol.kg}^{-1}$ (Figures S2, S3). Therefore
350 we applied a WOCE/GLODAP flag 3 for C_T data of this cruise and will not use the station data in 2014 for the
351 C_{ant} calculations and the trend analysis described in this study.

352

353 **2.2.4 CMEMS-LSCE-FFNN model**

354

355 As most of the cruises took place during austral summer and data are not available each year, we
356 completed the observations with the results from an ensemble of feed-forward neural network model (CMEMS-
357 LSCE-FFNN or FFNN for simplicity here, Chau et al., 2022). The FFNN model allows mapping at global scale
358 monthly surface $f\text{CO}_2$ given SOCAT gridded datasets and ancillary variables. The reconstructed $f\text{CO}_2$ is then
359 used to derive monthly surface pH fields as well as air-sea CO_2 fluxes. This data product enables to investigate
360 the trends for different seasons and to derive estimates of annual air-sea CO_2 fluxes to interpret the change in
361 CO_2 uptake, if any. For a full description of the model, access to the data and a statistical evaluation of $f\text{CO}_2$
362 reconstructions please refer to Chau et al. (2022). Within this study, we compared the FFNN $f\text{CO}_2$ with
363 observations from 35 cruises for the years between 1991 and 2020 (Table S3, Figure S2a). Excepted for a few
364 periods (January 1993 and January 2002), model-data differences are generally within $\pm 10 \mu\text{atm}$ with a mean
365 difference of $2.1 (\pm 7) \mu\text{atm}$ for the 35 co-located periods. Note that, as opposed to sea surface $f\text{CO}_2$, no temporal
366 trend was identified for the differences between the observed and reconstructed $f\text{CO}_2$ (Figure S2b), i.e. the trends
367 of sea surface $f\text{CO}_2$ derived from the observations and from the FFNN model should be the same. Aside from the
368 $f\text{CO}_2$ reconstructions, surface ocean alkalinity (A_T) fields are also provided by using the multivariate linear
369 regression model LIAR (Carter et al., 2016; 2018) based on sea surface temperature, salinity, and nutrient
370 concentration.

371

372 **2.2.5 Calculations of carbonate properties**

373

374 Based on the data available for each cruise ($f\text{CO}_2$, or A_T and C_T) or from the FFNN model ($f\text{CO}_2$ and
375 A_T), other carbonate system properties (pH, $[\text{H}^+]$, $[\text{CO}_3^{2-}]$ and Ω) were calculated using the CO2sys program
376 (version CO2sys_v2.5, Orr et al., 2018) developed by Lewis and Wallace (1998) and adapted by Pierrot et al.
377 (2006) with K1 and K2 dissociation constants from Lueker et al. (2000) as recommended (Dickson et al., 2007;
378 Orr et al., 2015; Wanninkhof et al., 2015). The total boron concentration was calculated according to Uppström
379 (1974) and KSO_4 from Dickson (1990). To calculate the properties with the underway surface $f\text{CO}_2$ dataset, we
380 used the A_T/S relationship based on A_T-C_T data from OISO cruises in 1998-2019 in the South Indian sector as
381 described by Leseurre et al. (2022):

382

$$383 A_T = 64.341 \times S + 106.764 \text{ (rmse} = 7.485 \mu\text{mol.kg}^{-1}, n = 4775) \text{ (Eq. 1)}$$

384



385 The use of other A_T/S relationships (e.g. Millero et al., 1998; Jabaud-Jan et al., 2004; Lee et al., 2006;
386 Carter et al., 2018) would change slightly the A_T concentrations but neither the A_T trend nor the interpretation of
387 the C_T , pH or Ω trends. However, as salinity is an important predictor in the calculation of A_T , C_T or pH from
388 fCO_2 data, we have assessed the original underway salinity data and found biases for few cruises in 1992, 1993
389 and 1995 (Table S1b). For these cruises or when salinity was not measured we used the salinity from the World
390 Ocean Atlas, WOA (Antonov et al., 2006) in the SOCAT data-sets (Pfeil et al., 2013, identified “WOA” in Table
391 S1b). Monthly fCO_2 and A_T data extracted from the CMEMS-LSCE-FFNN datasets at the station location
392 ($50.5^\circ S$ - $68.5^\circ E$) over 1985-2020 were used to calculate the carbonate properties in the same way as from
393 observations.

394

395 **2.2.6 Comparisons of different datasets and the FFNN model**

396

397 To validate the properties calculated using the fCO_2 data for 1991-2021 or from the FFNN model over
398 1985-2020 we compared the calculated values (A_T , C_T , pH, $[H^+]$, $[CO_3^{2-}]$, Ω) with those from A_T - C_T data
399 measured in the mixed-layer at stations occupied in 1985 and in 1993-2021. For this comparison, we averaged
400 the continuous underway fCO_2 data selected in a box around the station location ($50^\circ S$ - $51.5^\circ S/67.5$ - $69^\circ E$, yellow
401 box in Figure 1). Results of the comparisons between various datasets are detailed in the Supplementary Material
402 (Tables S3 and S4). During the period 1993-2021, there are 22 stations with co-located fCO_2 data for different
403 seasons (but mainly in summer). Since we found a close agreement between measured fCO_2 and the FFNN
404 model (Table S3, Figure S2), mismatches in all calculated carbonate system properties between the underway
405 fCO_2 dataset and the FFNN model are small, falling within the range of the errors associated with the
406 calculations (Orr et al., 2018). For example, for 35 co-located periods, the mean differences in calculated C_T of
407 $1.5 (\pm 5) \mu mol.kg^{-1}$ or pH of $-0.002 (\pm 0.008)$ are in the range of the theoretical error of about $5 \mu mol.kg^{-1}$ and
408 0.007 respectively when taking into account measurements errors on salinity, temperature, nutrients, fCO_2 and
409 A_T (Orr et al., 2018). On the other hand, compared to the station data in the mixed-layer (Table S4), bias for
410 calculated A_T using Equation 1 is slightly higher by about $5 \mu mol.kg^{-1}$. This explains the relatively high
411 differences for C_T (mean difference around $8 \mu mol.kg^{-1}$) and for pH (mean difference around 0.008) calculated
412 with fCO_2 and the A_T/S relationship. The differences of calculated values with observations in 1991-2021 are, on
413 average, in the range of uncertainties of the carbonate system calculations using A_T - C_T pairs (error for fCO_2
414 around $13 \mu atm$ and for pH around 0.0144). Importantly, there is no temporal trend for the differences between
415 calculated and observed properties (Figure S3b). We are thus confident using the selected fCO_2 data for the trend
416 analysis presented in this study. The independent comparison with A_T - C_T data at stations also indicates that the
417 FFNN model results for A_T , C_T , are close to the observations (Table S4, Table S5, Figure S4) as well as for
418 calculated pH, $[H^+]$, $[CO_3^{2-}]$, Ω_{Ca} and Ω_{Ar} . This somehow validates the use of the FFNN data for the trend
419 analysis over the period 1985-2020 and for different seasons, although the FFNN model was not constrained by
420 in-situ fCO_2 before 1991 or Chl-a satellite data before 1998. Interestingly, in 1985 the atmospheric fCO_2 was
421 around 335 - $339 \mu atm$ (Dlugokencky and Tans, 2022) and the oceanic fCO_2 from the FFNN model was higher
422 than in the atmosphere from March to October (Figure S4) resulting in an annual CO_2 source of $+0.8 mol.m^{-2}.yr^{-1}$
423 in 1985.

424



425 3 Results and discussion

426

427 3.1 Variability and trend of sea surface fCO₂ and air-sea CO₂ fluxes: 1985-2021

428

429 The fCO₂ observations around 50°S-68°E and their mean values for each cruise are shown in Figure 2a.
430 The fCO₂ data in 1991-2021 were available for different seasons but the sampling locations were mainly
431 reoccupied in austral summer (January-February). During austral summer, the ocean fCO₂ was generally lower
432 than in the atmosphere (i.e. the ocean was a CO₂ sink) whereas in March to October it was near equilibrium. The
433 same distribution is obtained from the FFNN model for 1991-2020 (Figure 2a). The model also indicates that in
434 1985-1998 the fCO₂ during austral winter (May-September) was always higher than the atmospheric fCO₂
435 leading to a CO₂ source during this period (Figure 3). The model estimates a decrease of the annual CO₂ source
436 in 1985-2001 followed by an increase of the source in 2001-2010 and an increase of the sink in 2010-2020.

437

438

439

440

441

442

443

444

445

446

447

448

449

450

451

452

453

454

455

456

457

458

459

460

461

462

463

464

465

466

467

468

469

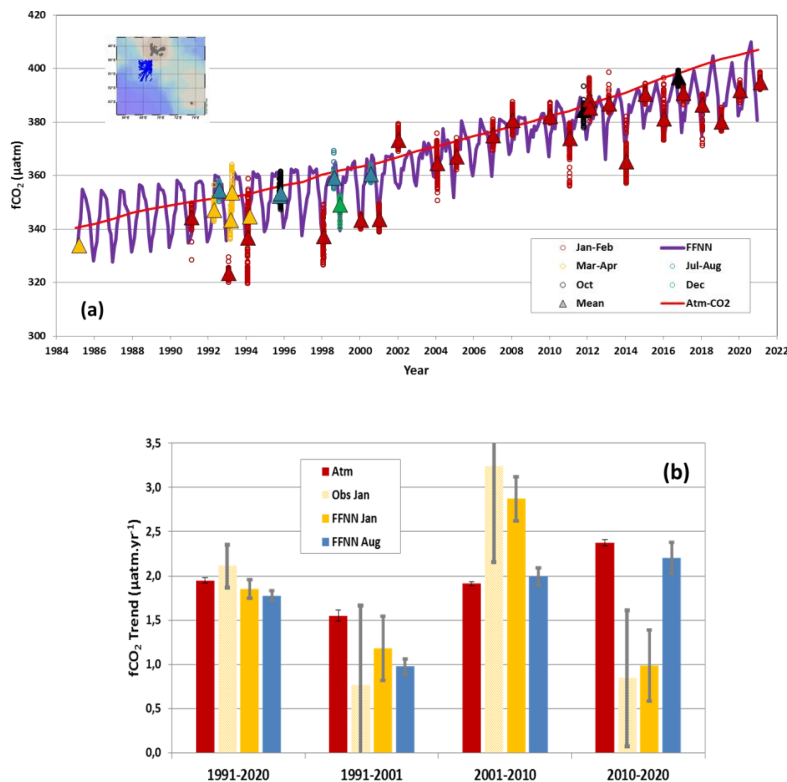


Figure 2: (a): Time-series of sea surface fCO₂ observations (µatm) South-West of Kerguelen Island in 1985-2021 (insert map shows the location of observations selected around station at 50°40'S-68°25'E). The color dots correspond to 5 seasons (January-February, March-April, July-August, October and December) and triangles the average for each period. The monthly sea surface fCO₂ from the FFNN model is presented for the period 1985-2020 (purple line) and the atmospheric fCO₂ represented by red line. In March 1985 there were no underway fCO₂ observations and the triangle corresponds to fCO₂ calculated with A_T-C_T data in the mixed-layer. (b): Trends of atmospheric and oceanic fCO₂ (µatm.yr⁻¹) for different season and periods based on observations (January) and the FFNN model (January or August).



470
471
472
473
474
475
476
477
478
479
480
481
482
483
484
485
486
487
488
489
490
491
492
493
494
495
496
497
498
499
500
501
502
503
504
505
506
507
508
509
510
511
512
513
514
515

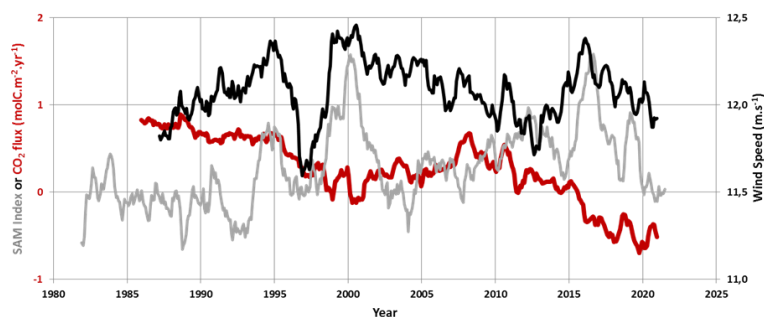


Figure 3: Time series of the SAM index (in grey) in the Southern Ocean, wind-speed (in black, m.s^{-1}) and air-sea CO_2 flux ($\text{molC.m}^{-2}.\text{yr}^{-1}$) from the FFNN model (in red) at location $50.5^\circ\text{S}-68.5^\circ\text{E}$. Positive (negative) flux represents CO_2 source (sink). Wind-speed and SAM are presented for respectively 12-months and 24-months running mean based on monthly values. Note the positive SAM in 1998-2003 and 2010-2020. SAM data from Marshall (2003), <http://www.nerc-bas.ac.uk/jcd/gjma/sam.html>, last access 14/8/2021. Wind speed data from ERA5 (Hersbach et al., 2020).

For the last cruise in February 2021, the average $f\text{CO}_2$ was $394.9 (\pm 1.5) \mu\text{atm}$ (Figure 2a), about 10 μatm lower than in the atmosphere (a small CO_2 sink). This is $+50.5 \mu\text{atm}$ higher than $f\text{CO}_2$ observed during the first cruise in February 1991 ($f\text{CO}_2 = 344.4 \pm 5.2 \mu\text{atm}$). During the same period, the atmospheric CO_2 increased from 354 ppm in 1991 to 411 ppm in 2021 in this region (recorded at Crozet Island, Dlugokencky and Tans, 2022). This first comparison of two cruises 30 years apart indicates that the ocean $f\text{CO}_2$ increased at a rate ($+1.7 \mu\text{atm.yr}^{-1}$) close to that of the atmosphere ($+1.9 \mu\text{atm.yr}^{-1}$). During the same period, we observed some variations in A_T (average $A_T = 2276.5 \pm 4.5 \mu\text{mol.kg}^{-1}$) and a clear increase in C_T (Figure 4a and S5).

The C_T concentration in the mixed-layer in summer 2021 was $2134.0 (\pm 1.8) \mu\text{mol.kg}^{-1}$, much higher than in summer 1993 ($C_T = 2115.8 \pm 2.6 \mu\text{mol.kg}^{-1}$). The difference over 28 years of $+22.1 \mu\text{mol.kg}^{-1}$ corresponds to an annual C_T increase of $+0.8 \mu\text{mol.kg}^{-1}.\text{yr}^{-1}$. At constant temperature and A_T , this would translate in an increase of oceanic $f\text{CO}_2$ of $+1.9 \mu\text{atm.yr}^{-1}$, i.e. equal to the atmospheric rate. The same comparison for October shows that $f\text{CO}_2$ in 2016 was $+43.8 \mu\text{atm}$ higher compared to 1995 (Figure 2a), i.e. a rate of $+2.1 \mu\text{atm.yr}^{-1}$. The C_T concentrations in October 2016 were also much higher than in 1993 (Figure 4a and S5). Over 23 years the observed C_T increase in October ($+22.6 \mu\text{mol.kg}^{-1}$) corresponds to a rate of $+0.98 \mu\text{mol.kg}^{-1}.\text{yr}^{-1}$ that is faster than the rate of $+0.8 \mu\text{mol.kg}^{-1}.\text{yr}^{-1}$ derived from summer data in 2021 and 1993. At constant A_T this would translate in an increase of oceanic $f\text{CO}_2$ of $+2.5 \mu\text{atm.yr}^{-1}$ in October, higher than the trend of $+2.1 \mu\text{atm.yr}^{-1}$ computed from $f\text{CO}_2$ data. Part of the difference may be explained by A_T that was slightly higher ($+6 \mu\text{mol.kg}^{-1}$) in October 2016 compared to 1993 (Figure S5).

Given the temporal variability of observed C_T in summer and the evolution of the annual air-sea CO_2 flux (Figure 3), decadal $f\text{CO}_2$ and pH trends as well as associated drivers need to be analyzed for different seasons and periods. This approach allows exploring links with the variability of primary production and/or the Southern Annual Mode (SAM). Shifts from a positive to a negative SAM index (Figure 3) will strengthen upwelling and impact ocean properties throughout the water column including C_T , nutrients, primary production or pH (e.g. Lovenduski and Gruber, 2005; Lenton et al., 2009; Hauck et al., 2013; Hoppema et al., 2015; Pardo et al., 2017).



516

517

518

519

520

521

522

523

524

525

526

527

528

529

530

531

532

533

534

535

536

537

538

539

540

541

542

543

544

545

546

547

548

549

550

551

552

553

554

555

556

557

558

559

560

561

562

563

564

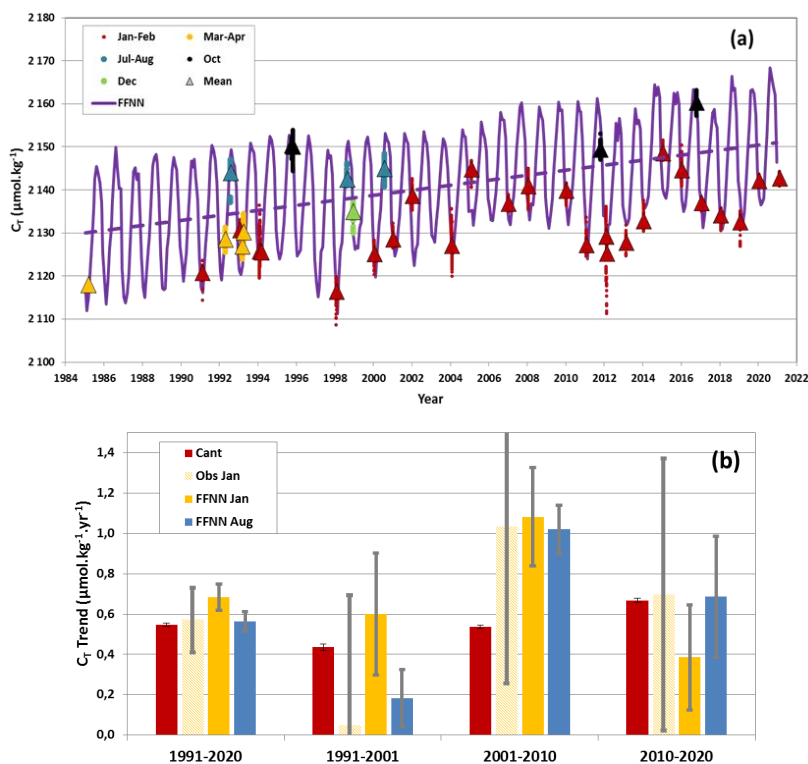


Figure 4: (a): Time-series of surface C_T ($\mu\text{mol.kg}^{-1}$) around station at $50^{\circ}40'S$ - $68^{\circ}25'E$ calculated from $f\text{CO}_2$ data (Figure 2) using the A_T/S relation (see text). The color dots correspond to 5 seasons (January-February, March-April, July-August, October and December) and triangles the average for each cruise. The monthly sea surface C_T from the FFNN model is presented for the period 1985-2020 (purple line). The annual C_T trend of $+0.58 \pm 0.05 \mu\text{mol.kg}^{-1}.\text{yr}^{-1}$ (dashed line) is derived from the FFNN monthly data. In March 1985 the triangle corresponds to the observed C_T in the mixed-layer. (b): Trends of sea surface C_T ($\mu\text{mol.kg}^{-1}.\text{yr}^{-1}$) for different season and periods based on observations (for January) and the FFNN model (for January or August). The trend for C_{ant} ($\mu\text{mol.kg}^{-1}.\text{yr}^{-1}$) is also shown (red bars) based on estimates in the winter water.

Summer data are characterized by a strong inter-annual variability between 1991-2021 (Figures 2a and 4a) with the ocean being a CO_2 source in January 2002, but a strong sink in January 1993, 1998, 2014, 2016 and 2019. In January 1998, when the surface ocean experienced a warm anomaly (Jabaud-Jan et al., 2004), the low $f\text{CO}_2$ of $337 \mu\text{atm}$ and the low C_T of $2110 \mu\text{mol.kg}^{-1}$ (Figure 4a and S5) co-occurred with intense primary production, probably supported by diatoms as suggested by very low DSi concentrations ($< 2 \mu\text{mol.kg}^{-1}$ down to 100m, Figure S6). In January 2014 and 2016, mixed-layer DSi concentrations were also remarkably small ($< 5 \mu\text{mol.kg}^{-1}$ down to 75m, Figure S6). In 2014 low DSi coincided with Chl-a levels that started to increase in mid-November 2013 and stayed at high level until February 2014 (Surface $\text{Chl-a} > 0.3 \text{ mg.m}^{-3}$, Figures 5 and S7). The intense primary production contributed to the low $f\text{CO}_2$ of $365 \mu\text{atm}$ reached by mid-January 2014, a value as low as in 2004 (Figure 2a). To the contrary, in 2002 relatively low Chl-a (mean $\text{Chl-a} < 0.2 \text{ mg.m}^{-3}$, Figure 5) was associated with higher levels of $f\text{CO}_2$ ($373 \mu\text{atm}$), C_T ($2128 \mu\text{mol.kg}^{-1}$, Figure 4a, Figure S5a) and DSi (Figure S6). This was also associated with higher salinity indicative of entrainment that might be related to storm



565 events that would occurred few days before the measurements leading to brief positive $f\text{CO}_2$ anomaly as recently
566 observed from Glider data in the subpolar South Atlantic (Nicholson et al., 2022). As opposed to the other
567 periods the ocean was a source of CO_2 in summer 2002 (this particular year was not well reconstructed by the
568 FFNN model, Figure 2a and Figure S2b). The important inter-annual variability observed in summer indicates
569 that in this region historically referred to as HNLC (Minas and Minas, 1992), primary production could
570 significantly impact $f\text{CO}_2$ level in summer (Jabaud-Jan et al., 2004; Pasquer et al., 2015; Gregor et al., 2018), a
571 result that needs to be taken into account when evaluating drivers of inter-annual variability (Rustogi et al.,
572 2023) and the decadal trends of $f\text{CO}_2$ or pH.

573 The Chl-a time-series derived from MODIS suggests higher concentrations in recent years with Chl-a
574 peaks identified in 2014, 2016, 2018, 2019 and 2021 (Figure 5 and S7) when the oceanic $f\text{CO}_2$ in summer was
575 well below the atmospheric level (Figure 2a).

576

577

578

579

580

581

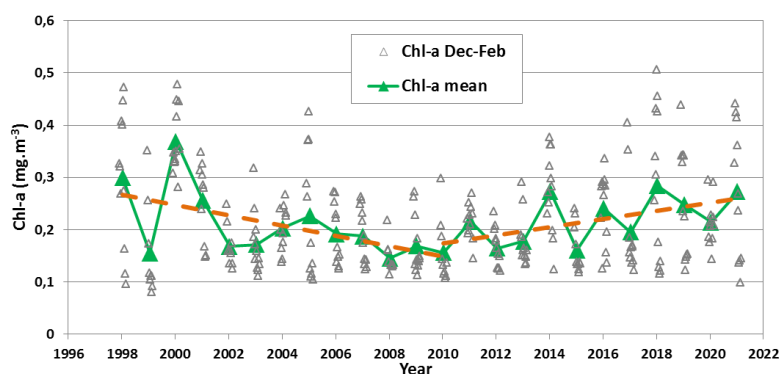
582

583

584

585

586



587 Figure 5: Time-series (1998-2021) of sea surface Chl-a ($\text{mg}\cdot\text{m}^{-3}$) in summer (December-February) from weekly satellite data
588 (SeaWiFS and MODIS, triangles) and associated mean (green triangles). The trends in 1998-2010 and 2010-2021 of
589 respectively $-0.0099 (\pm 0.0041)$ and $+0.0078 (\pm 0.0032) \text{ mg}\cdot\text{m}^{-3}\cdot\text{yr}^{-1}$ (dashed orange) indicate a decrease or increase of the
590 primary production that drives part of the $f\text{CO}_2$ and C_T stability observed in the recent period (Figure 2, Figure 4). The full
591 Chl-a record is shown in Supp. Mat. Figure S7.
592

593 The primary production lowers C_T concentrations and $f\text{CO}_2$, i.e. opposite to the C_T increase from
594 anthropogenic CO_2 uptake. These counteracting processes might explain the relatively stable $f\text{CO}_2$ previously
595 observed in the Indian POOZ in summer 2007-2019 with an annual $f\text{CO}_2$ rate of increase of only $+0.3 (\pm 0.2)$
596 $\mu\text{atm}\cdot\text{yr}^{-1}$ (Leseurre et al., 2022). This low rate is confirmed here with the new data obtained in 2020-2021
597 (Figure 2b and Figure S8). For the period 2010-2021, the oceanic $f\text{CO}_2$ trend in summer derived from
598 observations and the FFNN model is lower than $+1 \mu\text{atm}\cdot\text{yr}^{-1}$ (Table 1), i.e. much lower than the atmospheric
599 $f\text{CO}_2$ rate of $+2.4 \mu\text{atm}\cdot\text{yr}^{-1}$ and the oceanic $f\text{CO}_2$ trend of $+2.21 (\pm 0.17) \mu\text{atm}\cdot\text{yr}^{-1}$ in winter (Figure 2b). This
600 rate is also lower compared to the change observed in October ($+2.9 \mu\text{atm}\cdot\text{yr}^{-1}$) albeit being only based on 2
601 cruises in 2011 and 2016 (Figure 2a). As the low $f\text{CO}_2$ trend in recent years is detected for summer only this is
602 likely linked to an increase in primary production, as suggested by Chl-a records (Figure 5). In 1998-2010 the
603 summer Chl-a concentrations decreased at a rate of $-0.099 (\pm 0.041) \text{ mg}\cdot\text{m}^{-3}\cdot\text{decade}^{-1}$ whereas in 2010-2021 Chl-
604 a increased by $+0.078 (\pm 0.032) \text{ mg}\cdot\text{m}^{-3}\cdot\text{decade}^{-1}$ (Figure 5). These trends are coherent with previous studies, e.g.
605 the reduced net primary productivity reported in the Indian Antarctic zone in 1997-2007 (e.g. Arrigo et al., 2008;
606 Takao et al., 2012) and the shift of the Chl-a trend at large scale in the HNLC region of the Southern Ocean in
607 2010 (Basterretxea et al., 2023). As a consequence, after 2010 the difference between oceanic and atmospheric



608 $f\text{CO}_2$, $\Delta f\text{CO}_2$ (where $\Delta f\text{CO}_2 = f\text{CO}_2^{\text{occ}} - f\text{CO}_2^{\text{atm}}$) decreased in summer ($-1.4 \mu\text{atm.yr}^{-1}$) and the annual CO_2 flux
609 progressively varied from a source of $+0.45 \text{ molC.m}^{-2}.\text{yr}^{-1}$ in 2010 to a sink of $-0.63 \text{ molC.m}^{-2}.\text{yr}^{-1}$ in 2020
610 (Figure 3). In addition, because the wind speed was stable during this period ($12.0 \pm 0.9 \text{ m.s}^{-1}$ on average in
611 2010-2020, Figure 3), the variation of the air-sea CO_2 flux was mainly controlled by $\Delta f\text{CO}_2$ (e.g. Gu et al., 2023)
612 and the decadal variation of primary production imprinted a significant change on the $f\text{CO}_2$ trend and air-sea
613 CO_2 flux in this HNLC region. In the region investigated here, increasing Chl-a levels co-occurred with shifts of
614 the SAM index to a positive state (Figure 3), a link previously suggested south of the Polar Front in the SO but
615 for a short period 1997-2004 (Lovenduski and Gruber, 2005).

616 Another process to take into account for interpreting $f\text{CO}_2$ trends is the change in temperature in surface
617 waters. Previous analysis suggested a progressive warming in the region investigated here (Auger et al., 2021 for
618 summer 1993-2017). For 1998-2019 Leseurre et al. (2022) estimated a warming of Indian POOZ surface waters
619 of $+0.03 (\pm 0.02) \text{ }^\circ\text{C.yr}^{-1}$. Extending the time-series for the period 1991-2021 (Figure S9a) we note that the
620 surface temperature presents sub-decadal variability and that the ocean cooled after 2018 with a trend of -0.474
621 $(\pm 0.164) \text{ }^\circ\text{C.yr}^{-1}$ in 2018-2021 based on the monthly sea surface temperature (SST, Figure S9b). The trend
622 derived from our in-situ observations in summer 2018-2021 was $-0.253 (\pm 0.092) \text{ }^\circ\text{C.yr}^{-1}$.

623 In 2019, the lower temperature and relatively high Chl-a lead to low $f\text{CO}_2$ ($380 \mu\text{atm}$, Figure 2a) and
624 low C_T ($2128 \mu\text{mol.kg}^{-1}$) compared to 2018 ($f\text{CO}_2 = 386 \mu\text{atm}$; $C_T = 2137 \mu\text{mol.kg}^{-1}$, Figure 4a). The decrease in
625 observed $f\text{CO}_2$ from summer 2018 to 2019, also reconstructed by the FFNN model (Figure 2a), is contrary to the
626 expected $f\text{CO}_2$ and C_T increase due to anthropogenic uptake. In 2020, although the temperature was also lower,
627 the oceanic $f\text{CO}_2$ was higher ($392 \mu\text{atm}$) probably due to lower primary production as suggested by higher DSi
628 (Figure S6), as well as from C_T ($2135 \mu\text{mol.kg}^{-1}$, Figure 4a) and Chl-a records (Figure 5). In January 2021 the
629 temperature was close to that in January 2020, and both $f\text{CO}_2$ and C_T were slightly higher ($395 \mu\text{atm}$, 2139
630 $\mu\text{mol.kg}^{-1}$). A_T concentrations were stable between 2018 and 2021 ($2278.9 \pm 1.8 \mu\text{mol.kg}^{-1}$, Figure S5) indicating
631 no effect of A_T on the observed $f\text{CO}_2$ change in this region as opposed to the areas north of the Polar Front in the
632 Indian Ocean where A_T variations are often linked to coccolithophores blooms (Balch et al., 2016; Smith et al.,
633 2017).

634 The inter-annual variability observed in 1991-2021 highlights the competitive processes that drive C_T ,
635 $f\text{CO}_2$ or pH temporal variations. In summer 2018-2019, cooling and increased primary production both lead to
636 low $f\text{CO}_2$ counteracting the effect of anthropogenic CO_2 uptake. Given the changes of Chl-a, SST and air-sea
637 CO_2 flux, trends will be evaluated for three periods, 1991-2001, 2001-2010 and 2010-2020. In order to separate
638 natural and anthropogenic contributions, the anthropogenic CO_2 signal is estimated in the following section.

639

640 **3.2 Anthropogenic CO_2**

641

642 **3.2.1 Anthropogenic CO_2 in the water column**

643

644 To calculate anthropogenic CO_2 concentrations (C_{ant}), we used the TrOCA method developed by
645 Touratier et al. (2007) and previously applied in the southern Indian Ocean (Mahieu et al., 2020; Leseurre et al.,
646 2022). Such an indirect method is not suitable for evaluating C_{ant} concentrations in surface waters due to
647 biological activity and gas exchange and we restrict the C_{ant} calculations below the productive layer around



648 150m. In the region south of the Polar Front, a well-defined subsurface temperature minimum is observed each
649 year characterizing the winter water (WW) (Figure 6a).

650

651

652

653

654

655

656

657

658

659

660

661

662

663

664

665

666

667

668 Figure 6: Hovmoller section (Depth-Time) of potential temperature ($^{\circ}\text{C}$) and anthropogenic CO_2 (C_{ant} , $\mu\text{mol.kg}^{-1}$) in 1985-
669 2021 at station OISO-KERFIX ($50^{\circ}40'\text{S}$ - $68^{\circ}25'\text{E}$). The section for temperature is presented in the layer 0-500m and for
670 summer to highlight the temperature minimum around 200m (winter water, WW). The section for C_{ant} is limited below 200m.
671 Section produced with ODV (Schlitzer, 2018).
672

673

674

675

676

677

678

679

680

681

682

683

684

685 3.2.2 Anthropogenic CO_2 trend in the subsurface

686

687

688

689

To separate the natural and anthropogenic signals in surface waters for the driver analysis we assume that C_{ant} in the WW is representative of C_{ant} in the mixed-layer (ML). This is confirmed with few stations occupied during winter showing that C_{ant} concentrations in the WW in summer are almost equal to C_{ant} in the



690 ML during the preceding winter (Figure S11). The variation of C_{ant} in the WW for 1985-2021 is presented in
 691 Figure 7a for all seasons. In 1985 the C_{ant} concentration in the WW was $47.1 \mu\text{mol.kg}^{-1}$ and C_{ant} reached a
 692 maximum of $71.7 \mu\text{mol.kg}^{-1}$ in 2021. The data selected at 200m present some inter-annual variability like the
 693 relatively low C_{ant} in 1998, 2005 or 2020 probably related to natural variability. In 1998 and in 2020 the O_2
 694 concentrations were slightly lower in the WW ($< 300 \mu\text{mol.kg}^{-1}$) explaining the lower C_{ant} concentration (44.8
 695 $\mu\text{mol.kg}^{-1}$ in 1998 and $53.8 \mu\text{mol.kg}^{-1}$ in 2020). In 2005 anomalies of C_T , O_2 and temperature concur to explain
 696 the lower C_{ant} ($43.9 \mu\text{mol.kg}^{-1}$).

697

698

699

700

701

702

703

704

705

706

707

708

709

710

711

712

713

714

715

716

717

718

719

720

721

722

723

724

725

726

727

728

729

730

731

732

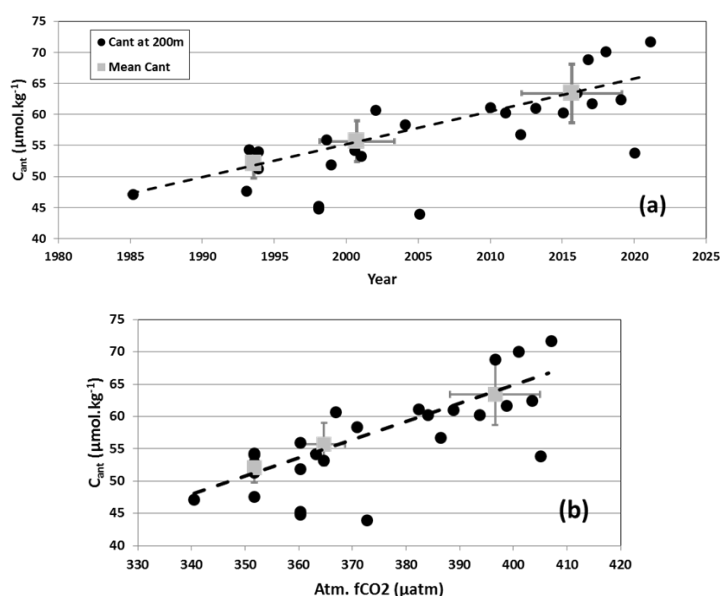


Figure 7: (a): Time-series of anthropogenic CO_2 (C_{ant} $\mu\text{mol.kg}^{-1}$) estimated in the winter water layer (WW around 200m, see figure 6) in 1985-2021 at station OISO-KERFIX ($50^{\circ}40'S$ - $68^{\circ}25'E$). Black dots are the individual data in the WW and the grey squares the average for the 1990s, 2000s and 2010s (anomalies in 1998, 2005 and 2020 filtered). The C_{ant} trend of $+0.53 (\pm 0.01) \mu\text{mol.kg}^{-1}.\text{yr}^{-1}$ is represented (dashed line). (b): same data for C_{ant} versus atmospheric $f\text{CO}_2$ (the slope is $+0.263 \pm 0.042 \mu\text{mol.kg}^{-1}.\mu\text{atm}^{-1}$).

From 1985 to 2021, we estimate a C_{ant} trend in WW of $+0.49 (\pm 0.09) \mu\text{mol.kg}^{-1}.\text{yr}^{-1}$. When the C_{ant} anomalies in 1998, 2005 and 2020 are discarded, this C_{ant} trend is $+0.53 (\pm 0.01) \mu\text{mol.kg}^{-1}.\text{yr}^{-1}$ (Figure 7a). As expected, the C_{ant} concentrations in the ocean are positively related to atmospheric CO_2 (slope $+0.263 \pm 0.042 \mu\text{mol.kg}^{-1}.\mu\text{atm}^{-1}$, Figure 7b). Interestingly the slope observed south of the PF in the Indian Ocean is close to that observed in the Antarctic Intermediate waters (AAIW) in the South Atlantic ($+0.23 \pm 0.05 \mu\text{mol.kg}^{-1}.\mu\text{atm}^{-1}$, Fontela et al., 2021). At large scale, Gruber et al. (2019 a, b) evaluated C_{ant} changes between 1994 and 2007 in the global ocean. In the South Indian sector, they estimated a mean C_{ant} accumulation in the surface of $+6.0 (\pm 1.1) \mu\text{mol.kg}^{-1}$ in the band 50 - 55°S south of the PF. At our station location (50 - $52^{\circ}\text{S}/68^{\circ}\text{E}$) in the layer 0 - 250m , the C_{ant} accumulated from 1994 to 2007 was $+5.67 (\pm 1.47) \mu\text{mol.kg}^{-1}$. In 13 years, this corresponds to a trend of $+0.44 (\pm 0.11) \mu\text{mol.kg}^{-1}.\text{yr}^{-1}$. Gruber et al. (2019 a, b) did not use the data presented here allowing for an independent comparison to the present study. Estimates of C_{ant} accumulation by Gruber et al. (2019 a, b) are in agreement with ours for 1991-2008 ($+0.46 \mu\text{mol.kg}^{-1}.\text{yr}^{-1}$) but lower than reported here between 2008 and 2021 ($+0.61 \mu\text{mol.kg}^{-1}.\text{yr}^{-1}$).



733

734 3.2.3 Anthropogenic and surface C_T seasonal trends

735

736 The C_{ant} trend in WW over 1985-2021 ($+0.53 \pm 0.01 \mu\text{mol.kg}^{-1}.\text{yr}^{-1}$) is slightly lower than the annual C_T
737 trend in surface derived from the FFNN model for 1985-2020 (C_T trend = $+0.58 \pm 0.05 \mu\text{mol.kg}^{-1}.\text{yr}^{-1}$ Figure 4a)
738 suggesting that anthropogenic CO_2 uptake explains 86% of the C_T increase in surface. In 1991-2020 the surface
739 C_T trend appears slightly higher in January ($+0.68 \pm 0.07 \mu\text{mol.kg}^{-1}.\text{yr}^{-1}$) than in August ($+0.56 \pm 0.04 \mu\text{mol.kg}^{-1}.\text{yr}^{-1}$,
740 Figure 4b). This suggests that in addition to the increase of C_T due to anthropogenic CO_2 other processes
741 count such as the variability of the biological activity, vertical mixing or upwelling. Indeed, as for $f\text{CO}_2$ (Figures
742 2b), the C_T growth rate also depends on seasons and decades (Figure 4b). In 1991-2001 the C_T trend from the
743 observations ($+0.05 \pm 0.64 \mu\text{mol.kg}^{-1}.\text{yr}^{-1}$) is highly uncertain due to few data and the large variability (Figures
744 4a, b). The FFNN model showed that the C_T trend in summer was faster than in winter and the winter C_T trend
745 lower than the C_{ant} trend in subsurface (Figure 4b). This is because during that decade, the higher primary
746 production in 1998 created a negative C_T anomaly (Figure 4a) not compensated by the accumulation of C_{ant} .

747 In 2001-2010 the C_T trends were much faster than in 1991-2001 and they were the same for both
748 seasons (around $1 \mu\text{mol.kg}^{-1}.\text{yr}^{-1}$, Figure 4b). For this decade the summer C_T trends from the observations and the
749 FFNN model are coherent. They were also twice the C_{ant} rate in WW that could be explained by enhanced
750 upwelling of C_T -rich deep waters during this period after the SAM reached a high positive index (Figure 3;
751 Lenton and Matear, 2007; Le Quéré et al., 2007; Hauck et al., 2013). However, in 2001-2010 we did not detect
752 any clear change at depth for ocean properties (except for C_T and C_{ant}) that would support this assumption
753 (enhanced upwelling). The rapid C_T (and $f\text{CO}_2$) trend for this decade is probably due to processes at the surface
754 rather than changes in the water column (vertical mixing or upwelling). In 2010-2020 C_T trends are lower than in
755 2001-2010 (Figure 4b). For summer, this is identified from both observations and the FFNN model. In winter the
756 C_T trend is close to C_{ant} indicative of the anthropogenic accumulation. The low C_T trend at the surface in
757 summer, about half the C_{ant} trend for the FFNN model, is likely due to the increase of primary production after
758 2010 as described above (Figure 5). It appears thus that the impact of biological activity and its variability in
759 summer could counteract that of anthropogenic CO_2 and explain the temporal change of the carbonate system in
760 surface.

761 Given the differences of the $f\text{CO}_2$ and C_T trends in summer and winter (Figures 2b and 4b) we explored
762 the temporal variations of the seasonality. For each year we estimated the differences between August and
763 January (Figure 8a). The seasonal amplitude for C_T was on average $26.1 (\pm 3.4) \mu\text{mol.kg}^{-1}$ and for $f\text{CO}_2$ $15.1 (\pm$
764 $5.6)$. Interestingly, the $f\text{CO}_2$ seasonal amplitude reached a minimum around 2008-2010 and increased over 2010-
765 2020. This signal appears correlated with surface Chl-a in summer (Figure 8b). The inter-annual variability of
766 the seasonality is clearly identified when comparing C_T with C_T calculated due only to C_{ant} accumulation after
767 2010 (Figure S12c). This supports the conclusion that in addition to the C_{ant} accumulation, the variations of
768 phytoplanktonic biomass imprinted inter-annual variability on C_T and $f\text{CO}_2$ in summer. This holds for the
769 seasonal amplitude as the results for winter follows the C_{ant} trend (Figure 4b, Figure S12a). The same is true for
770 pH for which reduced seasonal amplitude was found when the production was low (not shown). However, over
771 36 years (1985-2020) we did not identify a long-term trend of the seasonal amplitude for C_T or for $f\text{CO}_2$ as
772 suggested by other studies (Landschützer et al., 2018; Rodgers et al., 2023; Shadwick et al 2023). Our results
773 highlight a variability over 5-10 years (Figure 8a) and suggest a potential change in seasonality and annual CO_2



774 sink if primary production changes in the future (e.g. Bopp et al., 2013; Leung et al., 2015; Fu et al., 2016;
775 Kwiatkowski et al., 2020; Krumhardt et al., 2022; Seifert et al., 2023).

776

777

778

779

780

781

782

783

784

785

786

787

788

789

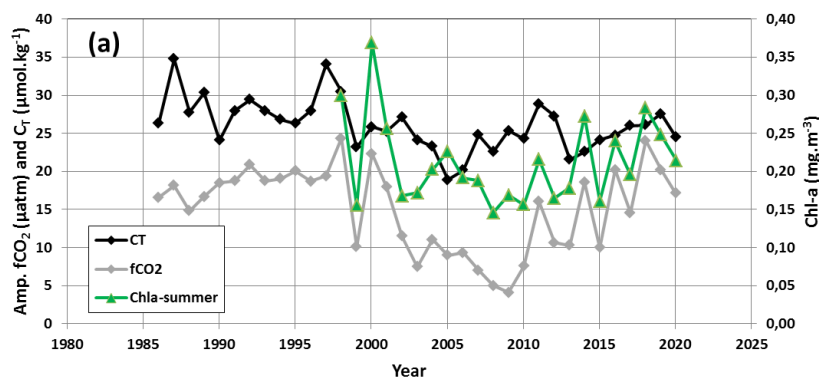
790

791

792

793

794



785

786

787

788

789

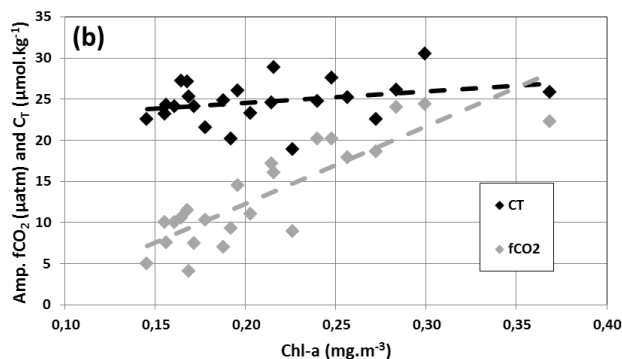
790

791

792

793

794



795

796

797

798

799

Figure 8: (a): Time-series of the seasonal amplitude (August minus January) for surface C_T (black, $\mu\text{mol.kg}^{-1}$) and $f\text{CO}_2$ (grey, μatm) from the FFNN model at station OISO-KERFIX ($50^{\circ}40'S-68^{\circ}25'E$). Also shown are the mean surface Chl-a (green, mg.m^{-3}) in summer in 1998-2021. (b): Seasonal amplitude of $f\text{CO}_2$ and C_T versus summer Chl-a for 1998-2020. The dashed lines indicate that the seasonal amplitude (August-January) increases when Chl-a is higher.

800 3.3 Anthropogenic CO_2 drives acidification in surface and the water column

801

802 3.3.1 Surface pH trend

803

804

805

806

807

808

809

810

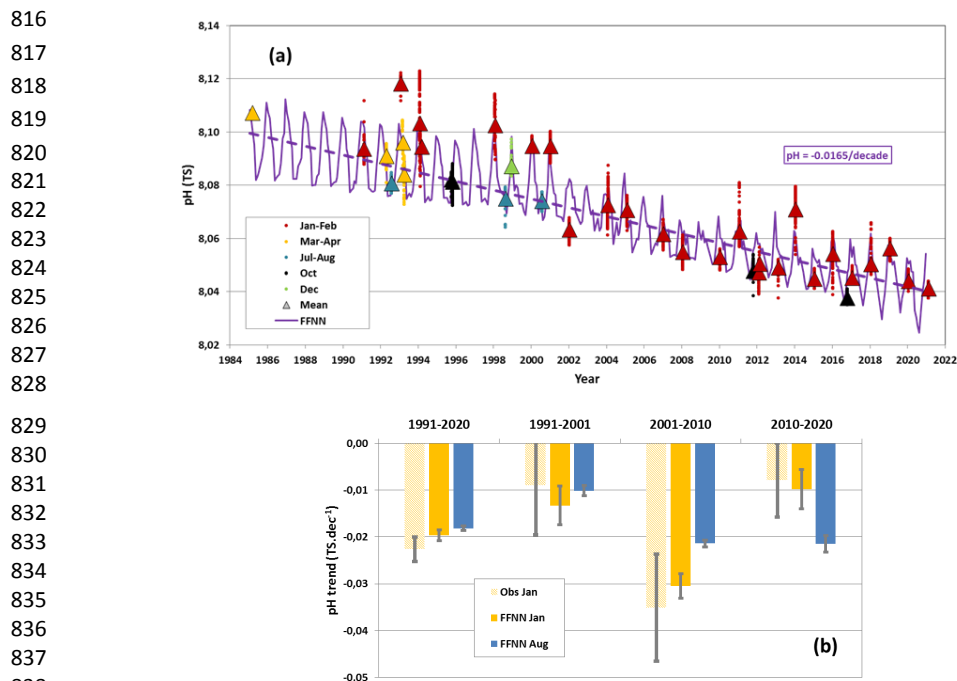
811

812

To explore the temporal change of pH in surface water we used the $f\text{CO}_2$ observations and the monthly results from the FFNN model. For both data-sets pH was calculated from $f\text{CO}_2$ and A_T reconstructed as described in section 2.2.5. Figure 9a presents the time-series of pH in the surface (the same time-series for $[\text{H}^+]$ concentrations is shown in Figure S13). For the full period, 1985-2020, the annual pH trend derived from the FFNN model is $-0.0165.\text{decade}^{-1}$ (± 0.0004) exactly the same as derived at large scale in the Southern Ocean (south of 44°S) for the period 1993-2018 (Iida et al., 2021, Table 1) but when restricted to this period, 1993-2018, the trend from the FFNN model appears slightly faster of $-0.0182.\text{decade}^{-1}$ (± 0.0006). This is less than the pH trend of -0.020 (± 0.002). decade^{-1} derived from $p\text{CO}_2$ data in the SO SubPolar Seasonally Stratified biome around $40-50^{\circ}\text{S}$ (SO-SPSS) for 1981-2011 (Table 1, Lauvset et al., 2015) and close to the pH trend of -0.0189 (\pm



813 0.0010).decade⁻¹ based on OceanSODA-ETH reconstructed fields in the SO-SPSS for the period 1982-2021 (Ma
814 et al., 2023). However, as for fCO₂ and C_T, different pH trends were estimated in summer and winter as well as
815 depending on the periods (Figure 9b, Table 1).



829
830
831
832
833
834
835
836
837
838
839
840 Figure 9: (a): Time-series of surface pH (TS) around station OISO-KERFIX (50°40'S-68°25'E) calculated from fCO₂ data
841 (Figure 2) using the A_T/S relation (see text). The color dots correspond to 5 seasons (January-February, March-April, July-
842 August, October and December) and triangles the average for each cruise. The monthly sea surface pH from the FFNN model
843 is presented for the period 1985-2020 (purple line). The annual pH trend in 1985-2020 of -0.0165.decade⁻¹ (± 0.0004)
844 (dashed line purple) is derived from the FFNN monthly data (the same figure for [H⁺] concentrations is presented in Supp.
845 Mat. Figure S13). (b): Trends of pH (TS.decade⁻¹) for different seasons and periods based on observations (January) and the
846 FFNN model (January or August).
847

848 The winter pH decreased was faster in recent years, mirroring the winter fCO₂ trend (Figure 2b). On the
849 opposite, in summer, the pH trend presents a large variability at decadal scale and was lower in 2010-2020. In
850 summer 2001-2010, the pH trend from the FFNN model was -0.0304.decade⁻¹ (± 0.0026) whereas in 2010-2020,
851 it was -0.0098.decade⁻¹ (± 0.0042) (Figure 9b, Table 1). Although the trends based on the observations are less
852 robust because the cruises were not conducted each year the reduced pH trend in summer after 2010 is confirmed
853 from in-situ data (-0.0351 ± 0.0114 .decade⁻¹ in 2001-2010 against -0.0078 ± 0.0079 .decade⁻¹ in 2010-2020,
854 Figure 9b, Table 1). These results show that the pH trend varied significantly from decade to decade and that the
855 decrease of pH since 1985 was mainly driven by anthropogenic CO₂. This is revealed in the winter water when
856 comparing pH and pre-industrial pH (Figure 10a). Here, the pre-industrial pH (pH-PI) was calculated after
857 subtracting C_{ant} values from the observed C_T concentrations for each sample in the WW layer. Interestingly the
858 pH trend in the WW of -0.0161 (± 0.0033).decade⁻¹ (here deduced from the station A_T-C_T data in 1985-2021) is
859 very close to the long-term trend in surface from the FFNN model in 1985-2020 (-0.0165.decade⁻¹ ± 0.0004).
860 This trend is slightly faster than the pH trends of -0.0134 (± 0.001).decade⁻¹ recently estimated in subsurface



861 waters (100-210m) of the Southern Ocean south of the PF and derived for years 1994-2017 from historical data
862 and BGC-Argo floats (Mazloff et al., 2023). For the same period, 1994-2017, at the OISO-KERFIX station we
863 estimate a pH trend in the WW of $-0.0168 (\pm 0.0043) \cdot \text{decade}^{-1}$ and of $-0.0186 (\pm 0.0006) \cdot \text{decade}^{-1}$ in surface
864 waters from the FFNN model.

865

866

867

868

869

870

871

872

873

874

875

876

877

878

879

880

881

882

883

884

885

886

887

888

889

890

891 Figure 10: (a): Time-series of pH (red dots) and pre-industrial pH (pH-PI, black dots) estimated in the winter water layer
892 (WW around 200m, see figure 6) in 1985-2021 at station OISO-KERFIX ($50^{\circ}40'S-68^{\circ}25'E$). pH-PI for each sample was
893 calculated after subtracting C_{ant} to C_T . The pH trend from the present days is $-0.0161 (\pm 0.0033) \cdot \text{decade}^{-1}$ (red dashed line).
894 No trend is observed for pH-PI (black dashed). The mean pH-PI in the WW is $8.173 (\pm 0.020, n = 45)$. (b): Profiles of pH and
895 pH-PI evaluated from March 1985 (black symbols) and February 2021 data (red symbols). The profiles for pH-PI are shown
896 below 150m only as C_{ant} estimates are not available in surface layer. Note that the pH-PI profiles are the same either using
897 1985 or 2021 data.

898

899

900

901

902

903

904

905

906

907

908

909

910

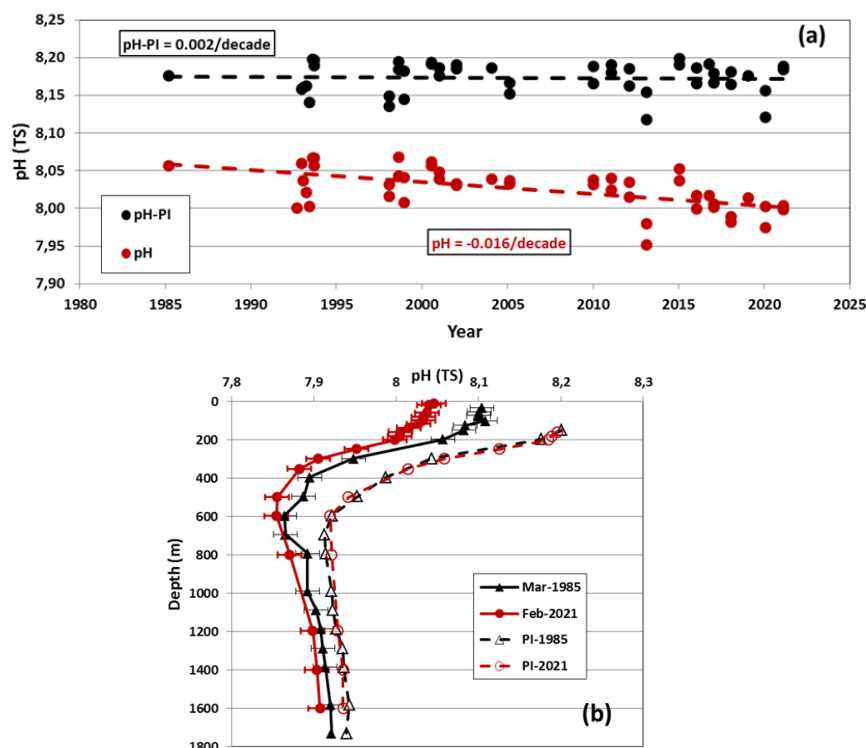
911

912

913

914

915



A for other properties (A_T , O_2 , temperature, salinity and nutrients), the pre-industrial pH (pH-PI) does not change over time in the WW (mean pH-PI = $8.173 \pm 0.020, n=45$, Figure 10a). The pH-PI in the WW is in the range of the pre-industrial surface pH value in the Southern Ocean (8.2 for year 1750 and 8.18 for year 1850) derived from Earth system Models (Jiang et al., 2023, their Table S9). In the WW at our location the modern pH (1985-2021) was on average $-0.147 (\pm 0.021)$ lower than pre-industrial pH. In 1985 pH in the WW was -0.119 lower than pH-PI and in 2021 it was -0.184 lower than pH-PI (Figure 10a). The progressive decrease of pH was clearly linked to C_{ant} concentrations in the WW layer and the pH decrease identified below that layer in the water column (Figure 10b).



908

909 3.3.2 Temporal change in the water column

910

911 From 1985 to 2021, signals of decreasing pH and increasing C_T in surface waters are propagated in the
912 water column down to about 500m. As mentioned above the data in 1985 (first occupation of the station) reveal
913 significant C_{ant} levels across the water column (Figure 6b). Therefore the pH down to 1400m was already lower
914 in 1985 than at pre-industrial times (Figure 10b). However, the largest C_{ant} increases were found in the top layers
915 and changes in pH from 1985 to 2021 were small below 500m (Figure 10b, Figure S14). While observations for
916 all years fall on a common linear relationship between C_{ant} and pH_{ant} for depths greater than 500 m, the change in
917 pH for a given level of C_{ant} increases with time for layers shallower than 500 m (Figure 11).

918

919

920

921

922

923

924

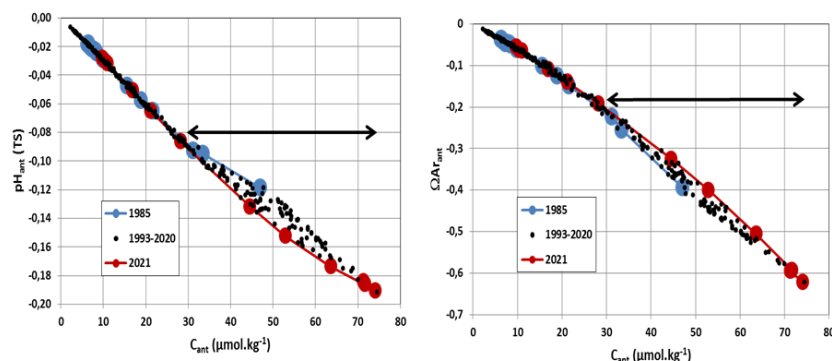
925

926

927

928

929



930

931

932 Figure 11: Anthropogenic pH (pH_{ant}) and anthropogenic Ω_{ar} ($\Omega_{ar,ant}$) versus anthropogenic CO_2 concentrations (C_{ant} ,
933 $\mu mol.kg^{-1}$) at station OISO-KERFIX ($50^{\circ}40'S-68^{\circ}25'E$). The data are selected in the layer 150-1600m for the periods 1985
934 (blue), 1993-2020 (black) and 2021 (red). The arrow identifies the data in the layer 150-500m (for $C_{ant} > 30 \mu mol.kg^{-1}$).
935 Below 500m no change of C_{ant} was observed from 1985 to 2021 and thus for pH_{ant} and $\Omega_{ar,ant}$.

936

937 The increase in C_{ant} concentrations over time (Figure 6b) also leads to a decrease of carbonate ion
938 concentrations [CO_3^{2-}] and of Ω_{ar} and Ω_{ca} (Figure S14, S15). These decreases are well identified since the pre-
939 industrial era in the whole water column but in the last 36 years, observations do not show any appreciable
940 changes below 500m (Figure 11). The aragonite saturation state ($\Omega_{ar}=1$) was found around 600m in 1985 and
941 around 400m in recent years (2015-2021, Figures S14, S15). Moreover, during the period covered by
942 observations (1985-2021), we did not detect abrupt change of the aragonite saturation horizon from one year to
943 the next (including from season to season, Figure S16). This contrasts with previous regional studies in the SO
944 and most notably with results from the layers close to the deep minimum of carbonate ion concentrations (Hauri
945 et al., 2015; Negrete-Garcia et al., 2019). At our station the [CO_3^{2-}] minimum lies around 500-600m (Figure S14,
946 S15) and, along with the superimposed C_{ant} accumulation, explains the upward shift of the aragonite and calcite
947 saturation between the pre-industrial and modern periods (Figure S15). At pre-industrial time under-saturation
948 with regard to aragonite ($\Omega_{ar}<1$) was found at the bottom only (1600m) whereas in 1985-2021 it was found in
949 the water column below 600 m or 400 m (Figure S15). The subsurface pre-industrial Ω_{ar} value was around 1.9-2
950 (Figure S15) and in the range of Ω_{ar} value in the Southern Ocean at pre-industrial time from ESM models (Jiang
951 et al., 2023, their Figure 4).



952 The aragonite under-saturation already occurred in 1985 at 500-600m (Figure S15) and a small increase
953 of C_T (via C_{ant} accumulation) close to the $[\text{CO}_3^{2-}]$ minimum would rapidly shift the aragonite saturation horizon
954 in layers above 500m. This might have already occurred and explains that Ω_{ar} value was 1.02 at 350m in 2021
955 (Figure S15). These results suggest that for pelagic calcifiers living in subsurface (150m or deeper) such as
956 pteropods and/or foraminifera (e.g. Hunt et al., 2008; Meilland et al., 2018) the impact of acidification might
957 occur sooner than in surface.

958 For the interpretation of the trend analysis based on observations, only data below 150m could be used
959 as C_{ant} was not evaluated in the surface layer. At 200m, based on A_T - C_T data, pH and Ω_{ar} decreased from 1985
960 to 2021 by -0.059 for pH (Figure 10b) and -0.16 for Ω_{ar} (Figure S15). In 36 years, this represents about 30% of
961 the total change since the pre-industrial era (-0.184 for pH and -0.6 for Ω_{ar} at 200m). This is mainly linked to the
962 C_{ant} change that represents also 30% increase in 36 years (+24.6 $\mu\text{mol.kg}^{-1}$ from 1985 to 2021 for a total of +71.7
963 $\mu\text{mol.kg}^{-1}$ CO_2 accumulated at 200m in 2021, Figure 7). We conclude that anthropogenic CO_2 drives the change
964 of the carbonate system in subsurface and probably also in surface waters.

965 In order to quantify the propagation of surface trends to depth, the temporal variations of carbonate
966 properties in the surface for both summer and winter derived from the FFNN model are compared to the changes
967 observed across the water column (Figure 12). The comparison shows that the seasonal amplitude of surface
968 waters properties was of a similar magnitude to the observed changes in the mixed layer between 1985 and 2021.
969 For example, the C_T and Ω_{ar} seasonality, respectively around 20 $\mu\text{mol.kg}^{-1}$ and 0.2, corresponds to the C_T
970 increase and Ω_{ar} decrease from 1985 to 2021. The comparisons also highlight that in summer the FFNN results
971 were close to observations in the mixed-layer (e.g. C_T was 2120 $\mu\text{mol.kg}^{-1}$ in 1985 and 2140 $\mu\text{mol.kg}^{-1}$ in 2021).
972 In winter the surface properties are different (C_T was higher, and pH, $[\text{CO}_3^{2-}]$, Ω_{ar} were lower) and intercept the
973 observations at depth close to the winter water (150-200m). This is true in 1985 and 2020/2021. Specifically,
974 surface C_T from the FFNN model in winter 1985 (2145.5 $\mu\text{mol.kg}^{-1}$) equaled the C_T measured at 150 m in
975 March 1985 (2148 $\mu\text{mol.kg}^{-1}$). In 2020, the winter C_T at the surface (2168.3 $\mu\text{mol.kg}^{-1}$) is equal to C_T
976 concentrations observed at 150-180 m in January 2020 or in 2021. For Ω_{ar} , the surface value derived from the
977 FFNN model in winter 1985 (1.6) equal to the Ω_{ar} observed at 125 m in March 1985. In 2020, the surface winter
978 estimate of Ω_{ar} (1.42) was equal to Ω_{ar} observed at 100-150 m in January 2020 or 2021. The same
979 correspondences between winter surface and WW data were identified for pH and $[\text{CO}_3^{2-}]$ (Figure 12). This
980 supports the use of winter and summer surface data from the FFNN model to investigate the seasonal Ω_{ar} trends
981 and their projection in the future.

982 The surface water Ω_{ar} (Ω_{ca}) trend from the FFNN model in summer of $-0.0059.\text{yr}^{-1}$ ($-0.0094.\text{yr}^{-1}$) was
983 stronger than in winter $-0.0050.\text{yr}^{-1}$ ($-0.0079.\text{yr}^{-1}$) and also higher than derived from observations in the WW ($-$
984 $0.0043.\text{yr}^{-1}$ for Ω_{ar} and $-0.0069.\text{yr}^{-1}$ for Ω_{ca}). The results indicate that the change of carbonate properties in the
985 years 1985-2021 were mainly driven by C_{ant} accumulation in surface waters and across the water column.
986 However, potential changes in primary productivity after 2010 mitigated the effects of increasing C_{ant}
987 accumulation in response to increasing atmospheric CO_2 leading to relatively stable summer C_T and $f\text{CO}_2$ and to
988 a stronger CO_2 sink (Figure 3). Consequently, when restricted to the period 2010-2020, the trend of Ω_{ar} in
989 surface waters in summer was much smaller, $-0.024.\text{decade}^{-1}$ (± 0.027) than during the preceding period. This
990 was much smaller than derived from the all data in 1985-2021 ($-0.048.\text{decade}^{-1}$) or estimated from reconstructed
991 fields in the SO-SPSS in 1982-2021 ($-0.0616.\text{decade}^{-1}$, Ma et al., 2023). It underscores the uncertainty in
992 extrapolating long-term time-series depending on the selection of data and periods.



993
 994
 995
 996
 997
 998
 999
 1000
 1001
 1002
 1003
 1004
 1005
 1006
 1007
 1008
 1009
 1010
 1011
 1012
 1013
 1014
 1015
 1016
 1017
 1018
 1019
 1020
 1021
 1022
 1023

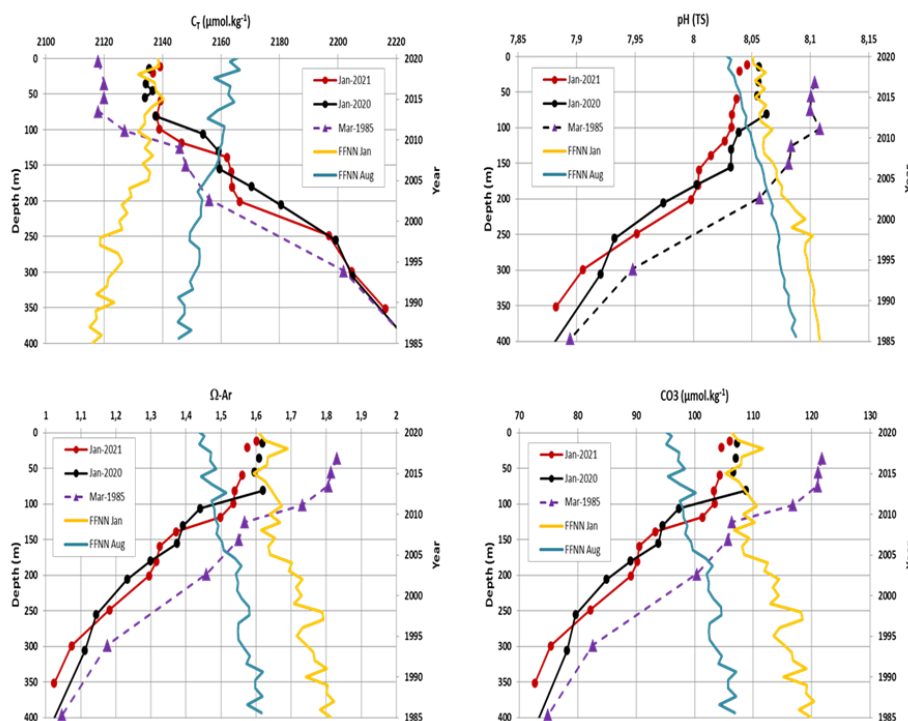


Figure 12: Profiles (0–400m left axis) of observed and calculated properties (C_T , pH, Ω -ar, $[CO_3^{2-}]$) at station OISO-KERFIX ($50^{\circ}40'S$ - $68^{\circ}25'E$) in March 1985, January 2020 and January 2021 along with surface time-series in 1985–2020 (right axis) of the same properties in January (yellow line) and August (blue line) from the FFNN model. The FFNN values in January 2020 are coherent with January 2020 observations in the mixed-layer and in January 1985 are close to the observations in March 1985. Note that the differences of properties between 2020–21 and 1985 have a similar magnitude as the seasonal amplitude (illustrated by the FFNN values for January and August).

1024
 1025
 1026
 1027
 1028
 1029
 1030
 1031
 1032
 1033

3.4 Long-term change in surface water, from the sixties to the future.

The data described above allowed evaluating the temporal variations of the properties of the carbonate system and C_{ant} over 1985–2021 along with a comparison to the pre-industrial state in the water column excluding the surface layer. The results over 36 years informed on the recent changes, inter-annual variations and trends, but the time-series appears somehow short to extrapolate the trends over time. What was the change of the carbonate system in surface water before 1985 and what will be its future evolution ?

3.4.1 Back to the sixties: observed trends since 1962.

1034
 1035
 1036
 1037

To explore the long-term change, we start by comparing our recent data with the observations from the LUSIAD cruise conducted in 1962–1963 (Keeling and Waterman, 1968). Some data from this cruise were obtained mid-November 1962 south of the Polar Front, in the region south-west off Kerguelen. Because of the seasonality, we compared the November 1962 data with our observations obtained in October–November in



1038 1995, 2011 and 2016, and with the FFNN model results for November (Figure 13). The C_T concentration, pH,
 1039 Ω_{ar} and Ω_{ca} for 1962 were calculated using fCO_2 data and A_T (from the A_T/S relationship Eq. 1).

1040

1041

1042

1043

1044

1045

1046

1047

1048

1049

1050

1051

1052

1053

1054

1055

1056

1057

1058

1059

1060

1061

1062

1063

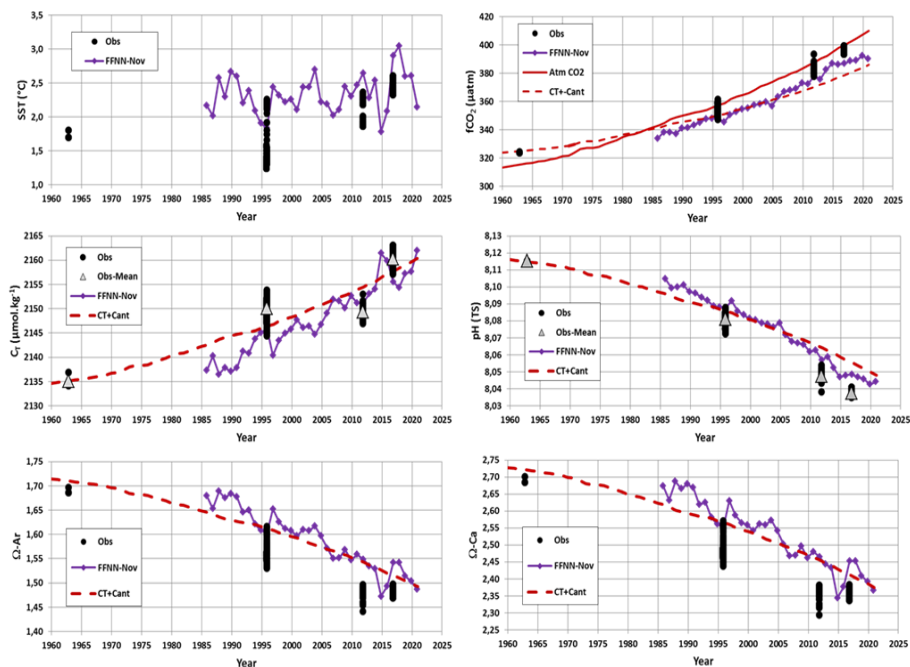
1064

1065

1066

1067

1068



1062 Figure 13: Observed (black dots) sea surface temperature ($^{\circ}C$), fCO_2 (μatm), C_T ($\mu mol.kg^{-1}$), pH (TS), Ω_{ar} and Ω_{ca} around
 1063 station OISO-KERFIX at $50^{\circ}40'S-68^{\circ}25'E$ for October-November. Also shown are the results for the FFNN model for November in 1985-2020 (Purple). The C_T concentrations, pH, Ω_{ar} and Ω_{ca} were calculated from fCO_2 data using the A_T/S
 1064 relation (Eq. 1). The red line is the atmospheric fCO_2 and red dashed-lines in each plot are the evolution of properties since
 1065 1960 corrected to C_{ant} where fCO_2 , pH, Ω_{ar} and Ω_{ca} were recalculated using C_T+C_{ant} , A_T constant at $2290 \mu mol.kg^{-1}$ and
 1066 SST at $2^{\circ}C$. Grey triangles identified the mean values for C_T and pH.
 1067
 1068

1069

1070

1071

1072

1073

1074

1075

1076

1077

1078

1079

1080

1081

1082

1083

First, we note that measured SST in November 1962 ($1.7^{\circ}C$) was slightly lower (on average about -
 0.6 $^{\circ}C$) compared to recent years, but SST as low as $1.8^{\circ}C$ for this season were also recorded in other periods
 (e.g. November 1995, 2014). The change in SST is unlikely to explain the long-term increase in fCO_2 or
 decrease in pH since 1962 (Figure 13). In 1962, the ocean fCO_2 was $324 \mu atm$ slightly higher than in the
 atmosphere ($\Delta fCO_2 = +8 \mu atm$, a small source), whereas in November 1985-2020 the ocean was a small CO_2 sink
 on average ($\Delta fCO_2 = -3.3 \pm 4.5 \mu atm$). The C_T concentration in 1962 ($2135 \mu mol.kg^{-1}$) was much lower than
 observed in the 90s and the pH (8.115) much higher than in recent years (Figure 13). Compared to 1962, pH in
 2016 was -0.078 lower, i.e. representing 70% of the pH decrease of -0.11 in the global ocean since the beginning
 of the industrial era (Jiang et al, 2019). In November 1962, surface C_T was lower by $-15.1 \mu mol.kg^{-1}$ compared to
 the data in October 1995, i.e. a trend of $+0.46 \mu mol.kg^{-1}.yr^{-1}$ in 33 years close to the C_{ant} trend observed in the
 WW in 1985-2021 as described above ($+0.53 \pm 0.01 \mu mol.kg^{-1}.yr^{-1}$). Having the C_T value in 1962, we can
 project the C_T in time by adding the C_{ant} concentration based on the relationship observed between C_{ant} and
 atmospheric CO_2 (Figure 7b) assuming that the anthropogenic CO_2 uptake since the sixties is representative of
 the C_T change (i.e. the change of C_T due to natural variability is small). This projection is shown for all
 properties (red dashed-lines in Figure 13) and confirms that the progressive C_{ant} accumulation explained most of



1084 the C_T and fCO_2 increase in surface since 1962. We note that the C_T derived from the FFNN model suggests
1085 slightly lower C_T compared to the C_{ant} projection especially before 2004. The difference of projected C_T and the
1086 FFNN model (on average $-2.2 \pm 2.7 \mu\text{mol.kg}^{-1}$) is within the uncertainty of C_T calculations (error is $\pm 5 \mu\text{mol.kg}^{-1}$
1087 when using the A_T/fCO_2 pairs) and the trend of the difference over 1985-2020 ($-0.15 \mu\text{mol.kg}^{-1}.\text{yr}^{-1}$) is too small
1088 to be related with confidence to changes associated with natural processes. On the other hand, the ocean fCO_2
1089 recalculated with the projected C_{ant} trend suggested that for this season (November) the ocean moved from a CO_2
1090 source in 1962-1985 ($\Delta fCO_2 > 0$) to a sink in 1986-2021 ($\Delta fCO_2 < 0$) in line with results from the FFNN model.
1091 The recalculated fCO_2 with C_{ant} (dashed red line in Figure 13) was close to that observed in 1995 or from the
1092 FFNN model in 1985-2014 (mean difference over 1985-2014 is $-1.2 \pm 5.2 \mu\text{atm}$). After 2016, the recalculated
1093 fCO_2 suggest a stronger sink and the difference with observations in 2011 and 2016 or the FFNN model is
1094 slightly higher (mean difference over 2016-2020 is $-8.8 \pm 1.5 \mu\text{atm}$). Although the differences are in the range of
1095 the error in fCO_2 calculation using A_T-C_T pairs ($\pm 13 \mu\text{atm}$), this might indicate that after 2016 a process could
1096 contribute to increase fCO_2 faster than the effect of C_{ant} only. This difference could be due to the warming that
1097 occurred after 2016 when SST was higher than 2°C and up to 3°C in November 2017 (Figure 13 and Figure S9).
1098 The same could be applied for pH that was slightly lower than the pH recalculated from C_{ant} trend after 2015 (the
1099 mean difference between recalculated pH and FFNN-pH over 1985-2020 is only 0.002 ± 0.006). Therefore, we
1100 conclude that for November the pH decrease since 1962 was mainly driven by anthropogenic CO_2 . Aragonite
1101 and calcite saturation states also show a clear decrease since 1962 (Figure 13), a diminution of 11% in 59 years
1102 for both Ω_{ar} and Ω_{ca} . Based on these results over almost 60 years that confirm the conclusions from the
1103 observations in 1985-2021, we now evaluate the long-term change of the carbonate system in surface water in
1104 the future.

1105

1106 3.4.2 Projecting the observed trends in the future

1107

1108 The trends of the properties based on observations in 1962-2021 and the FFNN model in 1985-2020
1109 indicate relatively linear trends linked to C_{ant} uptake albeit with some decadal variability in summer (Figure 4). A
1110 simple linear extrapolation of the trends in the future suggests that aragonite saturation in surface water would be
1111 reached in year 2110 for the winter season and 2120 for summer (Figure S17) whereas the trend in subsurface
1112 suggests under-saturation in 2090. In year 2100, surface pH and $[H^+]$ would be around 7.9 and 12 nmol.kg^{-1}
1113 (Figure S17). However, ESM CMIP6 models suggest that under a high emission scenario (SSP5-8.5), pH in
1114 2100 in the Southern Ocean near 50°S would be around 7.65 and $[H^+]$ around 22 nmol.kg^{-1} (Jiang et al., 2023,
1115 their figure 4). This suggests that the simple linear extrapolation based on recent observed trends (Figure S17)
1116 underestimated the future change of the carbonate system for a high emission scenario as previously shown in
1117 the South-Eastern Indian Ocean based on summer trends derived from observations in 1969-2003 (Midorikawa
1118 et al., 2012, their figure 4).

1119 To better investigate the changes in the next decades, we assumed that the C_{ant} trend for the modern
1120 period (Figure 7) that experienced a “business as usual” scenario after the sixties is representative of the future
1121 changes in the surface ocean carbonate system. For this analysis, we use two emissions scenarios (Shared
1122 Socioeconomic Pathways, SSP, Meinshausen et al., 2020) with atmospheric xCO_2 reaching 1135 ppm in 2100 (a
1123 “high” emission scenario SSP5-8.5) or xCO_2 reaching 603 ppm in 2100 after a stabilization around 2080
1124 (scenario SSP2-4.5). This enables to simulate future C_T concentrations for summer or winter (Figure 14) and to



1125 calculate other carbonate properties using C_T and A_T (Figure 15, Table 2) in response to approximated future
1126 changes in physical and geochemical properties excluding impacts of changes in atmospheric and oceanic
1127 circulation. As the calculated properties are sensitive to A_T values, we used a fixed A_T of $2280 \mu\text{mol.kg}^{-1}$ or
1128 applied a correction based on the long-term change of sea surface salinity observed in the last 6 decades (1960-
1129 2017), i.e. a freshening in the Southern Ocean of around -0.01 to $-0.02.\text{decade}^{-1}$ (Durack and Wijffels, 2010;
1130 Cheng et al., 2020b). The decrease in salinity in the South Indian Ocean ($-0.02.\text{decade}^{-1} \pm 0.01$) was recently
1131 analyzed by Akhoudas et al. (2023) who showed that in the years 1993-2021 the freshening was mainly due to
1132 an increase in the precipitation linked to the acceleration of the atmospheric hydrological cycle. From our data in
1133 the mixed-layer over 1985-2021, we estimated a trend in salinity of $-0.0207.\text{decade}^{-1}$ (± 0.0041). For the A_T
1134 sensitivity test we thus select a salinity trend of $-0.01.\text{decade}^{-1}$ in 1962-1985 and $-0.02.\text{decade}^{-1}$ after 1985 and
1135 apply these trends to simulate A_T over 1960-2100 using the $A_T/\text{Salinity}$ relationship (Equation 1). This leads to a
1136 salinity of 33.650 and A_T of $2272 \mu\text{mol.kg}^{-1}$ in year 2100, about $8 \mu\text{mol.kg}^{-1}$ lower than observed in 2021 (2280
1137 $\mu\text{mol.kg}^{-1}$). Compared to the C_T change from 2021 to 2100 ($+50$ and $+193 \mu\text{mol.kg}^{-1}$ for the “low” and “high”
1138 emissions scenario, Figure 14), the impact of A_T decrease has a minor effect on the future change for pH, $[\text{CO}_3^{2-}]$
1139 or Ω (Table 2). For example, in winter for the SSP5-8.5 scenario, when the A_T decrease is taken into account, pH
1140 in 2100 is 7.316 and Ω_{Ar} is 0.33 against 7.372 and 0.34 when A_T is constant (Table 2). In both cases, the
1141 aragonite saturation ($\Omega_{Ar}=1$) in winter occurred in 2055, whereas in summer it is identified in 2070. The effect of
1142 lower A_T in the future appeared also small compared to the seasonal differences of pH and Ω in 2100.

1143 As noted above, the Southern Ocean experienced a warming in recent decades (e.g. Auger et al., 2021)
1144 and it is projected that warming will continue in the future (IPCC, 2022). Therefore, to test the sensitivity of
1145 calculated properties to warming we applied a correction of $+0.0125^\circ\text{C.yr}^{-1}$ in 1985-2020 and $+0.025^\circ\text{C.yr}^{-1}$ after
1146 2020 (Azarian et al, 2023). As for A_T , these results are compared for winter using constant SST (Table 2). The
1147 effect of the long-term warming does mainly impact the projection of $[\text{H}^+]$ and pH (Table 2).

1148 These sensitivity tests for temperature and A_T showed that as for the observed period 1962-2021 (Figure
1149 13), the projection in the future depends mainly on the anthropogenic CO_2 accumulation. Here, the C_T
1150 concentrations were calculated using the C_{ant} versus atmospheric CO_2 relationship (Figure 7b). We thus tested
1151 the results for winter based on the error associated with this relationship (Figure S18). This leads to either higher
1152 or lower C_T compared to original calculation (Figure 14). For the SSP5-8.5 scenario, the winter C_T
1153 concentrations in 2100 range between 2328 and $2378 \mu\text{mol.kg}^{-1}$, higher than simulated in the ESM CMIP6
1154 models around 50°S ($2300 \mu\text{mol.kg}^{-1}$, Jiang et al., 2023). As in the ESM models for the SSP2-4.5 scenario, the
1155 projected C_T concentration in 2100 at our location is much lower $2217 \mu\text{mol.kg}^{-1}$ (Figure 14). The future change
1156 of the carbonate system is not significantly different using low or high C_{ant} accumulation (Figure S18) but this
1157 test gives a range of years to reach aragonite and calcite under-saturation. In winter (SSP5-8.5 scenario),
1158 aragonite would reach under-saturation between year 2050 and 2060 and between year 2070 and 2080 for
1159 calcite. Note that for summer we derived under-saturation for Ω_{Ar} in year 2065 and for Ω_{Ca} in year 2085. For the
1160 SSP2-4.5 scenario, where C_T is $143 \mu\text{mol.kg}^{-1}$ lower in 2100 compared to SSP5-8.5, aragonite under-saturation
1161 would not be reached before 2070 (Figure 15).

1162



1163
1164
1165
1166
1167
1168
1169
1170
1171
1172
1173
1174
1175
1176
1177
1178
1179
1180
1181
1182
1183
1184
1185
1186
1187
1188
1189
1190
1191
1192
1193
1194
1195
1196
1197
1198
1199
1200
1201
1202
1203
1204
1205
1206
1207
1208
1209
1210
1211
1212
1213
1214
1215
1216
1217
1218

Table 2: Results of the simulated properties for year 2020, 2050 and 2100 for two emission scenario (SSP5-8.5 or SSP2-4.5). For 2020 the results based on observations in January (Obs) and the FFNN model in January and August also listed. Sensitivity tests: “SSP85 W-T” is for winter with constant temperature and “SSP85 W-A-T” is for winter with constant A_T and temperature.

Method	Year	Atm-CO ₂ ppm	fCO ₂ µatm	C _T µmol.kg ⁻¹	A _T µmol.kg ⁻¹	pH TS	[H ⁺] nmol.kg ⁻¹	[CO ₃ ²⁻] µmol.kg ⁻¹	Ωca	Ωar
Obs Jan	2020	410.6	391.9	2142.2	2281.8	8.044	9.04	105.2	2.53	1.59
Std obs.			(2.0)	(0.7)	(0.3)	(0.002)	(0.04)	(0.5)	(0.01)	(0.01)
FFNN Jan	2020	410.6	385.1	2138.5	2280.1	8.051	8.90	106.3	2.55	1.61
SSP Summer	2020	414.9	375.4	2137.5	2282.1	8.061	8.70	108.0	2.60	1.63
FFNN Aug	2020	410.6	410.0	2168.3	2289.8	8.024	9.45	94.2	2.27	1.42
SSP Winter	2020	414.9	434.5	2167.3	2282.1	8.001	9.98	90.4	2.18	1.37
SSP85 Summer	2050	562.8	526.5	2177.2	2278.3	7.928	11.79	84.2	2.02	1.28
SSP85 Winter	2050	562.8	624.7	2207.0	2278.3	7.857	13.91	68.5	1.65	1.04
SSP85 W-A-T	2050	562.8	585.7	2207.0	2280.0	7.880	13.17	69.0	1.66	1.04
SSP85 W-T	2050	562.8	592.7	2207.0	2278.3	7.875	13.32	68.1	1.64	1.03
SSP45 Winter	2050	506.9	554.8	2192.0	2278.3	7.905	12.46	75.8	1.92	1.15
SSP85 Summer	2100	1135.2	1986.9	2330.6	2271.8	7.394	41.31	26.9	0.65	0.41
SSP85 Winter	2100	1135.2	2306.3	2360.4	2271.8	7.316	48.26	21.8	0.52	0.33
SSP85 W-A-T	2100	1135.2	1993.1	2360.4	2280.0	7.372	42.44	22.6	0.54	0.34
SSP85 W-T	2100	1135.2	2097.0	2360.4	2271.8	7.349	44.74	21.3	0.51	0.32
SSP45 Winter	2100	602.8	753.9	2217.7	2271.8	7.782	16.51	60.9	1.47	0.92

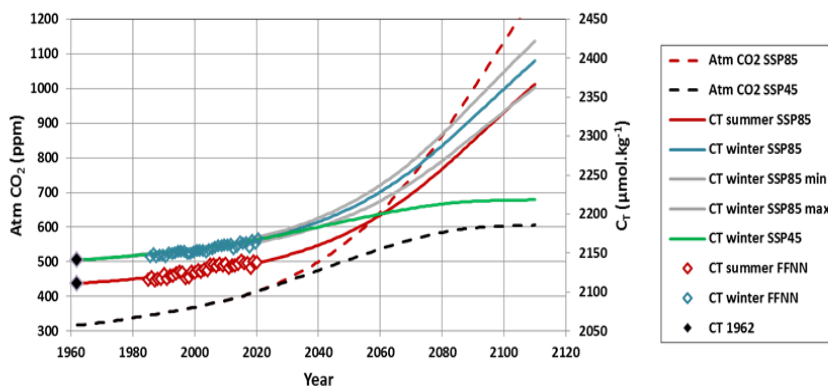


Figure 14: Evolution of atmospheric CO₂ (ppm) and sea surface C_T (µmol.kg⁻¹) in 1960-2110 evaluated for 2 scenarios (SSP2-4.5 black dashed and SSP5-8.5 red dashed), for summer (red line for SSP5-8.5) and winter (blue line for SSP5-8.5 and green line for SSP2-4.5). Grey lines are the high and low C_T for winter SSP5-8.5 based on the error in the C_{ant}/fCO₂ relationship (figure 7b). Also shown are the results for the FFNN model in 1985-2020 for summer (red diamonds) and winter (blue diamonds) and C_T in 1962 (black diamonds). The C_T values for different seasons and scenarios were used to calculate the carbonate properties in the future (Figure 15).



1219
 1220
 1221
 1222
 1223
 1224
 1225
 1226
 1227
 1228
 1229
 1230
 1231
 1232
 1233
 1234
 1235
 1236
 1237
 1238
 1239
 1240
 1241
 1242
 1243
 1244
 1245
 1246
 1247
 1248
 1249
 1250
 1251
 1252
 1253
 1254
 1255
 1256
 1257
 1258
 1259
 1260
 1261
 1262
 1263
 1264
 1265
 1266
 1267

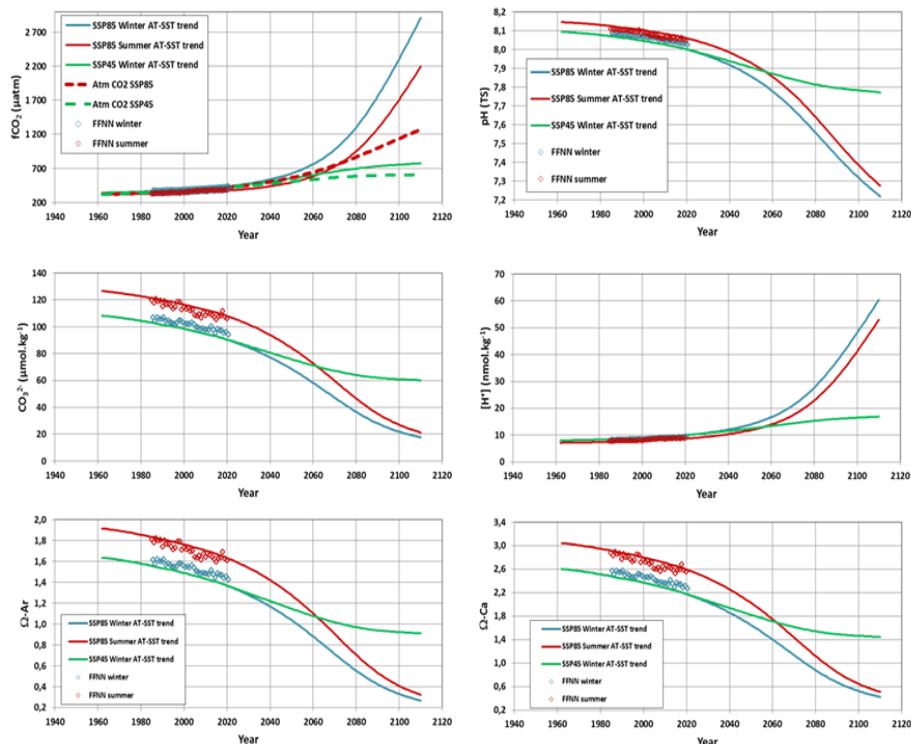


Figure 15: Evolution of sea surface fCO_2 (μatm), pH (TS), CO_3^{2-} ($\mu mol.kg^{-1}$), $[H^+]$ ($nmol.kg^{-1}$), $\Omega-Ar$ and $\Omega-Ca$ in 1960-2110 evaluated for the SSP5-8.5 scenario for winter (blue line) and summer (red line) taking into account both A_T and SST future trends. For winter results are also presented using the SSP2-4.5 scenario (green line). Also shown are the results for the FFNN model in 1985-2020 for summer (red diamonds) and winter (blue diamonds). Atmospheric fCO_2 is also shown for SSP5-8.5 (red dashed) and SSP2-4.5 (green dashed). Values in 2020, 2050 and 2100 for different sensitivity tests are listed in Table 2.

4 Summary and concluding remarks

The times-series of high quality observations in 1985-2021 and the results from the FFNN model at one location, south of the Polar Front in the Southern Indian Ocean ($50^\circ S-68^\circ E$) presented in this analysis offered new results on the inter-annual variability, decadal to long-term trends of the carbonate system in surface waters, air-sea CO_2 fluxes and associated drivers. The evaluation of anthropogenic CO_2 concentrations in the water column indicates that the trends of the carbonate species are mainly driven by the CO_2 uptake leading to a progressive acidification in surface waters and at depth.

In 1985, the C_{ant} concentrations were approaching $50 \mu mol.kg^{-1}$ at 200 m and C_{ant} was detected in the water column down to the bottom (1600m). This explains why aragonite under-saturation was observed at around 600m in 1985, where $[CO_3^{2-}]$ concentration was at minimum, whereas at pre-industrial era the water column was super-saturated (this study Figure S15; Lauvset et al., 2020, their Figure S15). 36 years later because of the anthropogenic CO_2 accumulation, we observed an upward migration of the aragonite saturation horizon that was found around 400 m in 2021 (a shoaling rate of around $-6 m.yr^{-1}$).



1268 At subsurface, in the winter water layer, the C_{ant} trend is estimated at $+0.53 (\pm 0.01) \mu\text{mol.kg}^{-1}.\text{yr}^{-1}$ in
1269 1985-2021 with a detectable increase in recent years (up to $72 \mu\text{mol.kg}^{-1}$ in 2021 compared to $47 \mu\text{mol.kg}^{-1}$ in
1270 1985). The C_{ant} concentrations in the ocean are closely related to the atmospheric CO_2 concentrations and the
1271 slope we observed south of the PF in the Indian sector of $+0.263 \pm 0.042 \mu\text{mol.kg}^{-1}.\mu\text{atm}^{-1}$ is close to that
1272 observed in the AAIW in the South Atlantic ($+0.23 \pm 0.05 \mu\text{mol.kg}^{-1}.\mu\text{atm}^{-1}$, Fontela et al., 2021). This suggests
1273 that local observations in the South Indian POOZ captured the link between C_{ant} and atmospheric CO_2 at larger
1274 scale.

1275 In surface waters, over 1991-2020 the oceanic $f\text{CO}_2$ increased at a rate close or slightly lower than in
1276 the atmosphere (Figure 2b) and the C_T trend followed the C_{ant} accumulation (Figure 4b, S12a). However in the
1277 last decade both observations and the FFNN model showed low $f\text{CO}_2$ trends in summer (less than $1 \mu\text{atm.yr}^{-1}$).
1278 The change in summer trend appears related to primary production as revealed by a decrease of Chl-a in 1998-
1279 2010 followed by an increase after 2010. Biological activity counteracts the C_T increase due to C_{ant} , resulting in
1280 rather stable C_T and $f\text{CO}_2$ in summer 2010-2020 ($+0.38 \pm 0.26 \mu\text{mol.kg}^{-1}.\text{yr}^{-1}$ and $+0.98 \pm 0.40 \mu\text{atm.yr}^{-1}$). As a
1281 result, the region moved from an annual source of $+0.8 \text{molC.m}^{-2}.\text{yr}^{-1}$ in 1985 to a sink of $-0.5 \text{molC.m}^{-2}.\text{yr}^{-1}$ in
1282 2020. The increase of the ocean CO_2 sink was particularly pronounced after 2011 (Figure 3) when phytoplankton
1283 biomass was stronger in this HNLC region and occurred when the SAM index was in a positive state.

1284 In 1959-1963, the SAM was also positive on average and moved to a negative phase in 1964 (Marshall,
1285 2003; King et al., 2023). Historical data from 1962 suggest that in November the region was a small CO_2 source
1286 ($\Delta f\text{CO}_2 = +8 \mu\text{atm}$). Assuming the seasonality was the same as in the 80s, we estimate that in 1962 the annual flux
1287 would be around $2.2 \text{molC.m}^{-2}.\text{yr}^{-1}$. Extrapolating to the entire South Indian POOZ ($50\text{-}58^\circ\text{S}/20\text{-}120^\circ\text{E}$, 6.5
1288 Mkm^2), this region was a CO_2 source of 0.17PgC.yr^{-1} in 1962, reduced to 0.06PgC.yr^{-1} in 1985 and a CO_2 sink
1289 of -0.04PgC.yr^{-1} in 2020. This could be compared with reconstructed fluxes from a data-based model that
1290 produced a CO_2 source in 1960-1990 and a sink in 2020 in the south Indian sector (Rödenbeck et al., 2022, their
1291 Figure 6).

1292 For November 1962, the estimated C_T concentration in surface ($2135 \mu\text{mol.kg}^{-1}$) is $21 \mu\text{mol.kg}^{-1}$ lower
1293 than observed mid-October 2016 in the mixed-layer ($2156 \mu\text{mol.kg}^{-1}$). This is almost equal to the increase of C_{ant}
1294 in 54 years ($+22.3 \mu\text{mol.kg}^{-1}$). As a result, surface ocean pH dropped from 8.11 in 1962 to 8.044 in 2020. Over
1295 multi-decadal time scale (30 years or more), acidification in the South Indian POOZ has been mainly controlled
1296 by uptake of anthropogenic CO_2 . However, our data also indicate a modulation of the summer pH trend by
1297 natural processes. After 2010, a very small pH trend was estimated in summer ($-0.0098.\text{decade}^{-1} \pm 0.0042$) when
1298 the region experienced higher primary productivity. On the opposite, in winter, the pH trends continuously
1299 increased with time, $-0.010.\text{decade}^{-1} (\pm 0.001)$ in 1991-2001 and $-0.021.\text{decade}^{-1} (\pm 0.002)$ in 2010-2020. In the
1300 subsurface (winter water layer), the trend of pH based on $A_T\text{-}C_T$ data in 1985-2021 of $-0.0161 (\pm 0.0033).\text{decade}^{-1}$
1301 is also almost equal to the annual surface trend from the FFNN model. A simple extrapolation of the trends in
1302 the WW indicated that under-saturation ($\Omega < 1$) would be reached at year 2090 for aragonite and year 2180 for
1303 calcite. However, as atmospheric CO_2 will desperately continue to rise and ocean C_T will increase in the future,
1304 the pH and Ω will decrease at a faster rate than observed in recent years. A projection of future C_T concentrations
1305 based on emissions scenario, excluding changes in ocean circulation, indicated that the winter surface pH in
1306 2100 would decrease to 7.32 for a high emission scenario (SSP5-8.5) or to 7.782 for a low emission scenario
1307 (SSP2-4.5). This is up to -0.86 lower than pre-industrial pH and -0.71 lower than pH observed in 2020. For the



1308 winter season the aragonite saturation in surface would be reached around 2050 for a high emissions scenario
1309 and 2070 for a low emission scenario.

1310 The time-series presented here for the Southern Ocean, along with other historical time-series of A_T - C_T
1311 in the water-column (BATS, HOT, ESTOC, KNOT, Iceland or Irminger seas; Bates et al., 2014; Lange et al.,
1312 2023) or the recent BG-Argo floats in the Southern Ocean (Mazloff et al., 2023) offer useful data for the
1313 evaluation of biogeochemical and Earth system models, especially the coupling of fCO_2 , C_T , A_T , and pH not well
1314 represented in current models at seasonal to decadal scale in the Southern Ocean (e.g. Hauck et al., 2023;
1315 Rodgers et al., 2023; Joos et al., 2023). Observing the decadal changes of the carbonate system in the water
1316 column is also an important step to extend the evaluation of biogeochemical and ESM models below the surface
1317 (Jiang et al., 2023). It is important to maintain such time-series for monitoring the future evolution of the ocean
1318 CO_2 sink, of the acidification and its impact on phytoplankton species and higher trophic levels. This is
1319 especially the case in Marine Protected Area such as the French Sub-Antarctic islands including the Kerguelen
1320 Archipelago which was listed as a UNESCO World Heritage site in 2019.

1321

1322 **Data availability:**

1323 Data used in this study are available in SOCAT (www.socat.info) for fCO_2 surface data, in GLODAP
1324 (www.glodap.info) for water-column data and at NCEI/OCADS (www.ncei.noaa.gov/access/ocean-carbon-data-system/oceans/VOS_Program/OISO.html). The CMEMS-LSCE-FFNN model data are available at E.U.
1325 Copernicus Marine Service Information (<https://resources.marine.copernicus.eu/products>).

1326

1327

1328 **Authors contributions:**

1329 CLM and NM are co-I of the ongoing OISO project. CLM, NM, CL and CR participated to OISO cruises.
1330 Underway fCO_2 was measured by CLM, NM, CL, and qualified by CLM and NM. Nutrients data were measured
1331 and qualified by CLM and CL. Chl-a data were measured and qualified by CR. Water column data were
1332 qualified by CLM, NM, CL, CR and GR. MG, FC and TTTC developed the CMEMS-LSCE-FFNN model and
1333 provided the model results. NM started the analysis, wrote the draft of the manuscript and prepared the figures
1334 All authors contributed to revising the draft manuscript.

1335

1336 **Competing interest:** The authors declare that they have no conflict of interest.

1337

1338 **Acknowledgments:** The OISO program was supported by the French institutes INSU (Institut National des
1339 Sciences de l'Univers) and IPEV (Institut Polaire Paul-Emile Victor), OSU Ecce-Terra (at Sorbonne Université),
1340 and the French program SOERE/Great-Gases. We thank the French oceanographic fleet ("Flotte
1341 océanographique française") for financial and logistic support for the OISO program
1342 (<https://campagnes.flotteoceanographique.fr/series/228/>). We thank the captains and crew of R.R.V. *Marion*
1343 *Dufresne* and the staff at IFREMER, GENAVIR and IPEV. We also thank Jonathan Fin and Claude Mignon for
1344 their help during the OISO cruises. The development of the neural network model benefited from funding by the
1345 French INSU-GMMC project "PPR-Green-Grog (grant no 5-DS-PPR-GGREOG), the EU H2020 project
1346 AtlantOS (grant no 633211), as well as through the Copernicus Marine Environment Monitoring Service (project
1347 83-CMEMS-TAC-MOB). We thank all colleagues that contributed to the quality control of ocean data made
1348 available through CARINA and GLODAP (www.glodap.info). The Surface Ocean CO_2 Atlas (SOCAT,



1349 www.socat.info) is an international effort, endorsed by the International Ocean Carbon Coordination Project
1350 (IOCCP), the Surface Ocean Lower Atmosphere Study (SOLAS) and the Integrated Marine Biogeochemistry
1351 and Ecosystem Research program (IMBER), to deliver a uniformly quality-controlled surface ocean CO₂
1352 database.

1353

1354 **References**

1355

1356 Akhoudas, C. H., Sallée, J.-B., Reverdin, G., Haumann, F. A., Pauthenet, E., Chapman, C. C., Margirier, F., Lo
1357 Monaco, C., Metzl, N., Meilland, J., and Stranne, C.: Isotopic evidence for an intensified hydrological cycle in
1358 the Indian sector of the Southern Ocean. *Nat Commun* 14, 2763. <https://doi.org/10.1038/s41467-023-38425-5>,
1359 2023

1360

1361 Aminot, A., and Kérouel, R.: *Hydrologie des écosystèmes marins: paramètres et analyses*. Ed. Ifremer, 336 p.,
1362 2004

1363

1364 Antonov, J. I., Locarnini, R. A., Boyer, T. P., Mishonov, A. V., and Garcia, H. E.: World Ocean Atlas 2005, in:
1365 Volume 2: Salinity, edited by: Levitus, S., NOAA Atlas NESDIS 62, US Government Printing Office,
1366 Washington, DC, 182 pp., <https://repository.library.noaa.gov/view/noaa/1127>, 2006.

1367

1368 Arrigo, K. R., van Dijken, G. L., and Bushinsky, S.: Primary production in the Southern Ocean, 1997–2006, *J.*
1369 *Geophys. Res.-Oceans*, 113, C08004, doi:doi:10.1029/2007jc004551, 2008.

1370

1371 Auger, M., Morrow, R., Kestenare, E., Sallée, J.-B., and Cowley, R.: Southern Ocean in-situ temperature trends
1372 over 25 years emerge from interannual variability, *Nat. Commun.*, 12, 514,
1373 <https://doi.org/10.1038/s41467-020-20781-1>, 2021

1374

1375 Azarian, C., Bopp, L., Pietri, A., Sallée, J.-B., and d'Ovidio, F.: Current and projected patterns of warming and
1376 marine heatwaves in the Southern Indian Ocean, *Progress in Oceanography*,
1377 doi:<https://doi.org/10.1016/j.pocean.2023.103036>, 2023

1378

1379 Bakker, D. C. E., Pfeil, B., Landa, C. S., Metzl, N., O'Brien, K. M., Olsen, A., Smith, K., Cosca, C., Harasawa,
1380 S., Jones, S. D., Nakaoka, S.-I., Nojiri, Y., Schuster, U., Steinhoff, T., Sweeney, C., Takahashi, T., Tilbrook, B.,
1381 Wada, C., Wanninkhof, R., Alin, S. R., Balestrini, C. F., Barbero, L., Bates, N. R., Bianchi, A. A., Bonou, F.,
1382 Boutin, J., Bozec, Y., Burger, E. F., Cai, W.-J., Castle, R. D., Chen, L., Chierici, M., Currie, K., Evans, W.,
1383 Featherstone, C., Feely, R. A., Fransson, A., Goyet, C., Greenwood, N., Gregor, L., Hankin, S., Hardman-
1384 Mountford, N. J., Harlay, J., Hauck, J., Hoppema, M., Humphreys, M. P., Hunt, C. W., Huss, B., Ibáñez, J. S.
1385 P., Johannessen, T., Keeling, R., Kitidis, V., Körtzinger, A., Kozyr, A., Krasakopoulou, E., Kuwata, A.,
1386 Landschützer, P., Lauvset, S. K., Lefèvre, N., Lo Monaco, C., Manke, A., Mathis, J. T., Merlivat, L., Millero, F.
1387 J., Monteiro, P. M. S., Munro, D. R., Murata, A., Newberger, T., Omar, A. M., Ono, T., Paterson, K., Pearce, D.,
1388 Pierrot, D., Robbins, L. L., Saito, S., Salisbury, J., Schlitzer, R., Schneider, B., Schweitzer, R., Sieger, R.,
1389 Skjelvan, I., Sullivan, K. F., Sutherland, S. C., Sutton, A. J., Tadokoro, K., Telszewski, M., Tuma, M., Van
1390 Heuven, S. M. A. C., Vandemark, D., Ward, B., Watson, A. J., and Xu, S.: A multi-decade record of high-
1391 quality fCO₂ data in version 3 of the Surface Ocean CO₂ Atlas (SOCAT), *Earth Syst. Sci. Data*, 8, 383–413,
1392 doi:10.5194/essd-8-383-2016, 2016.

1393

1394 Bakker, D. C. E. et al: Surface Ocean CO₂ Atlas Database Version 2022 (SOCATv2022) (NCEI Accession
1395 0253659). NOAA National Centers for Environmental Information. Dataset. <https://doi.org/10.25921/1h9f-nb73>.
1396 Last Accessed [21 June 2022], 2022

1397

1398 Balch, W.M., Bates, N.R., Lam, P.J., Twining, B.S., Rosengard, S. Z., Bowler, B.C., Drapeau, D.T., Garley, R.,
1399 Lubelczyk, L.C., Mitchell, C., and Rauschenberg, S.: Factors regulating the Great Calcite Belt in the Southern
1400 Ocean and its biogeochemical significance. *Global Biogeochem. Cycles*, 30, doi: 10.1002/2016GB005414, 2016



- 1401
1402 Basterretxea, G., Font-Muñoz, J. S., Hernández-Carrasco, I., and Sañudo-Wilhelmy, S. A.: Global variability of
1403 high-nutrient low-chlorophyll regions using neural networks and wavelet coherence analysis, *Ocean Sci.*, 19,
1404 973–990, <https://doi.org/10.5194/os-19-973-2023>, 2023.
- 1405
1406 Bates, N., Astor, Y., Church, M., Currie, K., Dore, J., González-Dávila, M., Lorenzoni, L., Muller-Karger, F.,
1407 Olafsson, J., and Santa-Casiano, M.: A Time-Series View of Changing Ocean Chemistry Due to Ocean Uptake
1408 of Anthropogenic CO₂ and Ocean Acidification, *Oceanography*, 27, 126–141,
1409 <https://doi.org/10.5670/oceanog.2014.16>, 2014.
- 1410
1411 Beaufort, L., Probert, I., de Garidel-Thoron, T., Bendif, E.M., Ruiz-Pino, D., Metzl, N., Goyet, C., Buchet, N.,
1412 Coupel, P., Grelaud, M., Rost, B., Rickaby, R.E.M., and de Vargas C.: Sensitivity of coccolithophores to
1413 carbonate chemistry and ocean acidification. *Nature*, doi:10.1038/nature10295. 2011
- 1414
1415 Bennington, V., Gloege, L., and McKinley, G. A.: Variability in the global ocean carbon sink from 1959 to 2020
1416 by correcting models with observations. *Geophysical Research Letters*, 49, e2022GL098632.
1417 <https://doi.org/10.1029/2022GL098632>, 2022
- 1418
1419 Benoiston, A.-S., Ibarbalz, F. M., Bittner, L., Guidi, L., Jahn, O., Dutkiewicz, S., and Bowler, C.: The evolution
1420 of diatoms and their biogeochemical functions. *Phil. Trans. R. Soc. B* 372: 20160397.
1421 <http://dx.doi.org/10.1098/rstb.2016.0397>, 2017
- 1422
1423 Bopp, L., Resplandy, L., Orr, J. C., Doney, S. C., Dunne, J. P., Gehlen, M., Halloran, P., Heinze, C., Ilyina, T.,
1424 Séférian, R., Tjiputra, J., and Vichi, M.: Multiple stressors of ocean ecosystems in the 21st century: projections
1425 with CMIP5 models, *Biogeosciences*, 10, 6225–6245, <https://doi.org/10.5194/bg-10-6225-2013>, 2013.
- 1426
1427 Brady, R. X., Maltrud, M. E., Wolfram, P. J., Drake, H. F., and Lovenduski, N. S.: The influence of ocean
1428 topography on the upwelling of carbon in the Southern Ocean. *Geophysical Research Letters*, 48,
1429 e2021GL095088. <https://doi.org/10.1029/2021GL095088>, 2021
- 1430
1431 Brandon, M., Goyet, C., Touratier, F., Lefèvre, N., Kestenare, E., and Morrow, R.: Spatial and temporal
1432 variability of the physical, carbonate and CO₂ properties in the Southern Ocean surface waters during austral
1433 summer (2005–2019), *Deep-Sea Research Part I*, <https://doi.org/10.1016/j.dsr.2022.103836>, 2022
- 1434
1435 Burger, F. A., John, J. G., and Frölicher, T. L.: Increase in ocean acidity variability and extremes under
1436 increasing atmospheric CO₂, *Biogeosciences*, 17, 4633–4662, <https://doi.org/10.5194/bg-17-4633-2020>, 2020
- 1437
1438 Bushinsky, S. M., Landschützer, P., Rödenbeck, C., Gray, A. R., Baker, D., Mazloff, M. R., Resplandy, L.,
1439 Johnson, K. S., and Sarmiento, J. L.: Reassessing Southern Ocean air-sea CO₂ flux estimates with the addition of
1440 biogeochemical float observations. *Global Biogeochemical Cycles*, 33. doi: 10.1029/2019GB006176, 2019
- 1441
1442 Caldeira, K., and Wickett, M.: Anthropogenic carbon and ocean pH. *Nature*, 425, 365. doi: 10.1038/425365a,
1443 2003
- 1444
1445 Canadell, J. G., Monteiro, P. M. S., Costa, M. H., Cotrim da Cunha, L., Cox, P. M., Eliseev, A. V., Henson, S.,
1446 Ishii, M., Jaccard, S., Koven, C., Lohila, A., Patra, P. K., Piao, S., Rogelj, J., Syampungani, S., Zaehle, S., and
1447 Zickfeld, K.: Global Carbon and other Biogeochemical Cycles and Feedbacks, in: *Climate Change 2021: The*
1448 *Physical Science Basis. Contribution of Working Group I to the Sixth Assessment Report of the*
1449 *Intergovernmental Panel on Climate Change*, edited by: Masson-Delmotte, V., Zhai, P., Pirani, A., Connors, S.
1450 L., Péan, C., Berger, S., Caud, N., Chen, Y., Goldfarb, L., Gomis, M. I., Huang, M., Leitzell, K., Lonnoy, E.,
1451 Matthews, J. B. R., Maycock, T. K., Waterfield, T., Yelekçi, O., Yu, R., and Zhou, B., Cambridge University
1452 Press, Cambridge, United Kingdom and New York, NY, USA, 673–816, doi:10.1017/9781009157896, 2021
- 1453



- 1454 Carpenter, J. H.: The Accuracy of the Winkler Method for Dissolved Oxygen Analysis, *Limnol. Oceanogr.*, 10,
1455 135–140, <https://doi.org/10.4319/lo.1965.10.1.0135>, 1965.
1456
1457 Carter, B. R., Williams, N. L., Gray, A. R., and Feely, R. A.: Locally interpolated alkalinity regression for global
1458 alkalinity estimation. *Limnol. Oceanogr.: Methods* 14: 268–277. doi:10.1002/lom3.10087, 2016
1459
1460 Carter, B. R., Feely, R. A., Williams, N. L., Dickson, A. G., Fong, M. B., and Takeshita, Y.: Updated methods
1461 for global locally interpolated estimation of alkalinity, pH, and nitrate. *Limnology and Oceanography: Methods*,
1462 16: 119-131. doi: 10.1002/lom3.10232, 2018
1463
1464 Carter, B. R., Feely, R. A., Wanninkhof, R., Kouketsu, S., Sonnerup, R. E., Pardo, P. C., et al: Pacific
1465 anthropogenic carbon between 1991 and 2017. *Global Biogeochemical Cycles*, 33, 597–617.
1466 <https://doi.org/10.1029/2018GB006154>, 2019
1467
1468 Chapman, C., Mcc Hogg, A., Kiss, A., and Rintoul, S.: The dynamics of Southern Ocean storm tracks. *Journal of*
1469 *Physical Oceanography*, 45 (3), pp.884 - 903. 10.1175/JPO-D-14-0075.1, 2015
1470
1471 Chau, T. T. T., Gehlen, M., and Chevallier, F.: A seamless ensemble-based reconstruction of surface ocean $p\text{CO}_2$
1472 and air–sea CO_2 fluxes over the global coastal and open oceans, *Biogeosciences*, 19, 1087–1109,
1473 <https://doi.org/10.5194/bg-19-1087-2022>, 2022.
1474
1475 Chen, H., Haumann, F. A., Talley, L. D., Johnson, K. S., and Sarmiento, J. L.: The deep ocean's carbon exhaust.
1476 *Global Biogeochemical Cycles*. doi: <https://doi.org/10.1002/essoar.10507757.1>, 2022
1477
1478 Cheng, L. J., Abraham, J., Zhu, J., Trenberth, K. E., Fasullo, J., Boyer, T., Locarnini, R., Zhang, B., Yu, F. J.,
1479 Wan, L. Y., Chen, X. R., Song, X. Z., Liu, Y. L., and Mann, M. E.: Record-setting ocean warmth continued in
1480 2019, *Adv. Atmos. Sci*, 37, 137-142. <https://doi.org/10.1007/s00376-020-9283-7>, 2020a
1481
1482 Cheng L., K. E. Trenberth, N. Gruber, J. P. Abraham, J. Fasullo, G. Li, M. E. Mann, X. Zhao, Jiang Zhu:
1483 Improved estimates of changes in upper ocean salinity and the hydrological cycle. *Journal of Climate*. doi:
1484 <https://doi.org/10.1175/JCLI-D-20-0366.1>, 2020b
1485
1486 Copin-Montégut, C.: A new formula for the effect of temperature on the partial pressure of CO_2 in seawater.
1487 *Marine Chemistry*, 25, 29-37. [https://doi.org/10.1016/0304-4203\(88\)90012-6](https://doi.org/10.1016/0304-4203(88)90012-6), 1988.
1488
1489 Copin-Montégut, C.: A new formula for the effect of temperature on the partial pressure of CO_2 in seawater.
1490 Corrigendum. *Marine Chemistry*, 27, 143-144. [https://doi.org/10.1016/0304-4203\(89\)90034-0](https://doi.org/10.1016/0304-4203(89)90034-0), 1989.
1491
1492 Coverly, S. C., Aminot, A., and R. Kérouel: Nutrients in Seawater Using Segmented Flow Analysis, In: *Practical*
1493 *Guidelines for the Analysis of Seawater*, Edited by: Oliver Wurl, CRC Press,
1494 <https://doi.org/10.1201/9781420073072>, 2009
1495
1496 Daniault, N., and Ménard, Y.: Eddy kinetic energy distribution in the Southern Ocean from altimetry and FGGE
1497 drifting buoys, *J. Geophys. Res.*, 90 (C6), 11877–11889, doi:10.1029/JC090iC06p11877, 1985
1498
1499 Demuynek, P., Tyrrell, T., Naveira Garabato, A., Moore, M. C., and Martin, A. P.: Spatial variations in silicate-
1500 to-nitrate ratios in Southern Ocean surface waters are controlled in the short term by physics rather than biology,
1501 *Biogeosciences*, 17, 2289–2314, <https://doi.org/10.5194/bg-17-2289-2020>, 2020.
1502
1503 DeVries, T., Yamamoto, K., Wanninkhof, R., Gruber, N., Hauck, J., Müller, J. D., et al: Magnitude, trends, and
1504 variability of the global ocean carbon sink from 1985-2018. *Global Biogeochemical Cycles*, 37,
1505 e2023GB007780, doi:10.1029/2023GB007780, 2023.
1506



- 1507 Dickson, A. G.: Standard potential of the reaction: $\text{AgCl(s)} + \frac{1}{2}\text{H}_2(\text{g}) = \text{Ag(s)} + \text{HCl(aq)}$, and the standard
1508 acidity constant of the ion HSO_4^- in synthetic sea water from 273.15 to 318.15 K. *J. Chem. Thermodyn.* **22**:
1509 113–127. doi:10.1016/0021-9614(90)90074-Z, 1990
1510
1511 Dickson, A. G., Sabine, C. L. and Christian, J. R. (Eds.): Guide to Best Practices for Ocean CO₂ Measurements.
1512 *PICES Special Publication* 3, 191 pp., [https://www.ncei.noaa.gov/access/ocean-carbon-acidification-data-](https://www.ncei.noaa.gov/access/ocean-carbon-acidification-data-system/oceans/Handbook_2007.html)
1513 [system/oceans/Handbook_2007.html](https://www.ncei.noaa.gov/access/ocean-carbon-acidification-data-system/oceans/Handbook_2007.html), 2007
1514
1515 Dlugokencky, E. and Tans, P.: Trends in atmospheric carbon dioxide, National Oceanic & Atmospheric
1516 Administration, Earth System Research Laboratory (NOAA/ESRL), available at: [http://](http://www.esrl.noaa.gov/gmd/ccgg/trends/global.html)
1517 www.esrl.noaa.gov/gmd/ccgg/trends/global.html, (last access: 8 January 2022), 2022
1518
1519 Doney, S. C., Fabry, V. J., Feely, R. A., and Kleypas, J. A.: Ocean Acidification: The Other CO₂ Problem,
1520 *Annu. Rev. Mar. Sci.*, **1**, 169–192, <https://doi.org/10.1146/annurev.marine.010908.163834>, 2009.
1521
1522 Doney, S. C., Ruckelshaus, M., Duffy, J. E., Barry, J. P., Chan, F., English, C. A., Galindo, H. M., Grebmeier, J.
1523 M., Hollowed, A. B., Knowlton, N., Polovina, J., Rabalais, N. N., Sydeman, W. J., and Talley, L. D.: Climate
1524 change impacts on marine ecosystems, *Annu. Rev. Mar. Sci.*, **4**, 11–37. 10.1146/annurev-marine-041911-
1525 111611, 2012.
1526
1527 Dove, L. A., Balwada D., Thompson, A. F., and Gray, A. R.: Enhanced ventilation in energetic regions of the
1528 Antarctic Circumpolar Current. *Geophys. Res. Lett.* **49**(13):e2021GL097574,
1529 <https://doi.org/10.1029/2021GL097574>. 2022.
1530
1531 Duncan, R.J., Nielsen, D.A., Sheehan, C.E., Deppeler, S., Hancock, A.M., Schulz, K.G., Davidson, A.T. and
1532 Petrou, K.: Ocean acidification alters the nutritional value of Antarctic diatoms. *New Phytol*, **233**: 1813-1827.
1533 <https://doi-org.insu.bib.cnrs.fr/10.1111/nph.17868>, 2022
1534
1535 Durack, P. J. and Wijffels, S. E.: Fifty-year trends in global ocean salinities and their relationship to broad-scale
1536 warming. *J. Climate*, **23**, 4342–4362, <https://doi.org/10.1175/2010JCLI3377.1>, 2010
1537
1538 Fabry, V. J., Seibel, B. A., Feely, R. A., and Orr, J. C.: Impacts of ocean acidification on marine fauna and
1539 ecosystem processes. – *ICES Journal of Marine Science*, **65**: 414–432, doi: 10.1093/icesjms/fsn048, 2008
1540
1541 Fassbender, A. J., Schlunegger, S., Rodgers, K. B., and Dunne, J. P.: Quantifying the role of seasonality in the
1542 marine carbon cycle feedback: An ESM2M case study. *Global Biogeochemical Cycles*, **36**, e2021GB007018.
1543 doi:10.1029/2021GB007018, 2022
1544
1545 Fay, A. R., Munro, D. R., McKinley, G. A., Pierrot, D., Sutherland, S. C., Sweeney, C., and Wanninkhof, R.:
1546 Updated climatological mean delta fCO₂ and net sea–air CO₂ flux over the global open ocean regions, *Earth*
1547 *Syst. Sci. Data Discuss.* [preprint], <https://doi.org/10.5194/essd-2023-429>, in review, 2023.
1548
1549 Fox-Kemper, B., Hewitt, H. T. , Xiao, C., Adalgeirsdóttir, G., Drijfhout, S. S., Edwards, T. L., Golledge, N. R.,
1550 Hemer, M., Kopp, R. E., Krinner, G., Mix, A., Notz, D., Nowicki, S., Nurhati, I. S., Ruiz, L., Sallée, J.-B.,
1551 Slangen, A. B. A., and Yu, Y.: *Climate Change 2021: The Physical Science Basis. Contribution of Working*
1552 *Group I to the Sixth Assessment Report of the Intergovernmental Panel on Climate Change*, chapter Ocean,
1553 Cryosphere and Sea Level Change, pages 1211-1362. Cambridge University Press, United Kingdom and New
1554 York, NY, USA, August 2021. doi:10.1017/9781009157896.
1555
1556 Fontela, M., Vélo, A., Gilcoto, M., and Pérez, F.: Anthropogenic CO₂ and Ocean Acidification in Argentine
1557 Basin Water Masses over Almost Five Decades of Observations. *Science of The Total Environment*, **779**.
1558 <https://doi.org/10.1016/j.scitotenv.2021.146570>, 2021
1559



- 1560 Franco, A. C., Ianson, D., Ross, T., Hamme, R. C., Monahan, A. H., Christian, J. R., et al.: Anthropogenic and
1561 climatic contributions to observed carbon system trends in the northeast Pacific. *Global Biogeochemical Cycles*,
1562 35, e2020GB006829. Doi: 10.1029/2020GB006829, 2021
1563
- 1564 Friedlingstein, P., O'Sullivan, M., Jones, M. W., Andrew, R. M., Gregor, L., Hauck, J., Le Quéré, C., Luijkx, I.
1565 T., Olsen, A., Peters, G. P., Peters, W., Pongratz, J., Schwingshackl, C., Sitch, S., Canadell, J. G., Ciais, P.,
1566 Jackson, R. B., Alin, S. R., Alkama, R., Arneeth, A., Arora, V. K., Bates, N. R., Becker, M., Bellouin, N., Bittig,
1567 H. C., Bopp, L., Chevallier, F., Chini, L. P., Cronin, M., Evans, W., Falk, S., Feely, R. A., Gasser, T., Gehlen,
1568 M., Gkritzalis, T., Gloege, L., Grassi, G., Gruber, N., Gürses, Ö., Harris, I., Hefner, M., Houghton, R. A., Hurtt,
1569 G. C., Iida, Y., Ilyina, T., Jain, A. K., Jersild, A., Kadono, K., Kato, E., Kennedy, D., Klein Goldewijk, K.,
1570 Knauer, J., Korsbakken, J. I., Landschützer, P., Lefèvre, N., Lindsay, K., Liu, J., Liu, Z., Marland, G., Mayot, N.,
1571 McGrath, M. J., Metz, N., Monacci, N. M., Munro, D. R., Nakaoka, S.-I., Niwa, Y., O'Brien, K., Ono, T.,
1572 Palmer, P. I., Pan, N., Pierrot, D., Pockock, K., Poulter, B., Resplandy, L., Robertson, E., Rödenbeck, C.,
1573 Rodriguez, C., Rosan, T. M., Schwinger, J., Séférian, R., Shutler, J. D., Skjelvan, I., Steinhoff, T., Sun, Q.,
1574 Sutton, A. J., Sweeney, C., Takao, S., Tanhua, T., Tans, P. P., Tian, X., Tian, H., Tilbrook, B., Tsujino, H.,
1575 Tubiello, F., van der Werf, G. R., Walker, A. P., Wanninkhof, R., Whitehead, C., Willstrand Wranne, A.,
1576 Wright, R., Yuan, W., Yue, C., Yue, X., Zaehle, S., Zeng, J., and Zheng, B.: Global Carbon Budget 2022, *Earth*
1577 *Syst. Sci. Data*, 14, 4811–4900, <https://doi.org/10.5194/essd-14-4811-2022>, 2022.
1578
- 1579 Frölicher, T. L., Sarmiento, J. L., Paynter, D. J., Dunne, J. P., Krasting, J. P., and Winton, M.: Dominance of the
1580 southern ocean in anthropogenic carbon and heat uptake in CMIP5 models. *Journal of Climate*, 28(2), 862–886.
1581 <https://doi.org/10.1175/JCLI-D-14-00117.1>, 2015
1582
- 1583 Fu, W., Randerson, J. T., and Moore, J. K.: Climate change impacts on net primary production (NPP) and export
1584 production (EP) regulated by increasing stratification and phytoplankton community structure in the CMIP5
1585 models, *Biogeosciences*, 13, 5151–5170, <https://doi.org/10.5194/bg-13-5151-2016>, 2016.
1586
- 1587 Gallego, M. A., Timmermann, A., Friedrich, T., and Zeebe, R. E.: Drivers of future seasonal cycle changes in
1588 oceanic $p\text{CO}_2$, *Biogeosciences*, 15, 5315–5327, <https://doi.org/10.5194/bg-15-5315-2018>, 2018.
1589
- 1590 Gangstø, R., Gehlen, M., Schneider, B., Bopp, L., Aumont, O., and Joos, F.: Modeling the marine aragonite
1591 cycle: changes under rising carbon dioxide and its role in shallow water CaCO_3 dissolution, *Biogeosciences*, 5,
1592 1057–1072, <https://doi.org/10.5194/bg-5-1057-2008>, 2008.
1593
- 1594 Gardner J., Peck, V. L., Bakker, D. C. E., Tarling, G. A. and Manno, C.: Contrasting life cycles of Southern
1595 Ocean pteropods alter their vulnerability to climate change. *Front. Mar. Sci.* 10:1118570.
1596 doi: 10.3389/fmars.2023.1118570, 2023
1597
- 1598 Gooya, P., Swart, N. C., and Hamme, R. C.: Time-varying changes and uncertainties in the CMIP6 ocean carbon
1599 sink from global to local scale, *Earth Syst. Dynam.*, 14, 383–398, <https://doi.org/10.5194/esd-14-383-2023>,
1600 2023.
1601
- 1602 Gray, A., Johnson, K. S., Bushinsky, S. M., Riser, S. C., Russell, J. L., Talley, L. D., et al.: Autonomous
1603 biogeochemical floats detect significant carbon dioxide outgassing in the high-latitude Southern Ocean.
1604 *Geophysical Research Letters*, 45, 9049–9057. <https://doi.org/10.1029/2018GL078013>, 2018.
1605
- 1606 Gray, A., R.: The Four-Dimensional Carbon Cycle of the Southern Ocean. *Annu. Rev. Mar. Sci.* 16:23.1–23.28.
1607 <https://doi.org/10.1146/annurev-marine-041923-104057>, 2024.
1608
- 1609 Gregor, L., Kok, S., and Monteiro, P. M. S.: Interannual drivers of the seasonal cycle of CO_2 in the Southern
1610 Ocean, *Biogeosciences*, 15, 2361–2378, <https://doi.org/10.5194/bg-15-2361-2018>, 2018.
1611



- 1612 Gruber, N., Clement, D., Carter, B. R., Feely, R. A., van Heuven, S., Hoppema, M., Ishii, M., Key, R. M.,
1613 Kozyr, A., Lauvset, S. K., Lo Monaco, C., Mathis, J. T., Murata, A., Olsen, A., Perez, F. F., Sabine, C. L.,
1614 Tanhua, T., and Wanninkhof, R.: The oceanic sink for anthropogenic CO₂ from 1994 to 2007, *Science* vol. 363
1615 (issue 6432), pp. 1193–1199. DOI: 10.1126/science.aau5153, 2019a.
1616
1617 Gruber, N., Clement, D., Carter, B. R., Feely, R. A., Heuven, S., van, Hoppema, M., Ishii, M., Key, R. M.,
1618 Kozyr, A., Lauvset, S. K., Lo Monaco, C., Mathis, J. T., Murata, A., Olsen, A., Perez, F. F., Sabine, C. L.,
1619 Tanhua, T., and Wanninkhof, R.: The oceanic sink for anthropogenic CO₂ from 1994 to 2007 – the data (NCEI
1620 Accession 0186034), NOAA National Centers for Environmental Information [data set],
1621 <https://doi.org/10.25921/wdn2-pt10>, 2019b.
1622
1623 Gruber, N., Landschützer, P., and Lovenduski, N. S.: The Variable Southern Ocean Carbon Sink, *Annu.*
1624 *Rev. Mar. Sci.*, Vol. 11, doi:10.1146/annurev-marine-121916-063407, 2019c.
1625
1626 Gu, Y., Katul, G. G., & Cassar, N. Multiscale temporal variability of the global air-sea CO₂ flux anomaly.
1627 *Journal of Geophysical Research: Biogeosciences*, 128, e2022JG006934. <https://doi.org/10.1029/2022JG006934>,
1628 2023
1629
1630 Hauri, C., Friedrich, T., and Timmermann, A.: Abrupt onset and prolongation of aragonite undersaturation
1631 events in the Southern Ocean, *Nature Climate Change*, doi:10.1038/nclimate2844, 2015.
1632
1633 Hauck J., Hoppema, M., Bellerby, R. G. J., Völker, C., and Wolf-Gladrow, D.: Data-based estimation of
1634 anthropogenic carbon and acidification in the Weddell Sea on a decadal timescale. *J. Geophys. Res.* 115,
1635 C03004. doi:10.1029/2009jc005479, 2010
1636
1637 Hauck, J., Völker, C., Wang, T., Hoppema, M., Losch, M., and Wolf-Gladrow, D. A.: Seasonally different
1638 carbon flux changes in the Southern Ocean in response to the southern annular mode. *Global Biogeochemical*
1639 *Cycles*, 27(4), 1236–1245. <https://doi.org/10.1002/2013GB004600>, 2013
1640
1641 Hauck, J., Volker, C., Wolf-Gladrow, D. A., Laufkotter, C., Vogt, M., Aumont, O., et al.: On the Southern
1642 Ocean CO₂ uptake and the role of the biological carbon pump in the 21st century. *Global Biogeochemical*
1643 *Cycles*, 29(9), 1451–1470. <https://doi.org/10.1002/2015GB005140>, 2015
1644
1645 Hauck, J., Zeising, M., Le Quéré, C., Gruber, N., Bakker, D. C. E., Bopp, L., Chau, T. T., Gürses, Ö., Ilyina, T.,
1646 Landschützer, P., Lenton, A., Resplandy, L., Rödenbeck, C., Schwinger, J., and Séférian, R.: Consistency and
1647 challenges in the ocean carbon sink estimate for the Global Carbon Budget. *Front. Mar. Sci.* doi:
1648 10.3389/fmars.2020.571720, 2020
1649
1650 Hauck, J., Nissen, C., Landschützer, P., Rödenbeck, C., Bushinsky, S., and Olsen, A.: Sparse observations
1651 induce large biases in estimates of the global ocean CO₂ sink: an ocean model subsampling experiment. *Phil.*
1652 *Trans. R. Soc. A* 381: 20220063. <https://doi.org/10.1098/rsta.2022.0063>, 2023
1653
1654 Hersbach, H., Bell, B., Berrisford, P., Hirahara, S., Horányi, A., Muñoz-Sabater, J., Nicolas, J., Peubey, C.,
1655 Radu, R., Schepers, D., Simmons, A., Soci, C., Abdalla, S., Abellan, X., Balsamo, G., Bechtold, P., Biavati, G.,
1656 Bidlot, J., Bonavita, M., De Chiara, G., Dahlgren, P., Dee, D., Diamantakis, M., Dragani, R., Flemming, J.,
1657 Forbes, R., Fuentes, M., Geer, A., Haimberger, L., Healy, S., Hogan, R. J., Hólm, E., Janisková, M., Keeley, S.,
1658 Laloyaux, P., Lopez, P., Lupu, C., Radnoti, G., de Rosnay, P., Rozum, I., Vamborg, F., Villaume, S., and
1659 Thépaut, J.-N.: The ERA5 global reanalysis, *Q. J. Roy. Meteor. Soc.*, 146, 1999–2049,
1660 <https://doi.org/10.1002/qj.3803>, 2020.
1661
1662 Hoppema, M., Bakker, K., van Heuven, S. M. A. C., van Ooijen, J. C., and de Baar, H. J. W.: Distributions,
1663 trends and inter-annual variability of nutrients along a repeat section through the Weddell Sea (1996–2011).
1664 *Marine Chemistry*, 177, 545–553. <https://doi.org/10.1016/j.marchem.2015.08.007>, 2015



- 1665
1666 Hunt, B. P. V., Pakhomov, E. A., Hosie, G. W., Siegel, V., Ward, P., and Bernard, K.: Pteropods in Southern
1667 Ocean ecosystems, *Progress in Oceanography*, Volume 78, Issue 3, Pages 193-221,
1668 <https://doi.org/10.1016/j.pocean.2008.06.001>, 2008
1669
1670 Iida, T., Odate, T., and Fukuchi, M.: Long-term trends of nutrients and apparent oxygen utilization south of the
1671 polar front in Southern Ocean intermediate water from 1965 to 2008. *PLoS One*, 8, e71766.
1672 <https://doi.org/10.1371/journal.pone.0071766>, 2013
1673
1674 Iida, Y., Takatani, Y., Kojima, A., and Ishii, M.: Global trends of ocean CO₂ sink and ocean acidification: an
1675 observation based reconstruction of surface ocean inorganic carbon variables, *J. Oceanogr.*, 77, 323–358,
1676 <https://doi.org/10.1007/s10872-020-00571-5>, 2021.
1677
1678 IPCC: Changing Ocean, Marine Ecosystems, and Dependent Communities. in *The Ocean and Cryosphere in a*
1679 *Changing Climate 447–588* (Cambridge University Press, 2022). doi:10.1017/9781009157964.007, 2022
1680
1681 Ito, T., Minobe, S., Long, M. C., Deutsch, C. Upper ocean O₂ trends: 1958–2015. *Geophysical Research Letters*
1682 44, 4214–4223, <https://doi.org/10.1002/2017GL073613>, 2017.
1683
1684 Jabaud-Jan, A., Metzl, N., Brunet, C., Poisson, A., and Schauer, B.: Variability of the Carbon Dioxide System in
1685 the Southern Indian Ocean (20°S-60°S): the impact of a warm anomaly in austral summer 1998. *Global*
1686 *Biogeochemical Cycles*, Vol. 18, No. 1, GB1042,10.1029/2002GB002017, 2004
1687
1688 Jeandel, C., Ruiz-Pino, D., Gjata, E., Poisson, A., Brunet, C., Charriaud, E., Dehairs, F., Delille, D., Fiala, M.,
1689 Fravalo, C., Miquel, J. C., Park, Y. H., Pondaven, P., Quéguiner, B., Razouls, S., Schauer, B., and Tréguer, P.:
1690 KERFIX, a time-series station in the Southern Ocean: a presentation. *Journal of Marine Systems*, 17, 1-4, 555-
1691 569., [https://doi.org/10.1016/S0924-7963\(98\)00064-5](https://doi.org/10.1016/S0924-7963(98)00064-5), 1998
1692
1693 Jiang, L.-Q., Feely, R. A., Carter, B. R., Greeley, D. J., Gledhill, D. K., and Arzayus K. M.: Climatological
1694 distribution of aragonite saturation state in the global oceans, *Global Biogeochem. Cycles*, 29, 1656–1673,
1695 doi:10.1002/2015GB005198, 2015.
1696
1697 Jiang, L.-Q., Carter, B. R., Feely, R. A., Lauvset, S. K., and Olsen, A.: Surface ocean pH and buffer capacity:
1698 past, present and future. *Sci Rep* 9, 18624, doi:10.1038/s41598-019-55039-4, 2019
1699
1700 Jiang, L.-Q., Dunne, J., Carter, B. R., Tjiputra, J. F., Terhaar, J., Sharp, J. D., et al.: Global surface ocean
1701 acidification indicators from 1750 to 2100. *Journal of Advances in Modeling Earth Systems*, 15,
1702 e2022MS003563. <https://doi.org/10.1029/2022MS003563>, 2023
1703
1704 Joos, F., Hameau, A., Frölicher, T. L., and Stephenson, D. B.: Anthropogenic attribution of the increasing
1705 seasonal amplitude in surface ocean pCO₂. *Geophysical Research Letters*, 50, e2023GL102857.
1706 <https://doi.org/10.1029/2023GL102857>, 2023
1707
1708 Jouandet, M.-P., Blain, S., Metzl, N., Brunet, C., Trull, T., and Obernosterer, I.: A seasonal carbon budget for a
1709 naturally iron fertilized bloom (Kerguelen I. Southern Ocean). *Deep-Sea Res II*, 55, 856-867.
1710 doi:10.1016/j.dsr2.2007.12.037, 2008
1711
1712 Jouandet M.P., Blain, S., Metzl, N., and Mongin, C.: Interannual variability of the net community production and
1713 air-sea CO₂ flux in a natural iron fertilization region of the Southern Ocean. (Kerguelen plateau), *Antarctic*
1714 *Science*, doi:10.1017/S0954102011000411, 2011
1715



- 1716 Kane, A., Moulin, C., Thiria, S., Bopp, L., Berrada, M., Tagliabue, A., Crépon, M., Aumont, O., and Badran, F.:
1717 Improving the parameters of a global ocean biogeochemical model via variational assimilation of in situ data at
1718 five time series stations, *J. Geophys. Res.*, 116, C06011, doi:10.1029/2009JC006005, 2011
1719
- 1720 Kawaguchi, S., Ishida, A., King, R. et al.: Risk maps for Antarctic krill under projected Southern Ocean
1721 acidification. *Nature Clim. Change*, 3, 843–847, DOI: 10.1038/NCLIMATE1937, 2013
1722
- 1723 Keeling, C. D., and Waterman, L. S.: Carbon dioxide in surface ocean waters: 3. Measurements on Lusiad
1724 Expedition 1962–1963, *J. Geophys. Res.*, 73(14), 4529– 4541, doi:10.1029/JB073i014p04529, 1968
1725
- 1726 Keppler, L. and Landschützer, P.: Regional Wind Variability Modulates the Southern Ocean Carbon Sink, *Sci.*
1727 *Rep.-UK*, 9, 7384, <https://doi.org/10.1038/s41598-019-43826-y>, 2019.
1728
- 1729 Kessler, A. and Tjiputra, J.: The Southern Ocean as a constraint to reduce uncertainty in future ocean carbon
1730 sinks, *Earth Syst. Dynam.*, 7, 295–312, doi:10.5194/esd-7-295-2016, 2016.
1731
- 1732 Key, R. M., Kozyr, A., Sabine, C. L., Lee, K., Wanninkhof, R., Bullister, J. L., Feely, R. A., Millero, F. J.,
1733 Mordy, C., and Peng, T. H.: A global ocean carbon climatology: Results from Global Data Analysis Project
1734 (GLODAP), *Global Biogeochemical Cycles*, 18, GB4031, <https://doi.org/10.1029/2004GB002247>, 2004.
1735
- 1736 Khatiwala, S., Tanhua, T., Mikaloff Fletcher, S., Gerber, M., Doney, S. C., Graven, H. D., Gruber, N.,
1737 McKinley, G. A., Murata, A., Ríos, A. F., and Sabine, C. L.: Global ocean storage of anthropogenic carbon,
1738 *Biogeosciences*, 10, 2169–2191, <https://doi.org/10.5194/bg-10-2169-2013>, 2013.
1739
- 1740 King, J., Anchukaitis, K. J., Allen, K. et al.: Trends and variability in the Southern Annular Mode over the
1741 Common Era. *Nat Commun* 14, 2324, <https://doi-org.insu.bib.cnrs.fr/10.1038/s41467-023-37643-1>, 2023
1742
- 1743 Krumhardt, K. M., Long, M. C., Sylvester, Z. T. and Petrik, C. M.: Climate drivers of Southern Ocean
1744 phytoplankton community composition and potential impacts on higher trophic levels. *Front. Mar. Sci.*
1745 9:916140. doi: 10.3389/fmars.2022.916140, 2022
1746
- 1747 Kwiatkowski, L., and Orr, J. C.: Diverging seasonal extremes for ocean acidification during the twenty-first
1748 century. *Nature Climate Change*, 8(2), 141–145. <https://doi.org/10.1038/s41558-017-0054-0>, 2018
1749
- 1750 Kwiatkowski, L., Torres, O., Bopp, L., Aumont, O., Chamberlain, M., Christian, J. R., Dunne, J. P., Gehlen, M.,
1751 Ilyina, T., John, J. G., Lenton, A., Li, H., Lovenduski, N. S., Orr, J. C., Palmieri, J., Santana-Falcón, Y.,
1752 Schwinger, J., Séférian, R., Stock, C. A., Tagliabue, A., Takano, Y., Tjiputra, J., Toyama, K., Tsujino, H.,
1753 Watanabe, M., Yamamoto, A., Yool, A., and Ziehn, T.: Twenty-first century ocean warming, acidification,
1754 deoxygenation, and upper-ocean nutrient and primary production decline from CMIP6 model projections,
1755 *Biogeosciences*, 17, 3439–3470, <https://doi.org/10.5194/bg-17-3439-2020>, 2020.
1756
- 1757 Lange, N., Fiedler, B., Álvarez, M., Benoit-Cattin, A., Benway, H., Buttigieg, P. L., Coppola, L., Currie, K.,
1758 Flecha, S., Honda, M., Huertas, I. E., Lauvset, S. K., Muller-Karger, F., Körtzinger, A., O'Brien, K. M.,
1759 Ólafsdóttir, S. R., Pacheco, F. C., Rueda-Roa, D., Skjelvan, I., Wakita, M., White, A., and Tanhua, T.: Synthesis
1760 Product for Ocean Time-Series (SPOTS) – A ship-based biogeochemical pilot, *Earth Syst. Sci. Data Discuss.*
1761 [preprint], <https://doi.org/10.5194/essd-2023-238>, in review, 2023.
1762
- 1763 Landschützer, P., Gruber, N., Haumann, F. A., Rödenbeck, C., Bakker, D. C. E., Van Heuven, S., Hoppema, M.,
1764 Metz, N., Sweeney, C., Takahashi, T., Tilbrook, B., and Wanninkhof, R.: The reinvigoration of the Southern
1765 Ocean carbon sink, *Science*, 349, 1221–1224, <https://doi.org/10.1126/science.aab2620>, 2015.
1766



- 1767 Landschützer, P., Gruber, N., Bakker, D. C. E., Stemmler, I., and Six, K. D.: Strengthening seasonal marine CO₂
1768 variations due to increasing atmospheric CO₂. *Nature Climate Change*, 8(2), 146–150.
1769 <https://doi.org/10.1038/s41558-017-0057-x>, 2018
1770
- 1771 Lauvset, S. K., Gruber, N., Landschützer, P., Olsen, A., and Tjiputra, J.: Trends and drivers in global surface
1772 ocean pH over the past 3 decades. *Biogeosciences*, 12, 1285–1298, doi:10.5194/bg-12-1285-2015, 2015
1773
- 1774 Lauvset, S. K., Carter, B. R., Perez, F. F., Jiang, L.-Q., Feely, R. A., Velo, A., and Olsen, A.: Processes Driving
1775 Global Interior Ocean pH Distribution, *Global Biogeochem. Cycles*, 34, e2019GB006 229,
1776 <https://doi.org/10.1029/2019GB006229>, 2020.
1777
- 1778 Lauvset, S. K., Lange, N., Tanhua, T., Bittig, H. C., Olsen, A., Kozyr, A., Álvarez, M., Becker, S., Brown, P. J.,
1779 Carter, B. R., Cotrim da Cunha, L., Feely, R. A., van Heuven, S., Hoppema, M., Ishii, M., Jeansson, E.,
1780 Jutterström, S., Jones, S. D., Karlsen, M. K., Lo Monaco, C., Michaelis, P., Murata, A., Pérez, F. F., Pfeil, B.,
1781 Schirnack, C., Steinfeldt, R., Suzuki, T., Tilbrook, B., Velo, A., Wanninkhof, R., Woosley, R. J., and Key, R. M.:
1782 An updated version of the global interior ocean biogeochemical data product, GLODAPv2.2021, *Earth Syst. Sci.*
1783 *Data*, 13, 5565–5589, <https://doi.org/10.5194/essd-13-5565-2021>, 2021a.
1784
- 1785 Lauvset, Siv K.; Lange, Nico; Tanhua, Toste; Bittig, Henry C.; Olsen, Are; Kozyr, Alex; Álvarez, Marta;
1786 Becker, Susan; Brown, Peter J.; Carter, Brendan R.; Cotrim da Cunha, Leticia; Feely, Richard A.; van Heuven,
1787 Steven M. A. C.; Hoppema, Mario; Ishii, Masao; Jeansson, Emil; Jutterström, Sara; Jones, Steve D.; Karlsen,
1788 Maren K.; Lo Monaco, Claire; Michaelis, Patrick; Murata, Akihiko; Pérez, Fiz F.; Pfeil, Benjamin; Schirnack,
1789 Carsten; Steinfeldt, Reiner; Suzuki, Toru; Tilbrook, Bronte; Velo, Antón; Wanninkhof, Rik; Woosley, Ryan J.;
1790 Key, Robert M.: Global Ocean Data Analysis Project version 2.2021 (GLODAPv2.2021) (NCEI Accession
1791 0237935). [subset used GLODAPv2.2021_Indian_Ocean.cvs]. NOAA National Centers for Environmental
1792 Information. Dataset. <https://doi.org/10.25921/ttgg-n825>, Accessed 2/8/2021. 2021b.
1793
- 1794 Lee, K., Tong, L. T., Millero, F. J., Sabine, C. L., Dickson, A. G., Goyet, C., Park, G. H., Wanninkhof, R., Feely,
1795 R. A., and Key, R. M.: Global relationships of total alkalinity with salinity and temperature in surface waters of
1796 the world's oceans. *Geophys. Res. Lett.* 33, L19605. doi:10.1029/2006GL027207, 2006.
1797
- 1798 Lenton, A., Codron, F., Bopp, L., Metzl, N., Cadule, P., Tagliabue, A., and Le Sommer, J.: Stratospheric ozone
1799 depletion reduces ocean carbon uptake and enhances ocean acidification. *Geophys. Res. Lett.*, 36, L12606, 2009.
1800 doi:10.1029/2009GL038227, 2009
1801
- 1802 Lenton, A., Tilbrook, B., Law, R. M., Bakker, D., Doney, S. C., Gruber, N., Ishii, M., Hoppema, M.,
1803 Lovenduski, N. S., Matear, R. J., McNeil, B. I., Metzl, N., Mikaloff Fletcher, S. E., Monteiro, P. M. S.,
1804 Rödenbeck, C., Sweeney, C., and Takahashi, T.: Sea–air CO₂ fluxes in the Southern Ocean for the period 1990–
1805 2009, *Biogeosciences*, 10, 4037–4054, <https://doi.org/10.5194/bg-10-4037-2013>, 2013.
1806
- 1807 Le Quéré, C., Rödenbeck, C., Buitenhuis, E. T., Conway, T. J., Langenfelds, R., Gomez, A., Labuschagne, C.,
1808 Ramonet, M., Nakazawa, T., Metzl, N., Gillett, N., and Heimann, M.: Saturation of the Southern Ocean CO₂
1809 Sink Due to Recent Climate Change, *Science*, 316, 1735–1738, <https://doi.org/10.1126/science.1136188>, 2007.
1810
- 1811 Lerner, P., Romanou, A., Kelley, M., Romanski, J., Ruedy, R., and Russell, G.: Drivers of air–sea CO₂ flux
1812 seasonality and its long-term changes in the NASA-GISS model CMIP6 submission. *Journal of Advances in*
1813 *Modeling Earth Systems*, 13, e2019MS002028. <https://doi.org/10.1029/2019MS002028>, 2021.
1814
- 1815 Leseurre, C., Lo Monaco, C., Reverdin, G., Metzl, N., Fin, J., Mignon, C., and Benito, L.: Summer trends and
1816 drivers of sea surface fCO₂ and pH changes observed in the southern Indian Ocean over the last two decades
1817 (1998–2019), *Biogeosciences*, 19, 2599–2625, <https://doi.org/10.5194/bg-19-2599-2022>, 2022.
1818



- 1819 Leung, S., Cabré, A., and Marinov, I.: A latitudinally banded phytoplankton response to 21st century climate
1820 change in the Southern Ocean across the CMIP5 model suite, *Biogeosciences*, 12, 5715–5734,
1821 <https://doi.org/10.5194/bg-12-5715-2015>, 2015.
- 1822
- 1823 Lewis E., and Wallace, D. W. R.: Program developed for CO₂ system calculations. ORNL/CDIAC-105. Carbon
1824 Dioxide Information Analysis Center, Oak Ridge National Laboratory, US. Dept. of Energy, Oak Ridge, TN,
1825 1998.
- 1826
- 1827 Lo Monaco, C., Goyet, C., Metzl, N., Poisson, A., and Touratier, F.: Distribution and inventory of anthropogenic
1828 CO₂ in the Southern Ocean: Comparison of three databased methods, *J. Geophys. Res.-Oceans*, 110, C09S02,
1829 <https://doi.org/10.1029/2004JC002571>, 2005.
- 1830
- 1831 Lo Monaco, C., Álvarez, M., Key, R. M., Lin, X., Tanhua, T., Tilbrook, B., Bakker, D. C. E., van Heuven, S.,
1832 Hoppema, M., Metzl, N., Ríos, A. F., Sabine, C. L., and Velo, A.: Assessing the internal consistency of the
1833 CARINA database in the Indian sector of the Southern Ocean, *Earth Syst. Sci. Data*, 2, 51–70,
1834 <https://doi.org/10.5194/essd-2-51-2010>, 2010.
- 1835
- 1836 Lo Monaco, C., Metzl, N., D’Ovidio, F., Llort, J., and Ridame, C.: Rapid establishment of the CO₂ sink
1837 associated with Kerguelen’s bloom observed during the KEOPS2/OISO20 cruise, *Biogeosciences Discuss.*, 11,
1838 17543–17578, <https://doi.org/10.5194/bgd-11-17543-2014>, 2014.
- 1839
- 1840 Lo Monaco, C.: OISO-30 cruise, RV Marion Dufresne, <https://doi.org/10.17600/18000679>, 2020.
- 1841
- 1842 Lo Monaco, C., Jeandel, C., and Planquette, H.: OISO-31 cruise, RV Marion Dufresne,
1843 <https://doi.org/10.17600/18001254>, 2021.
- 1844
- 1845 Long, M. C., Lindsay, K., Peacock, S., Moore, J. K., and Doney, S. C.: Twentieth-Century Oceanic Carbon
1846 Uptake and Storage in CESM1(BGC), *J. Climate*, 26 (18), 6775–6800, doi:10.1175/JCLI-D-12-00184.1, 2013.
- 1847
- 1848 Long, M. C., Stephens, B. B., McKain, K., Sweeney, C., Keeling, R. F., Kort, E. A., Morgan, E. J., Bent, J. D.,
1849 Chandra, N., Chevallier, F., Commane, R., Daube, B. C., Krummel, P. B., Loh, Z., Luijkx, I. T., Munro, D.,
1850 Patra, P., Peters, W., Ramonet, M., Rödenbeck, C., Stavert, A., Tans, P., and Wofsy, S. C.: Strong Southern
1851 Ocean carbon uptake evident in airborne observations, *Science*, 374, 1275–1280,
1852 <https://doi.org/10.1126/science.abi4355>, 2021.
- 1853
- 1854 Louanchi, F., Ruiz-Pino, D., and Poisson, A.: Temporal variations of mixed layer oceanic CO₂ at JGOFS-
1855 KERFIX time-series station: Physical versus biogeochemical processes. *Journal of Marine Research* 57(1): 165-
1856 187. <https://doi.org/10.1357/002224099765038607>, 1999.
- 1857
- 1858 Louanchi, F., Ruiz-Pino, D. P., Jeandel, C., Brunet, C., Schauer, B., Masson, A., Fiala, M., and Poisson, A.:
1859 Dissolved inorganic carbon, alkalinity, nutrient and oxygen seasonal and interannual variations at the Antarctic
1860 Ocean JGOFS-KERFIX site. *Deep Sea Research Part I: Oceanographic Research Papers* 48(7): 1581-1603,
1861 [https://doi.org/10.1016/S0967-0637\(00\)00086-8](https://doi.org/10.1016/S0967-0637(00)00086-8), 2001.
- 1862
- 1863 Lovenduski, N. S., and Gruber, N.: Impact of the Southern Annular Mode on Southern Ocean circulation and
1864 biology, *Geophys. Res. Lett.*, 32, L11603, doi:10.1029/2005GL022727, 2005.
- 1865
- 1866 Lueker, T. J., Dickson, A. G., and Keeling, C. D.: Ocean pCO₂ calculated from dissolved inorganic carbon,
1867 alkalinity, and equations for K-1 and K-2: validation based on laboratory measurements of CO₂ in gas and
1868 seawater at equilibrium. *Marine Chemistry* 70, 105-119. [https://doi.org/10.1016/S0304-4203\(00\)00022-0](https://doi.org/10.1016/S0304-4203(00)00022-0), 2000.
- 1869
- 1870 Ma, D., Gregor, L., and Gruber, N.: Four decades of trends and drivers of global surface ocean acidification.
1871 *Global Biogeochemical Cycles*, 37, e2023GB007765. [10.1029/2023GB007765](https://doi.org/10.1029/2023GB007765), 2023.



- 1872
1873 Mackay, N., Watson, A. J., Suntharalingam, P. et al.: Improved winter data coverage of the Southern Ocean CO₂
1874 sink from extrapolation of summertime observations. *Commun Earth Environ* 3, 265,
1875 <https://doi.org/10.1038/s43247-022-00592-6>, 2022.
1876
1877 Mahieu, L., Lo Monaco, C., Metzl, N., Fin, J., and Mignon, C.: Variability and stability of anthropogenic CO₂ in
1878 Antarctic Bottom Water observed in the Indian sector of the Southern Ocean, 1978–2018, *Ocean Sci.*, 16, 1559–
1879 1576, <https://doi.org/10.5194/os-16-1559-2020>, 2020.
1880
1881 Marshall, G. J.: Trends in the Southern Annular Mode from observations and reanalyses. *J. Clim.*, 16, 4134–
1882 4143, doi:10.1175/1520-0442%282003%29016<4134%3ATITSAM>2.0.CO%3B2, 2003.
1883
1884 Mayot, N., Le Quéré, C., Rödenbeck, C., Bernardello, R., Bopp, L., Djeutchouang, L. M., Gehlen, M., Gregor,
1885 L., Gruber, N., Hauck, J., Iida, Y., Ilyina, T., Keeling, R. F., Landschützer, P., Manning, A. C., Patara, L.,
1886 Resplandy, L., Schwinger, J., Séférian, R., Watson, A. J., Wright, R. M. and Zeng, J.: Climate-driven variability
1887 of the Southern Ocean CO₂ sink. *Phil. Trans. R. Soc. A*. 381: 20220055, <http://doi.org/10.1098/rsta.2022.0055>,
1888 2023
1889
1890 Mazloff, M. R., Verdy, A., Gille, S. T., Johnson, K. S., Cornuelle, B. D., and Sarmiento, J.: Southern Ocean
1891 acidification revealed by biogeochemical-Argo floats. *Journal of Geophysical Research: Oceans*, 128,
1892 e2022JC019530. <https://doi.org/10.1029/2022JC019530>, 2023.
1893
1894 McKinley, G. A., Bennington, V. S., Meinshausen, M., and Nicholls, Z.: Modern air-sea flux distributions
1895 reduce uncertainty in the future ocean carbon sink, *Environmental Research Letters*, 18, doi:10.1088/1748-
1896 9326/acc195, 2023.
1897
1898 McNeil, B. I. and Matear, R. J.: Southern Ocean acidification: A tipping point at 450-ppm atmospheric
1899 CO₂, *P. Natl. Acad. Sci. USA*, 105, 18860–18864, <https://doi.org/10.1073/pnas.0806318105>, 2008.
1900
1901 McNeil, B. I. and Sasse, T. P.: Future ocean hypercapnia driven by anthropogenic amplification of the natural
1902 CO₂ cycle, *Nature*, 529, 383–386, doi:10.1038/nature16156, 2016
1903
1904 McNeil, B. I., Metzl, N., Key, R. M., Matear, R. J. and Corbiere, A.: An empirical estimate of the Southern
1905 Ocean air-sea CO₂ flux, *Global Biogeochem. Cycles*, Vol. 21, No. 3, GB3011 10.1029/2007GB002991, 2007.
1906
1907 Meinshausen, M., Nicholls, Z. R. J., Lewis, J., Gidden, M. J., Vogel, E., Freund, M., et al.: The shared
1908 socioeconomic pathway (SSP) greenhouse gas concentrations and their extensions to 2500. *Geoscientific Model*
1909 *Development*, 13(8), 3571–3605. <https://doi.org/10.5194/gmd-13-3571-2020>, 2020.
1910
1911 Metzl, N., and Lo Monaco, C.: OISO- Océan Indien Service D'Observation,
1912 <https://doi.org/10.18142/228>, 1998.
1913
1914 Metzl, N., Brunet, C., Jabaud-Jan, A., Poisson, A., and Schauer, B.: Summer and winter air–sea CO₂ fluxes in
1915 the Southern Ocean, *Deep-Sea Res.*, 53, 1548–1563, <https://doi.org/10.1016/j.dsr.2006.07.006>, 2006.
1916
1917 Metzl, N.: Decadal increase of oceanic carbon dioxide in Southern Indian Ocean surface waters (1991–2007),
1918 *Deep-Sea Res. Pt. II*, 56, 607–619, <https://doi.org/10.1016/j.dsr2.2008.12.007>, 2009.
1919
1920 Midorikawa, T., Inoue, H. Y., Ishii, M., Sasano, D., Kosugi, N., Hashida, G., Nakaoka, S., and Suzuki, T.:
1921 Decreasing pH trend estimated from 35-year time series of carbonate parameters in the Pacific sector of the
1922 Southern Ocean in summer, *Deep-Sea Res.*, 61, 131–139, <https://doi.org/10.1016/j.dsr.2011.12.003>, 2012.
1923



- 1924 Millero, F. J., Lee, K., and Roche, M.: Distribution of alkalinity in the surface waters of the major oceans, *Mar.*
1925 *Chem.*, 60, 111–130, [https://doi.org/10.1016/S0304-4203\(97\)00084-4](https://doi.org/10.1016/S0304-4203(97)00084-4), 1998.
- 1926
- 1927 Minas, H. J., and Minas, M.: Net community production in high nutrient-low chlorophyll waters of the tropical
1928 and Antarctic oceans – grazing vs iron hypothesis, *Oceanol. Acta*, 15, 145–162, 1992.
- 1929
- 1930 Mongin, M., Nelson, D. M., Pondaven, P., and Tréguer, P.: Simulation of upper-ocean biogeochemistry with a
1931 flexible-composition phytoplankton model: C, N and Si cycling and Fe limitation in the Southern Ocean. *Deep*
1932 *Sea Research Part II: Topical Studies in Oceanography*, Elsevier, 2006, 53 (5-7), pp.601-619.
1933 [10.1016/j.dsr2.2006.01.021](https://doi.org/10.1016/j.dsr2.2006.01.021), 2006.
- 1934
- 1935 Mongin, M., Nelson, D. M., Pondaven P., and Tréguer, P.: Potential phytoplankton responses to iron and
1936 stratification changes in the Southern Ocean based on a flexible-composition phytoplankton model. *Global*
1937 *Biogeochemical Cycles* 21 (GB4020), [/http://dx.doi.org/10.1029/2007GB002972S](http://dx.doi.org/10.1029/2007GB002972S), 2007.
- 1938
- 1939 Mongin, M., Molina, E., and Trull, T. W.: Seasonality and scale of the Kerguelen plateau phytoplankton bloom:
1940 A remote sensing and modeling analysis of the influence of natural iron fertilization in the Southern Ocean.
1941 *Deep Sea Research Part II: Topical Studies in Oceanography*, Vol 55, Issues 5–7, Pages 880-892,
1942 <https://doi.org/10.1016/j.dsr2.2007.12.039>. 2008.
- 1943
- 1944 Mongwe, N. P., Vichi, M., and Monteiro, P. M. S.: The seasonal cycle of pCO₂ and CO₂ fluxes in the Southern
1945 Ocean: diagnosing anomalies in CMIP5 Earth system models, *Biogeosciences*, 15, 2851–2872,
1946 <https://doi.org/10.5194/bg-15-2851-2018>, 2018.
- 1947
- 1948 Mongwe, P., Gregor, L., Tjiputra, J., Hauck, J., Ito, T., Danek, C., Vichi, M., Thomalla S., and Monteiro, M. S.:
1949 A shift in the mechanism of CO₂ uptake in the Southern Ocean under high emission-scenario, DOI:
1950 [10.21203/rs.3.rs-2849464/v1](https://doi.org/10.21203/rs.3.rs-2849464/v1), 2023.
- 1951
- 1952 Moore, J. K. and Abbott, M. R.: Phytoplankton chlorophyll distributions and primary production in the Southern
1953 Ocean, *J. Geophys. Res.-Oceans*, 105, 28709–28722, <https://doi.org/10.1029/1999JC000043>, 2000
- 1954
- 1955 Moy, A. D., Palmer, M. R., Howard, W. R., Bijma, J., Cooper, M. J., Calvo, E., Pelejero, C., Gagan M. K. and
1956 Chalk, T. B.: Reduced calcification in modern Southern Ocean planktonic foraminifera. *Nature Geosci* 2, 276–
1957 280. <https://doi.org/insu.bib.cnrs.fr/10.1038/ngeo460>, 2009.
- 1958
- 1959 Negrete-García, G., Lovenduski, N. S., Hauri, C., Krumhardt, K. M., and Lauvset, S. K.: Sudden
1960 emergence of a shallow aragonite saturation horizon in the Southern Ocean. *Nature Climate Change*, 1758–
1961 6798, [10.1038/s41558-019-0418-8](https://doi.org/10.1038/s41558-019-0418-8), 2019.
- 1962
- 1963 Neveux, J., and Lantoiné, F.: Spectrofluorometric assay of chlorophylls and phaeopigments using the least
1964 squares approximation technique, *Deep-Sea Res. I*, 40(9), 1747-1765, [https://doi.org/10.1016/0967-](https://doi.org/10.1016/0967-0637(93)90030-7)
1965 [0637\(93\)90030-7](https://doi.org/10.1016/0967-0637(93)90030-7), 1993.
- 1966
- 1967 Nicholson S. A., Whitt, D. B., Fer, I., du Plessis, M. D., Lebéhot A. D., et al.: Storms drive outgassing of CO₂ in
1968 the subpolar Southern Ocean. *Nat. Commun.* 13:158. <https://doi.org/10.1038/s41467-021-27780-w>, 2022
- 1969
- 1970 Olafsson, J., Olafsdottir, S. R., Benoit-Cattin, A., Danielsen, M., Arnarson, T. S., and Takahashi, T.: Rate of
1971 Iceland Sea acidification from time series measurements. *Biogeosciences* 6, 2661–2668.
1972 <https://doi.org/10.5194/bg-6-2661-2009>, 2009.
- 1973
- 1974 Olafsson, J., Olafsdottir, S. R., Benoit-Cattin, A., and Takahashi, T.: The Irminger Sea and the Iceland Sea time
1975 series measurements of sea water carbon and nutrient chemistry 1983–2006. *Earth Syst. Sci. Data* 2, 99–104.
1976 <https://doi.org/10.5194/essd-2-99-2010>, 2010.



- 1977
1978 Olsen, A., Key, R. M., van Heuven, S., Lauvset, S. K., Velo, A., Lin, X., Schirnack, C., Kozyr, A., Tanhua, T.,
1979 Hoppema, M., Jutterström, S., Steinfeldt, R., Jeansson, E., Ishii, M., Pérez, F. F., and Suzuki, T.: The Global
1980 Ocean Data Analysis Project version 2 (GLODAPv2) – an internally consistent data product for the world ocean,
1981 Earth Syst. Sci. Data, 8, 297–323, <https://doi.org/10.5194/essd-8-297-2016>, 2016.
1982
1983 Olsen, A., Lange, N., Key, R. M., Tanhua, T., Álvarez, M., Becker, S., Bittig, H. C., Carter, B. R., Cotrim da
1984 Cunha, L., Feely, R. A., van Heuven, S., Hoppema, M., Ishii, M., Jeansson, E., Jones, S. D., Jutterström, S.,
1985 Karlsen, M. K., Kozyr, A., Lauvset, S. K., Lo Monaco, C., Murata, A., Pérez, F. F., Pfeil, B., Schirnack, C.,
1986 Steinfeldt, R., Suzuki, T., Telszewski, M., Tilbrook, B., Velo, A., and Wanninkhof, R.: GLODAPv2.2019 – an
1987 update of GLODAPv2, Earth Syst. Sci. Data, 11, 1437–1461, <https://doi.org/10.5194/essd-11-1437-2019>, 2019.
1988
1989 Olsen, A., Lange, N., Key, R. M., Tanhua, T., Bittig, H. C., Kozyr, A., Álvarez, M., Azetsu-Scott, K., Becker, S.,
1990 Brown, P. J., Carter, B. R., Cotrim da Cunha, L., Feely, R. A., van Heuven, S., Hoppema, M., Ishii, M.,
1991 Jeansson, E., Jutterström, S., Landa, C. S., Lauvset, S. K., Michaelis, P., Murata, A., Pérez, F. F., Pfeil, B.,
1992 Schirnack, C., Steinfeldt, R., Suzuki, T., Tilbrook, B., Velo, A., Wanninkhof, R., and Woosley, R. J.: An updated
1993 version of the global interior ocean biogeochemical data product, GLODAPv2.2020, Earth Syst. Sci. Data, 12,
1994 3653–3678, <https://doi.org/10.5194/essd-12-3653-2020>, 2020.
1995
1996 Orr, J. C., Fabry, V. J., Aumont, O., Bopp, L., Doney, S. C., Feely, R. A., Gnanadesikan, A., Gruber, N., Ishida,
1997 A., Joos, F., Key, R. M., Lindsay, K., Maier-Reimer, E., Matear, R., Monfray, P., Mouchet, A., Najjar, R. G.,
1998 Plattner, G.-K., Rodgers, K. B., Sabine, C. L., Sarmiento, J. L., Schlitzer, R., Slater, R. D., Totterdell, I. J.,
1999 Weirig, M.-F., Yamanaka, Y., and Yool, A.: Anthropogenic ocean acidification over the twenty-first century and
2000 its impact on calcifying organisms, *Nature*, 437, 681–686, <https://doi.org/10.1038/nature04095>, 2005.
2001
2002 Orr, J. C., Epitalon, J.-M., and Gattuso, J.-P.: Comparison of ten packages that compute ocean carbonate
2003 chemistry, *Biogeosciences*, 12(5), 1483–1510, doi:10.5194/bg-12-1483-2015, 2015.
2004
2005 Orr, J. C., Epitalon, J.-M., Dickson, A. G., and Gattuso, J.-P.: Routine uncertainty propagation for the marine
2006 carbon dioxide system, *Marine Chemistry*, Vol. 207, 84–107, doi:10.1016/j.marchem.2018.10.006., 2018.
2007
2008 Oschlies, A., Brandt, P., Stramma, L., and Schmidtko, S.: Drivers and mechanisms of ocean deoxygenation. *Nat.*
2009 *Geosci.* 11, 467–473. doi: 10.1038/s41561-018-0152-2, 2018.
2010
2011 Pardo, P. C., Pérez, F. F., Khatiwala, S., and Ríos, A. F.: Anthropogenic CO₂ estimates in the Southern Ocean:
2012 Storage partitioning in the different water masses, *Prog. Oceanogr.*, 120, 230–242,
2013 <https://doi.org/10.1016/j.pcean.2013.09.005>, 2014.
2014
2015 Pardo, P. C., Tilbrook, B., Langlais, C., Trull, T. W., and Rintoul, S. R.: Carbon uptake and biogeochemical
2016 change in the Southern Ocean, south of Tasmania. *Biogeosciences*, 14(22), 5217–5237.
2017 <https://doi.org/10.5194/bg-14-5217-2017>, 2017.
2018
2019 Pasquer, B., Metzl, N., Goosse, H., and Lancelot, C.: What drives the seasonality of air-sea CO₂ fluxes in the
2020 ice-free zone of the Southern Ocean: A 1D coupled physical-biogeochemical model approach. *Marine*
2021 *Chemistry*, 177 (3): 554-565. [doi:10.1016/j.marchem.2015.08.008](https://doi.org/10.1016/j.marchem.2015.08.008), 2015.
2022
2023 Pauthenet, E., Roquet, F., Madec, G., Guinet, C., Hindell, M., McMahon, C. R., Harcourt, R., and Nerini, D.:
2024 Seasonal Meandering of the Polar Front Upstream of the Kerguelen Plateau, *Geophys. Res. Lett.*, 45, 9774–
2025 9781, <https://doi.org/10.1029/2018GL079614>, 2018.
2026
2027 Petrou, K., Baker, K. G., Nielsen, D. A., Hancock, A. M., Schulz, K. G. and Davidson, A. T.: Acidification
2028 diminishes diatom silica production in the Southern Ocean. *Nature Climate Change*, 9, 781-786,
2029 <https://doi.org/10.1038/s41558-019-0557-y>, 2019.



- 2030
2031 Pierrot, D., Lewis, E., and Wallace, D. W. R.: MS Excel Program Developed for CO₂ System Calculations
2032 ORNL/CDIAC-105, Carbon Dioxide Inf. Anal. Cent., Oak Ridge Natl. Lab., U. S. Dept. of Energy, Oak Ridge,
2033 Tenn., https://cdiac.ess-dive.lbl.gov/ftp/co2sys/CO2SYS_calc_XLS_v2.1/ (last access: 3 March 2022), 2006.
2034
2035 Pilcher, D. J., Brody, S. R., Johnson, L., and Bronselaer, B.: Assessing the abilities of CMIP5 models to
2036 represent the seasonal cycle of surface ocean pCO₂, *J. Geophys. Res. Oceans*, 120, 4625–4637,
2037 doi:10.1002/2015JC010759, 2015.
2038
2039 Pfeil, B., Olsen, A., Bakker, D. C. E., Hankin, S., Koyuk, H., Kozyr, A., Malczyk, J., Manke, A., Metzl, N.,
2040 Sabine, C. L., Akl, J., Alin, S. R., Bates, N., Bellerby, R. G. J., Borges, A., Boutin, J., Brown, P. J., Cai, W.-J.,
2041 Chavez, F. P., Chen, A., Cosca, C., Fassbender, A. J., Feely, R. A., González-Dávila, M., Goyet, C., Hales,
2042 B., Hardman-Mountford, N., Heinze, C., Hood, M., Hoppema, M., Hunt, C. W., Hydes, D., Ishii, M.,
2043 Johannessen, T., Jones, S. D., Key, R. M., Körtzinger, A., Landschützer, P., Lauvset, S. K., Lefèvre, N.,
2044 Lenton, A., Lourantou, A., Merlivat, L., Midorikawa, T., Mintrop, L., Miyazaki, C., Murata, A., Nakadate, A.,
2045 Nakano, Y., Nakaoka, S., Nojiri, Y., Omar, A. M., Padin, X. A., Park, G.-H., Paterson, K., Perez, F. F., Pierrot,
2046 D., Poisson, A., Ríos, A. F., Santana-Casiano, J. M., Salisbury, J., Sarma, V. V. S. S., Schlitzer, R.,
2047 Schneider, B., Schuster, U., Sieger, R., Skjelvan, I., Steinhoff, T., Suzuki, T., Takahashi, T., Tedesco, K.,
2048 Telszewski, M., Thomas, H., Tilbrook, B., Tjiputra, J., Vandemark, D., Veness, T., Wanninkhof, R., Watson,
2049 A. J., Weiss, R., Wong, C. S., and Yoshikawa-Inoue, H.: A uniform, quality controlled Surface Ocean CO₂ Atlas
2050 (SOCAT), *Earth Syst. Sci. Data*, 5, 125–143, doi:10.5194/essd-5-125-2013, 2013.
2051
2052 Poisson, A.: INDIGO 1 - MD 43 cruise, RV Marion Dufresne, <https://doi.org/10.17600/85000111>, 1985.
2053
2054 Poisson, A., Schauer, B., and Brunet, C. : MD43/INDIGO 1, Cruise report; Les rapports des campagnes à la mer,
2055 85(06). Les publications de la Mission de Recherche des Terres Australes et Antarctiques Françaises, Paris, 267
2056 pp., 1988.
2057
2058 Poisson, A., Metzl, N., Brunet, C., Schauer, B., Bres, B., Ruiz-Pino, D., and Louanchi, F.: Variability of sources
2059 and sinks of CO₂ in the western Indian and southern oceans during the year 1991, *J. Geophys. Res. Oceans*, 98,
2060 22759–22778, <https://doi.org/10.1029/93JC02501>, 1993.
2061
2062 Pondaven, P., Fravalo, C., Ruiz-Pino, D., Tréguer, P., Quéguiner, B., and Jeandel, C.: Modelling the silica pump
2063 in the Permanently Open Ocean Zone of the Southern Ocean, *J. Mar. Syst.*, 17, 1–4, 587–619,
2064 [https://doi.org/10.1016/S0924-7963\(98\)00066-9](https://doi.org/10.1016/S0924-7963(98)00066-9), 1998.
2065
2066 Pondaven, P., Ruiz-Pino, D., Fravalo, C., Tréguer, P., and Jeandel, C.: Interannual variability of Si and N cycles
2067 at the time-series station KERFIX between 1990 and 1995 – a 1-D modelling study, *Deep-Sea Res. Pt. I*, 47, 2,
2068 223–257, [https://doi.org/10.1016/S0967-0637\(99\)00053-9](https://doi.org/10.1016/S0967-0637(99)00053-9), 2000.
2069
2070 Prend, C. J., Gray, A. R., Talley, L. D., Gille, S. T., Haumann, F. A., Johnson, K. S., et al.: Indo-Pacific sector
2071 dominates Southern Ocean carbon outgassing. *Global Biogeochemical Cycles*, 36, e2021GB007226.
2072 <https://doi.org/10.1029/2021GB007226>, 2022.
2073
2074 Racapé, V., Lo Monaco, C., Metzl, N., and Pierre, C.: Summer and winter distribution of $\delta^{13}\text{C}_{\text{DIC}}$ in surface
2075 waters of the South Indian Ocean (20°S–60°S). *Tellus-B*, DOI: 10.1111/j.1600-0889.2010.00504, 2010.
2076
2077 Reynolds, R. W., Rayner, N. A., Smith, T. M., Stokes, D. C., and Wang, W.: An improved in situ and satellite
2078 SST analysis for climate. *J. Clim.* 15, 1609–1625. [https://doi.org/10.1175/1520-0442\(2002\)015<1609:AIHSAS>2.0.CO;2](https://doi.org/10.1175/1520-0442(2002)015<1609:AIHSAS>2.0.CO;2), 2002.
2079
2080



- 2081 Rödenbeck, C., Keeling, R. F., Bakker, D. C. E., Metzl, N., Olsen, A., Sabine, C., and Heimann, M.: Global
2082 surface-ocean pCO₂ and sea-air CO₂ flux variability from an observation-driven ocean mixed-layer scheme,
2083 *Ocean Sci.*, 9, 193–216, <https://doi.org/10.5194/os-9-193-2013>, 2013.
2084
- 2085 Rödenbeck, C., DeVries, T., Hauck, J., Le Quéré, C., and Keeling, R. F.: Data-based estimates of
2086 interannual sea-air CO₂ flux variations 1957–2020 and their relation to environmental drivers,
2087 *Biogeosciences*, 19, 2627–2652, <https://doi.org/10.5194/bg-19-2627-2022>, 2022.
2088
- 2089 Rodgers, K. B., Schwinger, J., Fassbender, A. J., Landschützer, P., Yamaguchi, R., Frenzel, H., et al.: Seasonal
2090 variability of the surface ocean carbon cycle: A synthesis. *Global Biogeochemical Cycles*, 37, e2023GB007798.
2091 <https://doi.org/10.1029/2023GB007798>, 2023
2092
- 2093 Rustogi, P., Landschützer, P., Brune, S. et al.: The impact of seasonality on the annual air-sea carbon flux and its
2094 interannual variability. *Clim. Atmos. Sci.*, 6, 66, <https://doi.org/10.1038/s41612-023-00378-3>, 2023.
2095
- 2096 Sabine, C. L., Key, R. M., Johnson, K. M., Millero, F. J., Poisson, A., Sarmiento, J. L., Wallace, D. W. R., and
2097 Winn, C. D.: Anthropogenic CO₂ inventory of the Indian Ocean, *Global Biogeochemical Cycles*, 13, 179–198,
2098 <https://doi.org/10.1029/1998GB900022>, 1999.
2099
- 2100 Sabine, C. L., Feely, R. A., Gruber, N., Key, R. M., Lee, K., Bullister, J. L., Wanninkhof, R., Wong, C. S.,
2101 Wallace, D. W. R., Tilbrook, B., Millero, F. J., Peng, T.-H., Kozyr, A., Ono, T., and Rios, A. F.: The Oceanic
2102 Sink for Anthropogenic CO₂, *Science*, 305, 367–371, <https://doi.org/10.1126/science.1097403>, 2004.
2103
- 2104 Sasse, T. P., McNeil, B. I., Matear, R. J., and Lenton, A.: Quantifying the influence of CO₂ seasonality on future
2105 aragonite undersaturation onset, *Biogeosciences*, 12, 6017–6031, <https://doi.org/10.5194/bg-12-6017-2015>,
2106 2015.
2107
- 2108 Schlitzer, R.: Ocean Data View, Ocean Data View, <http://odv.awi.de> (last access: 13 March 2019), 2018.
2109
- 2110 Schmidtko, S., Stramma, L., and Visbeck, M.: Decline in global oceanic oxygen content during the past five
2111 decades, *Nature*, 542, 335–339, <https://doi.org/10.1038/nature21399>, 2017.
2112
- 2113 Seifert, M., Nissen, C., Rost, B., Vogt, M., Völker, C., and Hauck, J.: Interaction matters: Bottom-up driver
2114 interdependencies alter the projected response of phytoplankton communities to climate change. *Global Change*
2115 *Biology*, 00, 1– 25. <https://doi.org/10.1111/gcb.16799>, 2023.
2116
- 2117 Shadwick, E. H., Wynn-Edwards, C. A., Matear, R.J., Jansen, P., Schulz, E. and Sutton, A. J.: Observed
2118 amplification of the seasonal CO₂ cycle at the Southern Ocean Time Series. *Front. Mar. Sci.* 10:1281854. doi:
2119 10.3389/fmars.2023.1281854, 2023
2120
- 2121 Skjelvan, I., Lauvset, S. K., Johannessen, T., et al.: Decadal trends in Ocean Acidification from the Ocean
2122 Weather Station M in the Norwegian Sea, *Journal of Marine Systems*,
2123 <https://doi.org/10.1016/j.jmarsys.2022.103775>, 2022.
2124
- 2125 Smith, H. E. K., Poulton, A. J., Garley, R., Hopkins, J., Lubelczyk, L. C., Drapeau, D. T., Rauschenberg, S.,
2126 Twining, B. S., Bates, N. R., and Balch, W. M.: The influence of environmental variability on the biogeography
2127 of coccolithophores and diatoms in the Great Calcite Belt, *Biogeosciences*, 14, 4905–4925,
2128 <https://doi.org/10.5194/bg-14-4905-2017>, 2017.
2129
- 2130 Strickland, J. D. H. and Parsons, T. R.: A Practical Hand Book of Seawater Analysis. Fisheries Research Board
2131 of Canada Bulletin, 2nd Edition., 310 p. pp., 1972.
2132



- 2133 Sutton, A. J., Williams, N. L., and Tilbrook, B.: Constraining Southern Ocean CO₂ Flux Uncertainty Using
2134 Uncrewed Surface Vehicle Observations, *Geophys. Res. Lett.*, 48, e2020GL091748,
2135 <https://doi.org/10.1029/2020GL091748>, 2021.
2136
2137 Takahashi, T., Olafsson, J., Goddard, J. G., Chipman, D. W., and Sutherland, S. C.: Seasonal variation of CO₂
2138 and nutrients in the high-latitude surface oceans: A comparative study, *Global Biogeochem. Cycles*, 7(4), 843–
2139 878, doi:10.1029/93GB02263, 1993.
2140
2141 Takahashi, T., Sutherland, S. C., Wanninkhof, R., Sweeney, C., Feely, R. A., Chipman, D. W., Hales, B.,
2142 Friederich, G., Chavez, F., Sabine, C., Watson, A., Bakker, D. C. E., Schuster, U., Metzl, N., Yoshikawa-Inoue,
2143 H., Ishii, M., Midorikawa, T., Nojiri, Y., Körtzinger, A., Steinhoff, T., Hoppema, M., Olafsson, J., Arnarson, T.
2144 S., Tilbrook, B., Johannessen, T., Olsen, A., Bellerby, R., Wong, C. S., Delille, B., Bates, N. R., and de Baar, H.
2145 J. W.: Climatological mean and decadal change in surface ocean pCO₂, and net sea–air CO₂ flux over the
2146 global oceans, *Deep-Sea Res. Pt. II*, 56, 554–577, <https://doi.org/10.1016/j.dsr2.2008.12.009>, 2009a.
2147
2148 Takahashi, T., Sutherland, S. C., Wanninkhof, R., Sweeney, C., Feely, R. A., Chipman, D. W., Hales, B.,
2149 Friederich, G., Chavez, F., Sabine, C., Watson, A., Bakker, D. C. E., Schuster, U., Metzl, N., Yoshikawa-Inoue,
2150 H., Ishii, M., Midorikawa, T., Nojiri, Y., Körtzinger, A., Steinhoff, T., Hoppema, M., Olafsson, J., Arnarson, T.
2151 S., Tilbrook, B., Johannessen, T., Olsen, A., Bellerby, R., Wong, C. S., Delille, B., Bates, N. R., and de Baar, H.
2152 J. W.: Corrigendum to “Climatological mean and decadal change in surface ocean pCO₂, and net sea–air CO₂
2153 flux over the global oceans” [*Deep Sea Res. II* 56 (2009) 554–577], *Deep Sea Research Part I: Oceanographic
2154 Research Papers*, 56, 11, 2075–2076, <https://doi.org/10.1016/j.dsr.2009.07.007>, 2009b.
2155
2156 Takao, S., Hirawake, T., Wright, S. W., and Suzuki, K.: Variations of net primary productivity and
2157 phytoplankton community composition in the Indian sector of the Southern Ocean as estimated from ocean color
2158 remote sensing data, *Biogeosciences*, 9, 3875–3890, doi:10.5194/bg-9-3875-2012, 2012.
2159
2160 Talley, L. D.: Closure of the global overturning circulation through the Indian, Pacific, and Southern Oceans:
2161 Schematics and transports. *Oceanography*, 26(1), 80–97. <https://doi.org/10.5670/oceanog.2013.07>, 2013.
2162
2163 Tanhua, T., Hoppema, M., Jones, E. M., Stöven, T., Hauck, J., Dávila, M. G., Santana-Casiano, M., Álvarez, M.,
2164 and Strass, V. H.: Temporal changes in ventilation and the carbonate system in the Atlantic sector of the
2165 Southern Ocean, *Deep Sea Res. Part II Top. Stud. Oceanogr.*, 138, 26–38,
2166 <https://doi.org/10.1016/j.dsr2.2016.10.004>, 2017.
2167
2168 Touratier, F., Azouzi, L. and Goyet, C.: CFC-11, $\Delta 14C$ and $3H$ tracers as a means to assess anthropogenic CO₂
2169 concentrations in the ocean. *Tellus B*, 59(2), 318–325, doi:10.1111/j.1600-0889.2006.00247.x, 2007.
2170
2171 Tréguer, P., and Le Corre, P.: Manuel d’analyse des sels nutritifs dans l’eau de mer (utilisation de
2172 l’autoanalyseur II Technicon), 2nd ed., 110 pp., L.O.C.U.B.O., Brest, 1975.
2173
2174 Uppström, L. R.: The boron/chlorinity ratio of deep-sea water from the Pacific Ocean, *Deep Sea Research and
2175 Oceanographic Abstracts*, 21, 161–162, [https://doi.org/10.1016/0011-7471\(74\)90074-6](https://doi.org/10.1016/0011-7471(74)90074-6), 1974.
2176
2177 van Heuven, S. M. A. C., Hoppema, M., Huhn, O., Slagter, H. A., and de Baar, H. J. W.: Direct observation of
2178 increasing CO₂ in the Weddell Gyre along the Prime Meridian during 1973–2008, *Deep-Sea Res. Pt. II*, 58,
2179 2613–2635, <https://doi.org/10.1016/j.dsr2.2011.08.007>, 2011.
2180
2181 Vázquez-Rodríguez, M., Touratier, F., Lo Monaco, C., Waugh, D. W., Padin, X. A., Bellerby, R. G. J., Goyet,
2182 C., Metzl, N., Ríos, A. F., and Pérez, F. F.: Anthropogenic carbon distributions in the Atlantic Ocean: data-based
2183 estimates from the Arctic to the Antarctic, *Biogeosciences*, 6, 439–451, <https://doi.org/10.5194/bg-6-439-2009>,
2184 2009.
2185



- 2186 Wanninkhof, R., and Trinanes, J.: The impact of changing wind speeds on gas transfer and its effect on
2187 global air-sea CO₂ fluxes, *Global Biogeochem. Cycles*, 31, doi:10.1002/2016GB005592, 2017.
2188
- 2189 Wanninkhof, R., Barbero, L., Byrne, R., Cai, W.-J., Huang, W.-J., Zhang, J.-Z., Baringer, M., and Langdon, C.:
2190 Ocean acidification along the Gulf Coast and East Coast of the USA, *Continental Shelf Research*, 98, 54-71,
2191 <https://doi.org/10.1016/j.csr.2015.02.008>, 2015
2192
- 2193 Weir, I., Fawcett, S., Smith, S., Walker, D., Bornman, T., and Fietz, S.: Winter biogenic silica and diatom
2194 distributions in the Indian sector of the Southern Ocean, *Deep Sea Research Part I: Oceanographic Research*
2195 *Papers*, Volume 166, 103421, <https://doi.org/10.1016/j.dsr.2020.103421>, 2020.
2196
- 2197 Weiss, R. F. and Price, B. A.: Nitrous oxide solubility in water and seawater. *Marine Chemistry*, 8(4), 347–359,
2198 doi:10.1016/0304-4203(80)90024-9, 1980.
2199
- 2200 Wright, R. M., Le Quéré, C., Mayot, N., Olsen, A., and Bakker, D.: Fingerprint of climate change on Southern
2201 Ocean carbon storage. *Global Biogeochemical Cycles*, 37, e2022GB007596. Doi: 10.1029/2022GB007596,
2202 2023.
2203
- 2204 Xue, L., Cai, W. J., Takahashi, T. et al.: Climatic modulation of surface acidification rates through summertime
2205 wind forcing in the Southern Ocean. *Nat. Commun.*, 9, 3240, Doi:10.1038/s41467-018-05443-7, 2018.
2206
- 2207 Yun, J., Jeong, S., Gruber, N., Gregor, L., Ho, C.-H., Piao, S., Ciais, P., Schimel, D., and Kwon, E. Y.: Enhance
2208 seasonal amplitude of atmospheric CO₂ by the changing Southern Ocean carbon sink, *Science Advances*, 8, 41,
2209 doi: 10.1126/sciadv.abq0220, 2022.
2210